Defense Nuclear Agency
Alexandria, VA 22310-3398



DNA-TR-95-43

# Seismic Hard In-Situ Source Test (SHIST)
## CRALE 1D and 2D Scoping Calculations

Victor E. Koik
Jim R. Rocco
Jeffrey M. Thomsen
Titan Corporation (The)
Titan Research & Technology Divsn
9410 Topanga Canyon Blvd
Suite 104
Chatsworth, CA 91311-5771

October 1995

Technical Report

Destroy this report when it is no longer needed. Do not return to sender.

PLEASE NOTIFY THE DEFENSE NUCLEAR AGENCY, ATTN: CSTI, 6801 TELEGRAPH ROAD, ALEXANDRIA, VA 22310-3398, IF YOUR ADDRESS IS INCORRECT, IF YOU WISH IT DELETED FROM THE DISTRIBUTION LIST, OR IF THE ADDRESSEE IS NO LONGER EMPLOYED BY YOUR ORGANIZATION.

# DISTRIBUTION LIST UPDATE

This mailer is provided to enable DNA to maintain current distribution lists for reports. (We would appreciate your providing the requested information.)

**NOTE:**
**Please return the mailing label from the document so that any additions, changes, corrections or deletions can be made easily. For distribution cancellation or more information call DNA/IMAS (703) 325-1036.**

☐ Add the individual listed to your distribution list.

☐ Delete the cited organization/individual.

☐ Change of address.

NAME: _____

ORGANIZATION: _____

| OLD ADDRESS | CURRENT ADDRESS |
|---|---|
| _____ | _____ |
| _____ | _____ |
| _____ | _____ |

TELEPHONE NUMBER: ( ) _____

| DNA PUBLICATION NUMBER/TITLE | CHANGES/DELETIONS/ADDITIONS, etc. *(Attach Sheet if more Space is Required)* |
|---|---|
| _____ | _____ |
| _____ | _____ |
| _____ | _____ |

DNA OR OTHER GOVERNMENT CONTRACT NUMBER: _____

CERTIFICATION OF NEED-TO-KNOW BY GOVERNMENT SPONSOR (if other than DNA):

SPONSORING ORGANIZATION: _____

CONTRACTING OFFICER OR REPRESENTATIVE: _____

SIGNATURE: _____

CUT HERE AND RETURN

DEFENSE NUCLEAR AGENCY
ATTN: IMAS
6801 TELEGRAPH ROAD
ALEXANDRIA, VA 22310-3398

DEFENSE NUCLEAR AGENCY
ATTN: IMAS
6801 TELEGRAPH ROAD
ALEXANDRIA, VA 22310-3398

# REPORT DOCUMENTATION PAGE

*Form Approved*
*OMB No. 0704-0188*



| 1. AGENCY USE ONLY (Leave blank) | 2. REPORT DATE | 3. REPORT TYPE AND DATES COVERED |
|---|---|---|
| | 951001 | Technical 930915 – 950315 |

**4. TITLE AND SUBTITLE**
Seismic Hard In-Situ Source Test (SHIST)
CRALE 1D and 2D Scoping Calculations

**5. FUNDING NUMBERS**

**6. AUTHOR(S)**
Victor E. Koik, Jim R. Rocco and Jeffrey M. Thomsen

**7. PERFORMING ORGANIZATION NAME(S) AND ADDRESS(ES)**
Titan Corporation (The)
Titan Research & Technology Divsn
9410 Topanga Canyon Blvd
Suite 104
Chatsworth, CA 91311-5771

**8. PERFORMING ORGANIZATION REPORT NUMBER**
TRT-FR-3346

**9. SPONSORING/MONITORING AGENCY NAME(S) AND ADDRESS(ES)**
Defense Nuclear Agency
6801 Telegraph Road
Alexandria, VA 22310-3398
FCTT/Rinehart

**10. SPONSORING/MONITORING AGENCY REPORT NUMBER**
DNA-TR-95-43

**11. SUPPLEMENTARY NOTES**

**12a. DISTRIBUTION/AVAILABILITY STATEMENT**
Approved for public release; distribution is unlimited.

**12b. DISTRIBUTION CODE**

**13. ABSTRACT** (*Maximum 200 words*)

SHIST (Seismic Hard rock In-Situ Source Test) was a proposed prototype High Explosive (HE) seismic source function experiment designed to provide a benchmark data set for seismic source function models in hard rock geology, and also to provide a threshold of detection calibration point for regional seismic monitoring systems. The experiment was to consist of 20 tons of HE in a fully contained sphere detonated in a granite test bed. The test was subsequently canceled. This report describes preliminary material models developed for the site and 1D and 2D finite-difference scoping calculations performed to serve as a starting point should the test (or other HE test requiring a hard rock geology) be revived in the future. The intent of this study was to investigate the details of the shock wave propagation into granite, and to determine the seismic transition point (the range at which the stress wave developed by the HE source began to decay as an elastic wave) to assist with gage placement activities. 3D effects, such as the surface slope variation and ground fault lines, found to exist at the proposed SHIST Site, were neglected.

| 14. SUBJECT TERMS | | 15. NUMBER OF PAGES |
|---|---|---|
| SHIST | Granite | 132 |
| HE Testing | Seismic Sources | 16. PRICE CODE |

| 17. SECURITY CLASSIFICATION OF REPORT | 18. SECURITY CLASSIFICATION OF THIS PAGE | 19. SECURITY CLASSIFICATION OF ABSTRACT | 20. LIMITATION OF ABSTRACT |
|---|---|---|---|
| UNCLASSIFIED | UNCLASSIFIED | UNCLASSIFIED | SAR |

NSN 7540-280-5500

Standard Form 298 (Rev.2-89)
Prescribed by ANSI Sts. 239-18
298-102

CLASSIFIED BY:

N/A since Unclassified.

DECLASSIFY ON:

N/A since Unclassified.

| Accesion For | |
|---|---|
| NTIS CRA&I | ☑ |
| DTIC TAB | ☐ |
| Unannounced | ☐ |
| Justification | |
| By | |
| Distribution / | |
| Availability Codes | |
| Dist | Avail and / or Special |
| A-1 | |

## SUMMARY

All three tasks for the above referenced contract have been completed. The available material properties of the SHIST site were evaluated and simple scoping Equations of State models for weathered and jointed granite were developed. These models were then used in a number of CRALE 1D and 2D finite-difference calculations to examine the free-field environment generated from a 20 ton QM-100/R HE charge buried at a depth of 35 meters. The 1D calculations indicate that the shock wave transitions to one with elastic characteristics (with an elastic attenuation of $R^{-1.1}$ ) at a range of approximately 30 m and stress level of 0.3 kbar. The 2D calculations showed that the environment is spherical up to the time when the relief wave arrives from either the 15 meter deep layer interface or from the free surface. They also indicate the shot appears to be deep enough so gages at depth should not be susceptible to serious free surface or layering effects. Stress, velocity, and displacement time history waveforms from the 2D CRALE prediction calculations have been included at the current experimental gage locations.

This study found that both bulk porosity and shock velocity to stresses on the order of 0.5 kbar are important factors in determining the range at which the elastic transition occurs. For future test planning, it is recommended that additional material properties tests be performed. These include Uniaxial stress response from 0.5 to 2 kbar on large enough samples to capture the in-situ jointing, and Triaxial stress tests to better understand the weathered material's failure envelope.

The CRALE 1D and 2D codes have been successfully ported to the DNA Field Command Silicon Graphics Crimson workstation. Both codes are fully operational, and since the 2D SHIST prediction calculation (case 2DSHIST03) was run on that platform, the data files are available to DNAFC for local postprocessing. The analytic approach used here could be easily extended to other explosive test configurations (such as decoupled cavity shots) and calculated on the DNAFC in-house workstations.

## CONVERSION TABLE

CONVERSION FACTORS FOR U.S. CUSTOMARY TO METRIC (SI) UNITS OF MEASUREMENT

MULTIPLY ⟶ BY ⟶ TO GET
TO GET ⟵ BY ⟵ DIVIDE

| | | |
|---|---|---|
| angstrom | 1.000 000 X E -10 | meters (m) |
| atmosphere (normal) | 1.013 250 X E +2 | kilo pascal (kPa) |
| bar | 1.000 000 X E +2 | kilo pascal (kPa) |
| barn | 1.000 000 X E -28 | meter$^2$ (m$^2$) |
| british thermal unit (thermochemical) | 1.054 350 X E +3 | joule (J) |
| calorie (thermochemical) | 4.184 000 | joule (J) |
| cal (thermochemical)/cm$^2$ | 4.184 000 X E -2 | mega joule/m$^2$(MJ/m$^2$) |
| curie | 3.700 000 X E +1 | *giga becquerel (GBq) |
| degree (angle) | 1.745 329 X E -2 | radian (rad) |
| degree Celsius | $t_k = t_{oC} = 273.15$ | degree kelvin (K) |
| degree Fahrenheit | $t_k = (t_{o*f} + 459.67)/1.8$ | degree kelvin (K) |
| electron volt | 1.602 19 X E -19 | joule (J) |
| erg | 1.000 000 X E -7 | joule (J) |
| erg/second | 1.000 000 X E -7 | watt (W) |
| foot | 3.048 000 X E -1 | meter (m) |
| foot-pound-force | 1.355 818 | joule (J) |
| gallon (U.S. liquid) | 3.785 412 X E -3 | meter$^3$ (m$^3$) |
| inch | 2.540 000 X E -2 | meter (m) |
| jerk | 1.000 000 X E +9 | joule (J) |
| joule/kilogram (j/kg) (radiation dose absorbed) | 1.000 000 | Gray (Cy) |
| kilotons | 4.184 | terajoules (TJ) |
| kip (1000 lbf) | 4.448 222 X E +3 | newton (N) |
| kip/inch$^2$ (ksi) | 6.894 757 X E +3 | kilo pascal (kPa) |
| ktap | 1.000 000 X E +2 | newton-second/m$^2$ (N-s/m$^2$) |
| micron | 1.000 000 X E -6 | meter (m) |
| mil | 2.540 000 X E -5 | meter (m) |
| mile (international) | 1.609 344 X E +3 | meter (m) |
| ounce (advoirdupois) | 2.834 952 X E -2 | kilogram (kg) |
| pound-force (lbs avoirdupois) | 4.448 222 | newton (N) |
| pound-force inch | 1.129 848 X E -1 | newton-meter (N-m) |
| pound-force/inch | 1.751 268 X E +2 | newton/meter (N/m) |
| pound-force/foot$^2$ | 4.788 026 X E -2 | kilo pascal (kPa) |
| pound-force/inch$^2$ (psi) | 6.894 757 | kilo pascal (kPa) |
| pound-mass (lbm avoirdupois) | 4.535 924 X E -1 | kilogram (kg) |
| pound-mass-foot$^2$ (moment of inertia) | 4.214 011 X E -2 | kilogram-meter$^2$ (kg-m$^2$) |
| pound-mass/foot$^3$ | 1.601 846 X E +1 | kilogram/meter$^3$ (kg/m$^3$) |
| rad (radiation dose absorbed) | 1.000 000 x E -2 | **gray (Gy) |
| roentgen | 2.580 000 X E -4 | coulomb/kilogram (C/Kg) |
| shake | 1.000 000 X E -8 | second (s) |
| slug | 1.459 390 X E +1 | kilogram (kg) |
| torr (mm Hg, 0°C) | 1.333 22 X E -1 | kilo pascal (kPa) |

* The becquerel (Bq) is the SI unit of radioactivity; 1 Bq = 1 event/s.

** The Gray (Gy) is the SI unit of absorbed radiation; 1 Gy = 1 J/kg.

A more complete listing of conversions may be found in "Metric Practice Guide E 380-74," American Socity for Testing Materials

## TABLE OF CONTENTS

## FIGURES

## FIGURES (Continued)

## FIGURES (Continued)

## FIGURES (Continued)

# SECTION 1
# INTRODUCTION

## 1.1 BACKGROUND.

SHIST (Seismic Hard rock In-situ Source Test) was a proposed prototype High Explosive (HE) seismic source function experiment that was designed to provide a benchmark data set for seismic source function models in hard rock geology. It was also intended to provide a threshold of detection calibration point for regional seismic monitoring. The experiment was to consist of 20 tons of a fully contained HE charge (QM-100/R) detonated in a granite test bed. The test cavity was to be located at a depth of 35 meters and excavated into a sphere by drilling an blasting, with the intent to reduce any possible edge effects that could result from the use of a cylindrical charge. Instrumentation was to be placed in the hydrodynamic region and in the transition region between the hydrodynamic and seismic region.

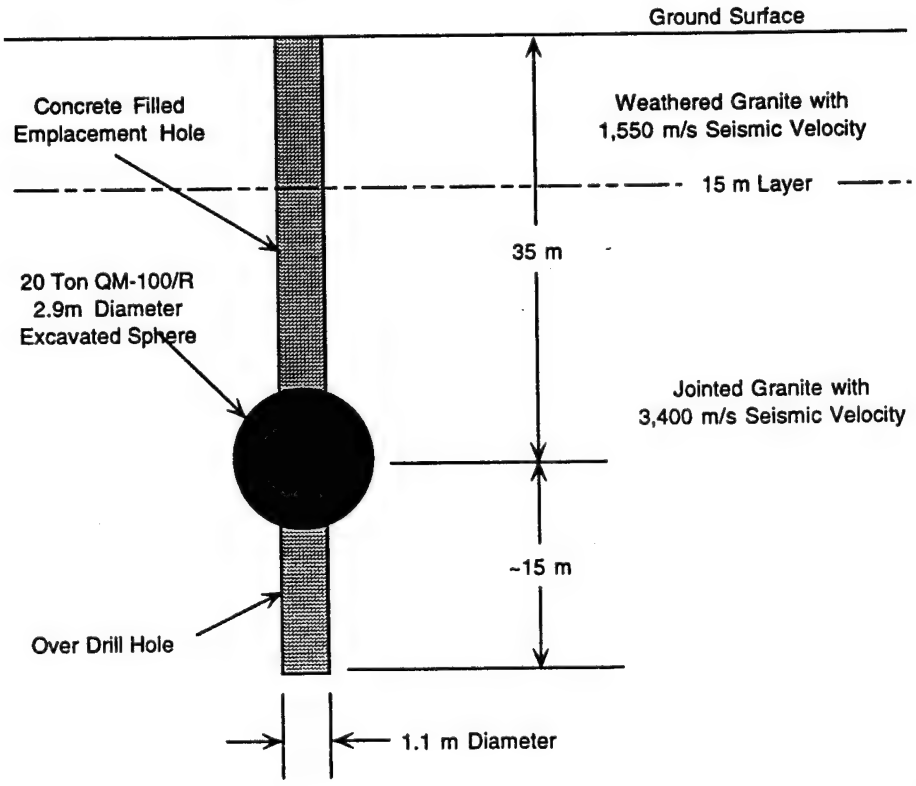


Figure 1-1. Proposed SHIST test configuration and emplacement hole profile.

The proposed SHIST test site is located in Lincoln County, New Mexico, adjacent to the Oscura mountains in the northeast portion of the White Sands Missile Range (WSMR). The site is in the Oscura Gap area, in the NW 1/4 of sec. 16, T.9 S, R.6 E, and includes the SPERRE site where WES conducted HE cratering experiments in 1979. The SHIST working point was to be situated in a region where a combination of age and tectogenetic factors have produced a granitic test bed that is jointed and weathered. The site geology was simplified in preliminary scoping calculations presented here to consist of a top layer of highly weathered granite overlaying a bed of jointed and fractured granite. Air-filled void (AFV) porosities range from 1-2% with In-situ seismic velocities ranging from 1,500 to 3,500 m/s (competent granite has a seismic velocity on the order of 5000 m/s). Since the proposed site is at the foot of the Oscura mountains, the ground surface has a slight slope to it with a potential vertical variation of 25 ft along any one gage radial. The proposed site also has known fault lines in the vicinity of the test bed, however the closest fault was considered to be sufficiently far away to be neglected in this study.

Currently, the SHIST test has been postponed, however Titan Research and Technology (TRT) had been tasked to develop preliminary material models for the site and conduct 1D and 2D finite-difference scoping calculations to serve as a starting point should the test (or other HE test requiring a hard rock) be revived in the next year or two. The intent of this study was to investigate the details of the shock wave propagation into the granite site and to determine the seismic transition point (the range at which the stress wave developed by the HE source begins to decay as an elastic wave) to assist in future gage placement. Three dimensional effects, such as the surface slope variation and ground fault lines, were neglected at this time. Should the program be reactivated in the future, these effects should be examined in closer detail.

TRT was also tasked to install the suite of CRALE codes (1D, 2D) and post-processing tools onto the DNAFC Silicon Graphics workstation. The SHIST scoping study was then to be used to verify the operation of these codes on this platform.

## 1.2 APPROACH.

The SHIST scoping study was completed as three separate tasks. Task 1: Evaluate the material properties of the SHIST site and develop simple scoping Equation of State (EOS) models for jointed granite. Due to the uncertainty in the material properties data for the SHIST site, the study was extended to include material model excursions from the prescribed SHIST lithology. Task 2: Take the granite models developed in Task 1 and use them in a series of 1-D finite-difference calculations (using the CRALE 1D code) to investigate the effect of changes to material properties on the free-field environment generated in the testbed. The intent of these calculations was to evaluate the potential effects material property variations may have on the seismic transition point. Task 3: Take the "best-estimate" material properties for the site and use them in a 2-D finite-difference calculation (using the CRALE 2D code) to investigate the details of the interaction of the shock with the surrounding stemming materials and granite. An assessment of the degree of sphericity of the ground shock could also be made by comparing the calculated 2-D results from Task 3 with the 1-D calculations of Task 2.

This report details the modeling and calculational efforts performed by TRT in support of the SHIST test. The material modeling is discussed Section 2, the 1-D free field environment calculations in Section 3, and the 2-D SHIST scoping calculations in Section 4. Appendices are included to document the specifics of the material models used in this study.

Though the proposed SHIST experiment is fully coupled, the same analytical approach reported here could be used to characterize the wave in the seismic region for decoupled sources. Both CRALE 1D and 2D codes could be used to calculate the shock wave resulting from an explosive source placed inside an open cavity. Surface effects and reflections from layering could also be examined in either 1D or 2D geometries.

## SECTION 2

## MATERIAL MODELS FOR GRANITE AND CONCRETE (TASK 1)

### 2.1 GENERIC GRANITE MODEL DESCRIPTIONS.

Prior to the suspension of the SHIST program, TRT developed a generic 1% (AFV) weak granite equation of state (EOS) which was considered to be the best one to use for SHIST p[1]re-shot calculations until additional experimental data became available [1]. This model was developed using an older version of the SHEL EOS that is no longer compatible with the current version of the CRALE code (CRALEPL3). Therefore, under the current effort, new granite material models with characteristics similar to those reported in Reference 1 were developed using the current version of the SHEL EOS.

The generic granite model discussed in Reference 1 (material model GRAN3A, which in this report will be referred to as GENERIC1) was shown to produce a reasonable overall match to data obtained from underground unclear tests at the Nevada Test Site (NTS) [2]. The model, having a seismic velocity of 4,500 m/s, is one representative of weak, jointed granitic rock, and produces waveforms which agree well with those measured in the HARDHAT test [2], peaks and scaled nuclear cavity radii consistent with the U.S. Granite experience at NTS ($R_c$ = 11.5 m/kt$^{1/3}$). The generic model incorporates 1% air filled porosity to simulate the effect of natural joints and fractures in otherwise competent Granite. The failure surface parameter for GENERIC1 is a simple linear Drucker-Prager / Von-Mises yield surface of the form:

---

[1] The current SHEL EOS formulation is discussed in Appendix A.

$$Y = \max\left\{\begin{array}{l}\dfrac{P}{P_y} + Y_o \\ Y_{vm}\end{array}\right. \qquad (2.1)$$

where

$Y_{vm}$ = the limiting yield strength

$Y_o$ = the yield strength at zero pressure (cohesion)

$P$ = the current pressure, and

$1/P_y$ = the Drucker-Prager slope.

To maintain compatibility with the current CRALE code, two new generic granite models (material models GRAN1C and GRAN1E, which in this report will be referred to as GENERIC2 and GENERIC3) were developed using the current EOS model to match the characteristics of the earlier model (GENERIC1). Both of the new models have 1% air filled porosity and the identical maximum Von-Mises yield surface as GENERIC1, however two different yield surface functions were used. The GENERIC2 uses the same linear Drucker-Prager yield surface function as GENERIC1 (Equation 2.1). GENERIC3 on the other hand uses an exponential yield surface function of the form:

$$Y = Y_{vm} - (Y_{vm} - Y_o)e^{-P/P_y} \qquad (2.2)$$

where

$Y_{vm}$ = the limiting yield strength

$Y_o$ = the yield strength at zero pressure (cohesion)

$P$ = the current pressure, and

$P_y$ = the pressure at which the yield function ~$(2/3\ Y_m + 1/3\ Y_o)$.

The exponential form of the yield surface eliminates the "non-physical" sharp corner that appears in Equation 2.1 at the intersection of the Drucker-Prager slope with the Von-Mises limit. Both formulations are available in the current CRALE code.

The bulk properties and failure surface parameters for the generic granite models in Table 2-1 (specific CRALE EOS parameters for GENERIC2 and GENERIC3 can be found in Appendix A and Appendix B).

Table 2-1. Properties of the generic models for weak granite with 1% AFV.

| Model | Density g/cc | Grain density g/cc | %AFV | Poisson's ratio | Cohesion* (bar) | Slope 1/Py | Exponential Constant 1/Py | VonMises* limit (kbar) |
|---|---|---|---|---|---|---|---|---|
| GENERIC1 (GRAN3A) | 2.643 | 2.67 | 1.0 | 0.25 | 100 | 0.3 | N/A | 12.5 |
| GENERIC2 (GRAN1C) | 2.624 | 2.65 | 1.0 | 0.25 | 100 | 0.3 | N/A | 12.5 |
| GENERIC3 (GRAN1E) | 2.624 | 2.65 | 1.0 | 0.25 | 100 | N/A | 30.0 | 12.5 |

* $\sqrt{J_2'}$

Both GENERIC2 and GENERIC3 have a grain density of 2.65 g/cc (lower than that of GENERIC1) to be more consistent with the SHIST material properties data.

The uniaxial stress-strain response of materials GENERIC1, GENERIC2, and GENERIC3 are shown in Figures 2-1a,b and 2-2a,b,c below. The Hugoniots for the three models are shown in Figure 2-3 along with the currently available granite shock data.

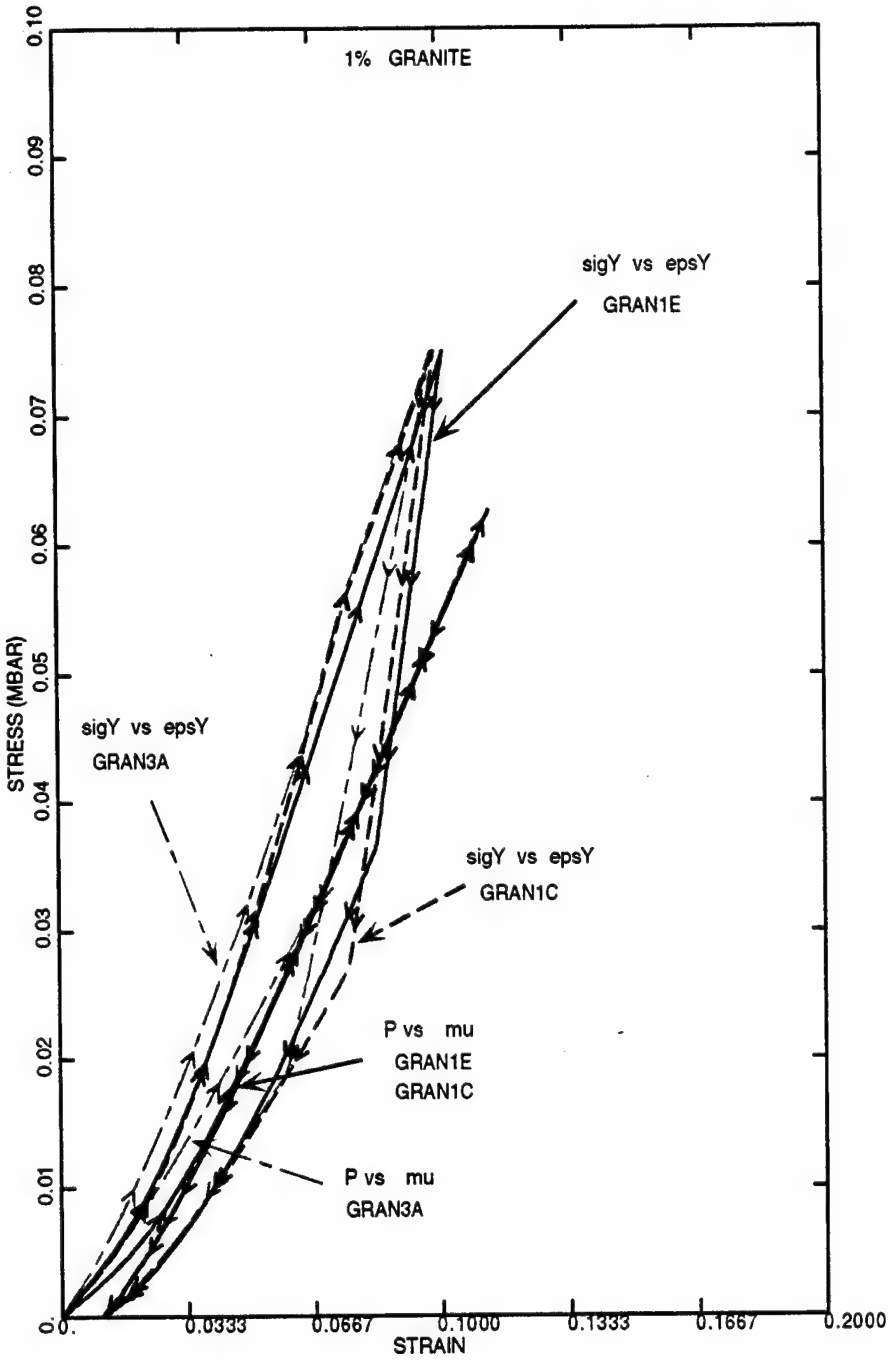


(a) stress-strain

Figure 2-1. Uniaxial stress response of GENERIC1 (GRAN3A), GENERIC2 (GRAN1C), and GENERIC3 (GRAN1E) to 80 kbar.

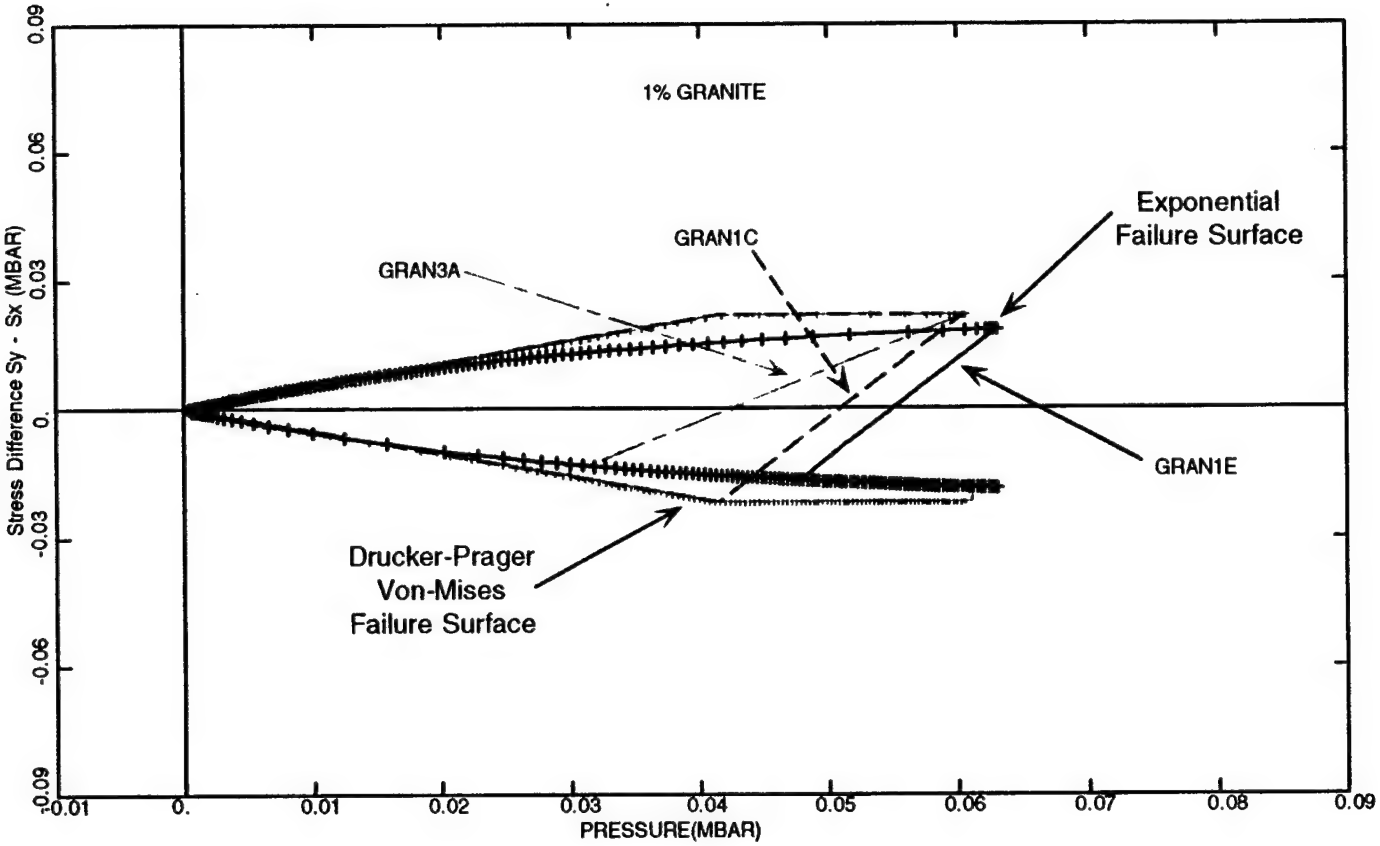


(b) stress difference

Figure 2-1. Uniaxial stress response from uniaxial loading of GENERIC1 (GRAN3A), GENERIC2 (GRAN1C), and GENERIC3 (GRAN1E) to 80 kbar. (Continued)

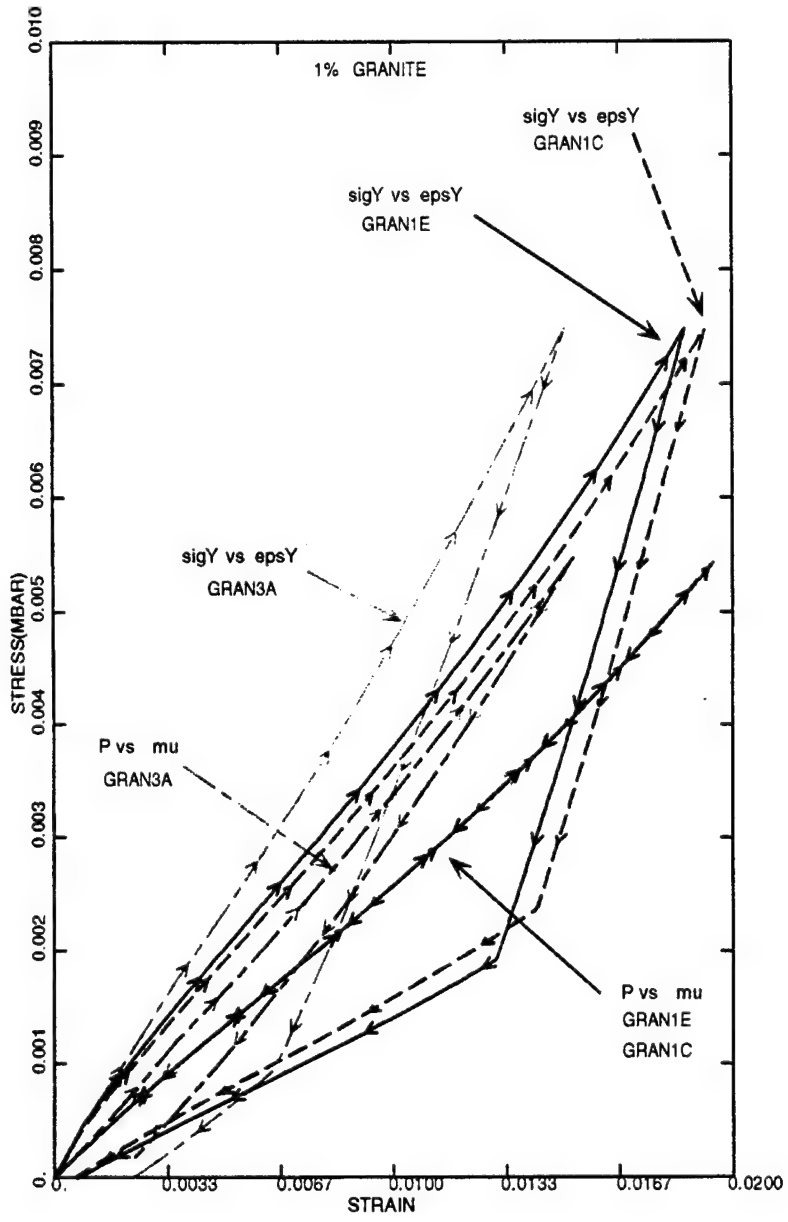


(a) stress-strain

Figure 2-2. Uniaxial stress response of GENERIC1 (GRAN3A), GENERIC2 (GRAN1C), and GENERIC3 (GRAN1E) to 8 kbar.

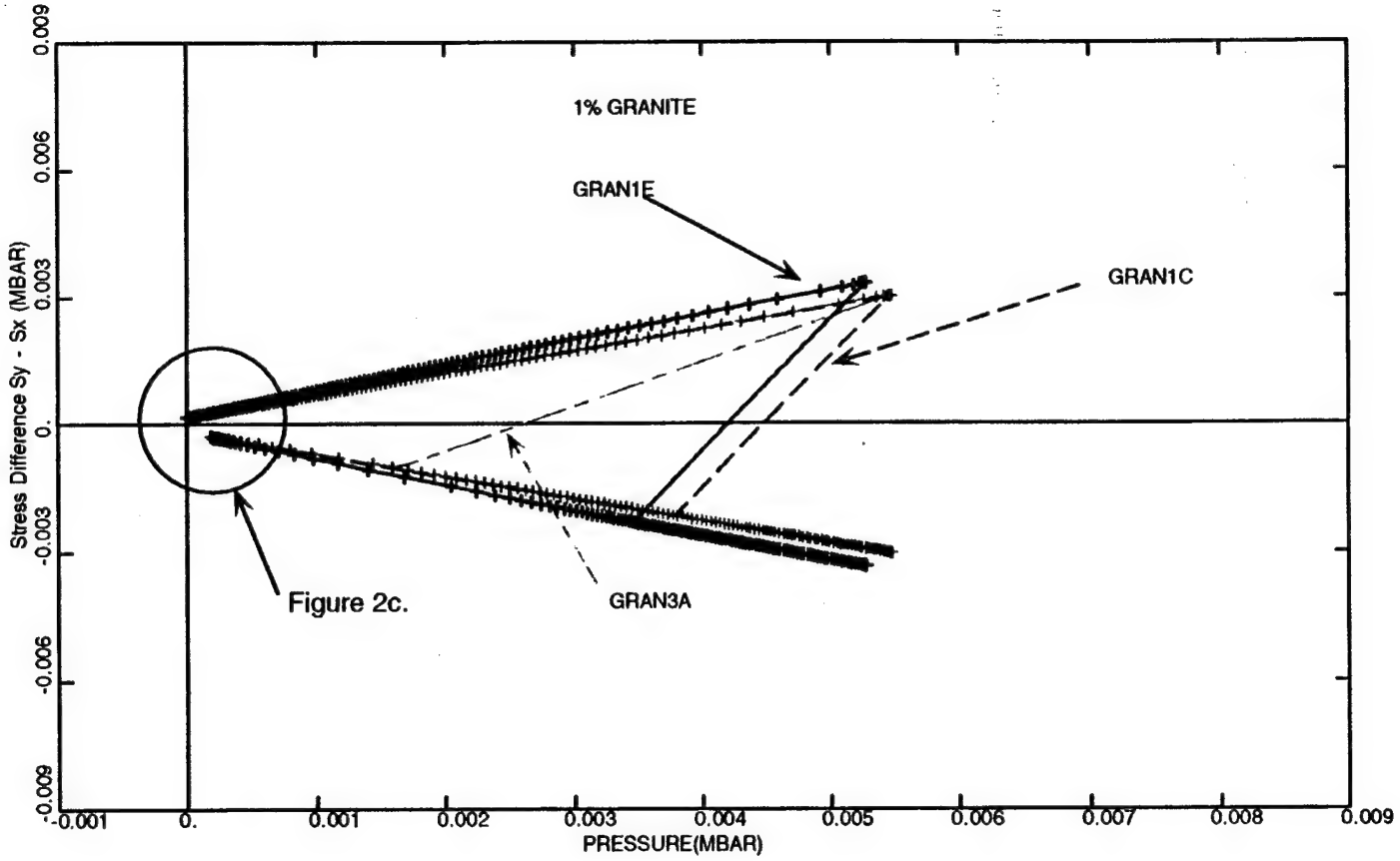


(b) stress-strain

Figure 2-2. Uniaxial stress response from uniaxial loading of GENERIC1 (GRAN3A), GENERIC2 (GRAN1C), and GENERIC3 (GRAN1E) to 80 kbar. (Continued)

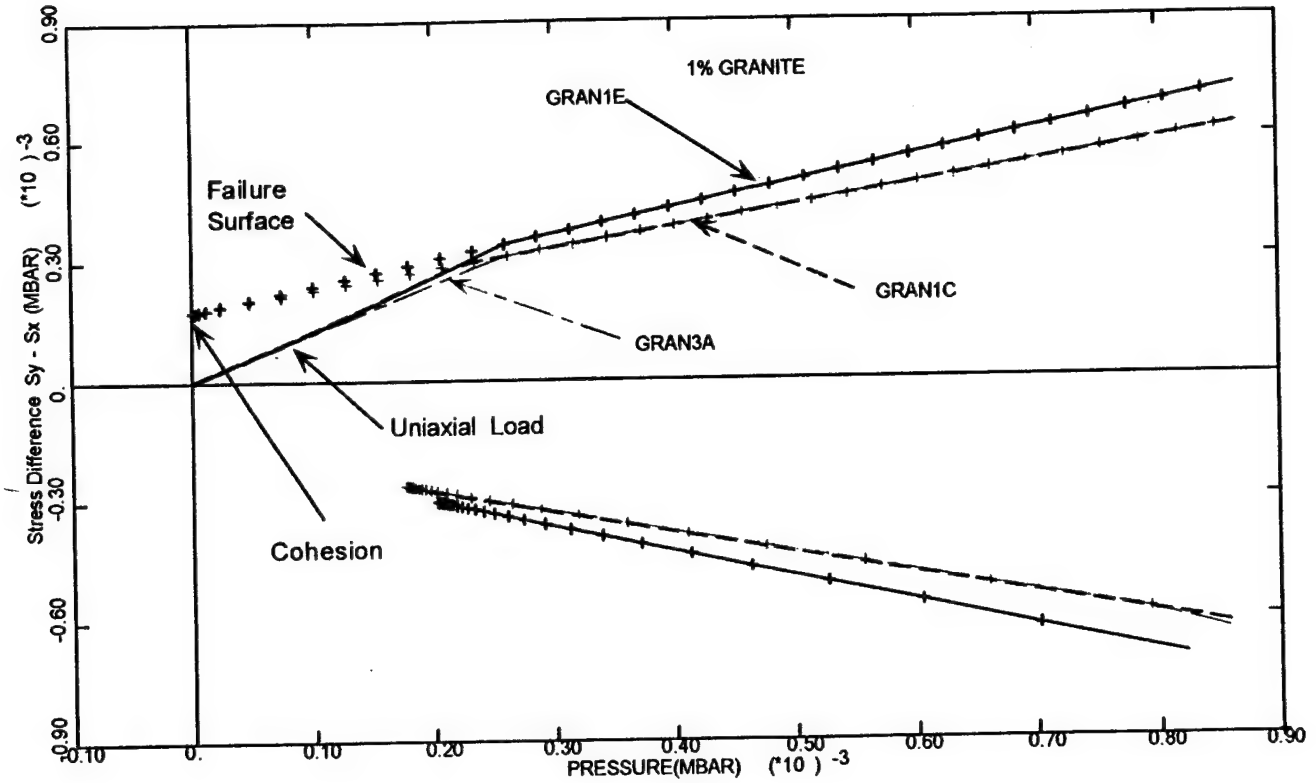


(c) Stress-Difference

Figure 2-2. Uniaxial Stress response from uniaxial loading of GENERIC1 (GRAN3A), GENERIC2 (GRAN1C), and GENERIC3 (GRAN1E). (Continued)

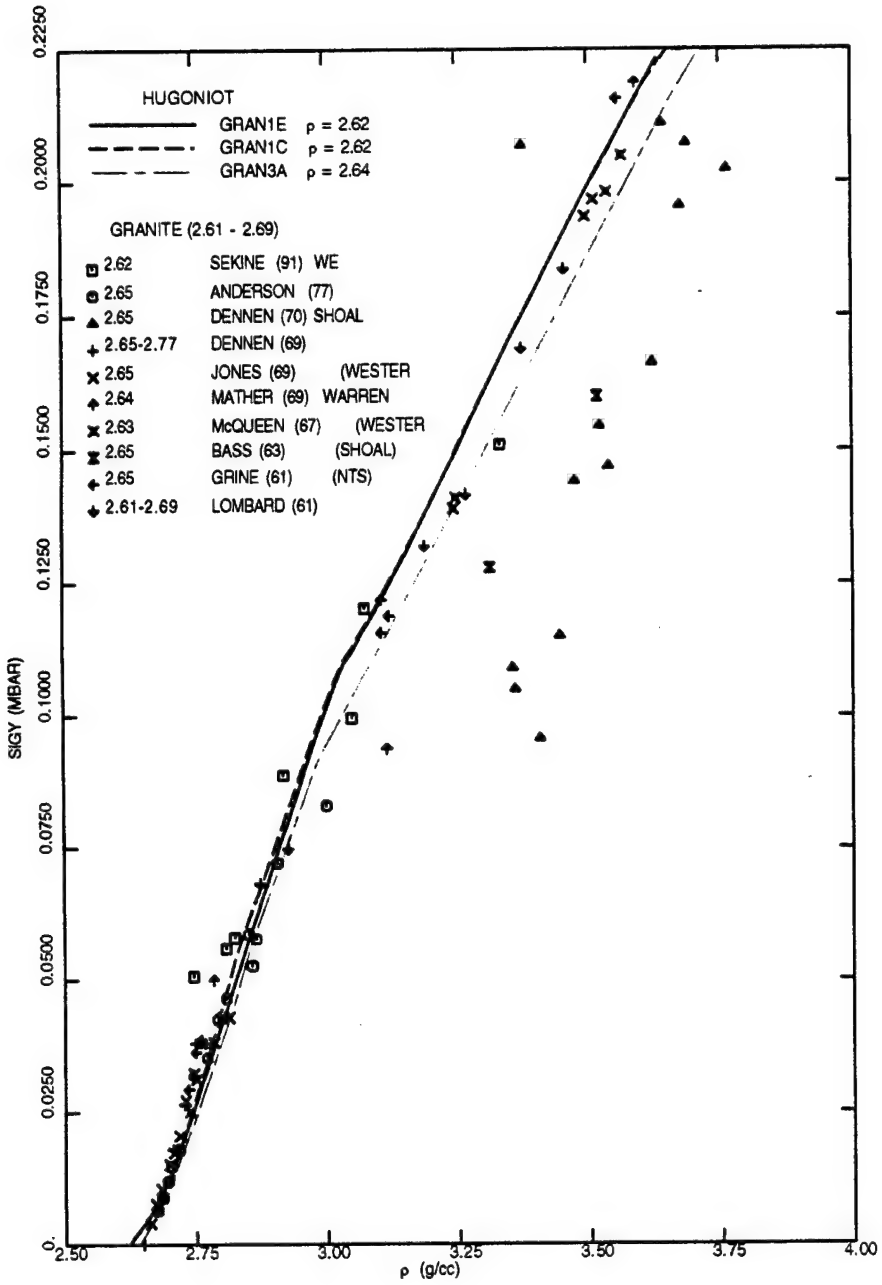


Figure 2-3. Hugoniots of GENERIC1 (GRAN3A), GENERIC2 (GRAN1C), and GENERIC3 (GRAN1E) and representative experimental data points to 225 kbar.

## 2.2 GENERIC GRANITE MODEL CHECKOUT AGAINST EXISTING NUCLEAR DATA.

The peak velocity vs. range obtained from a fully contained 1 kt nuclear calculation employing the model GENERIC1 (GRAN3A) and the two new models GENERIC2 (GRAN1C) and GENERIC3 (GRAN1E) are compared to available granite test data in Figure 2-4.

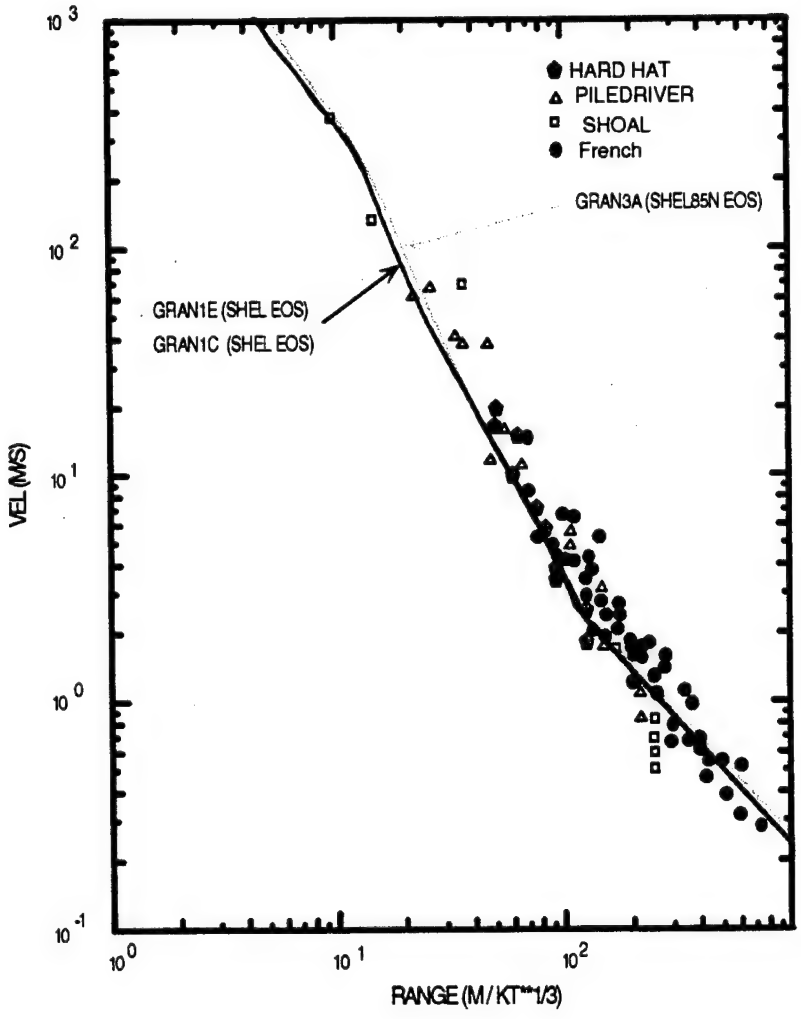


Figure 2-4. Calculated peak velocity vs. range for GENERIC1 (GRAN3A), GENERIC2 (GRAN1C), and GENERIC3 (GRAN1E) models compared to granite data base (Nuclear source).

As can be seen, both new generic granite models give virtually the same results as the older GENERIC1 model discussed in Reference 1. Therefore these models, both with a seismic velocity of 4,500 m/s, will be used as material model excursions for the current SHIST scoping study.

## 2.3 GRANITE MATERIAL MODELS DEVELOPED SPECIFICALLY FOR THE SHIST SITE.

The SHIST site is situated on and adjacent to the pediment along the western base of the southern Oscura Mountains. The Oscura Mountains are an east-dipping north-south structural block with relatively gentle slopes on the east and a steep precipitous scarp along the west. The scarp is the result of normal faulting, an expression of which has been observed to bisect the SHIST site. For this scoping study, the fault was considered to be far enough away from the test bed so that it could be ignored at this time.

The site profile in the vicinity of the test bed is one of highly weathered and jointed Precambrian granite. Small sample laboratory data reports indicate that the total porosities range from 1.2 to 1.9%, with seismic velocities ranging from 4,300 to 5,300 m/s [4]. However, these small scale properties are not considered representative of the in-situ characteristics of the SHIST test bed since geophone data suggest that the SHIST site has seismic velocities significantly lower than the lab data suggests.

The GENERIC models discussed above have seismic velocities consistent with small scale tests (4,500 m/s) and can be considered material model excursions for the SHIST site The actual SHIST in-situ seismic velocities range from 1,200 m/s in the surface layers to 4,000 m/s in the deeper layers. Through previous discussions with Dr. Robert Reinke DNA/FCTT, for this scoping study we decided to represent the SHIST site with two distinct layers. The top 15 meters were modeled with a seismic velocity of 1,550 m/s below 15 meters was a layer of material with a seismic velocity of 3,400 m/s. Since there is no experimental data to indicate the stress level for joint "lock up", simple models were developed to approximate the behavior of the jointed material.

Previous work on jointed material [5] has indicated that the joints will "lock up" anywhere from 0.5 to 1 kbar after which the material behaves as though jointing did not exist. Since we don't have any experimental data for jointing characteristics of the SHIST site, it was assumed that the joints would lock up at approximately 0.5 kbar. Two new models with seismic velocities of 3,400 m/s (material model GRAN5B, which in this report will be referred to as SHIST2) and 1,500 m/s (material model GRAN4B, which in this report will be referred to as SHIST1) were developed using the material model GENERIC3 as a starting point. The initial wave speeds were lowered to the appropriate values and the porosity increased so that stress-strain response of the jointed material models would intersect with the baseline model at 0.5 kbar, Figure 2-5.

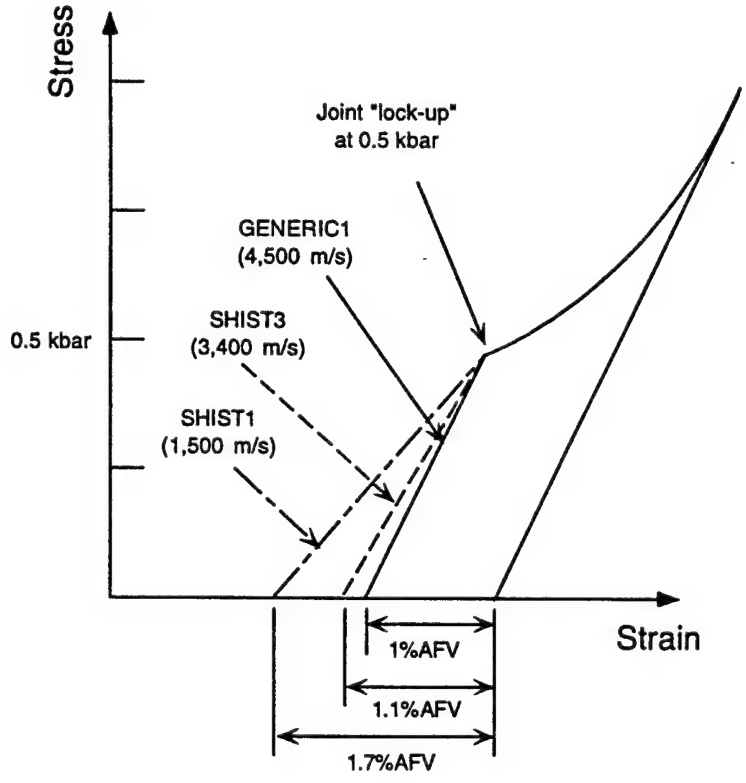


Figure 2-5. Schematic representation of elastic stress-strain assumption used in the development of SHIST1 and SHIST2 jointed granite material models.

Since it is assumed that the material is elastic for stresses below 0.5 kbar, a closed form solution for this intersection is possible. The constrained modulus, M, can be calculated from the seismic velocity, c, and the initial density, $\rho_o$, by the relationship

$$M = \rho_o c^2 \tag{2.3}$$

With a Poisson's ratio of 0.25, the bulk modulus, K, can be calculated as

$$K = \frac{M(1+\upsilon)}{3(1-\upsilon)} = \frac{M}{1.8} = \frac{\rho_o c^2}{1.8} \tag{2.4}$$

Also, for uniaxial strain, the stress, $\sigma$, can be calculated as a function of compression, $\mu$, or density, $\rho$, by the relationship

$$\sigma = M\mu = 1.8K\frac{\rho - \rho_o}{\rho_o} \tag{2.5}$$

Using the model GENERIC3 as the baseline "NTS like" jointed material (seismic velocity of 4,500 m/s and bulk modulus of 0.3 Mbar) the density at which the granite reaches 0.5 kbar in uniaxial strain is 2.626 (or 0.09% strain). Assuming that the SHIST jointed granite will lock up at this same stress and density, that it's stress strain behavior converges with model GENERIC3, the initial density of model SHIST2 (seismic velocity of 3,400 m/s and bulk modulus of 0.169 Mbar) is 2.621 g/cc and the initial density of model SHIST1 (seismic velocity of 1,550 m/s and bulk modulus of 0.035 Mbar) is 2.605 g/cc.

The SHIST material models developed by this elastic approximation are intended only for use in the current SHIST scoping calculation series. The in-situ seismic velocities used here were obtained from low stress geophone data, and there are large uncertainties in the stress level at which the joints close. If the SHIST program is reactivated in the future, it is recommended that additional bulk material properties data be obtained and laboratory tests conducted at various loading rates for use in the development of more representative material models.

The properties of material models SHIST1, SHIST2 and GENERIC3 are summarized in Table 2-2 below. For reference purposes, the SHEL equation of sate input parameters have been included in Appendix A and the CRALE input decks in Appendix B.

Table 2-2. Properties of granite material models SHIST1, SHIST2, and GENERIC3.

| Model | Density g/cc | Grain density g/cc | %AFV | Initial K Mbar | Seismic Velocity (m/s) | SHIST Site Layer |
|---|---|---|---|---|---|---|
| GENERIC1 (GRAN1E) | 2.624 | 2.65 | 1.0 | 0.3 | 4,500 | ------ |
| SHIST2 (GRAN5B) | 2.621 | 2.65 | 1.1 | 0.169 | 3,400 | > 15 m |
| SHIST1 (GRAN4B) | 2.605 | 2.65 | 1.7 | 0.035 | 1,550 | 0 - 15 m |

* $\sqrt{J_2'}$

Uniaxial stress-strain response curves for SHIST1 (GRAN4B) and SHIST2 (GRAN5B) are shown in Figures 2-6a,b and 2-7a,b. In each of these figures, GENERIC3 (GRAN1E) is shown with the equivalent strain offset used in the calculations above to estimate joint lockup at 0.5 kbar. As can be seen, the highly jointed SHIST materials come close to approximating the NTS GENERIC3 granite response for stresses above 0.5 kbar. Since these "jointed" models were intended to be used for first order scoping calculations, the differences observed above 0.5 kbar were not considered critical at this time. If future work is warranted, they will be modified so that a better match with the generic model occurs after joint lockup. It can be seen in Figure 2-7 that the SHIST1 (GRAN4B) model does not converge with the GENERIC3 model until stresses exceed 1.5 kbar. This is due to the differences between the exponential nature of the SHEL EOS and the linear elastic approximations made in the development of GRAN4B. These differences are less apparent in SHIST2 (GRAN5B, 1.1% AFV) since it is less hysteretic than SHIST1 (GRAN4B, 1.7% AFV).

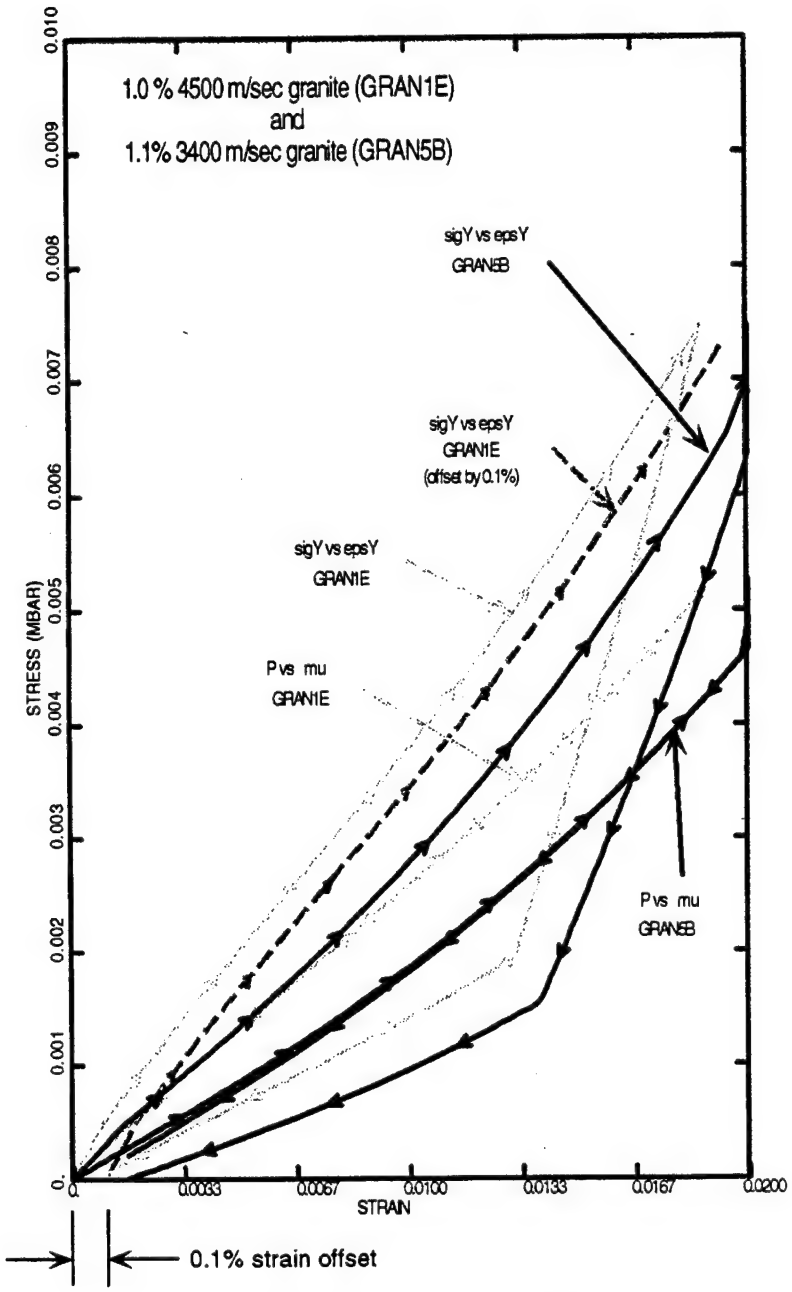


(a) stress-strain to 8 kbar

Figure 2-6. Uniaxial stress response of SHIST2 (GRAN5B) and GENERIC3 (GRAN1E). GENERIC3 is also shown with a 0.1% strain offset.

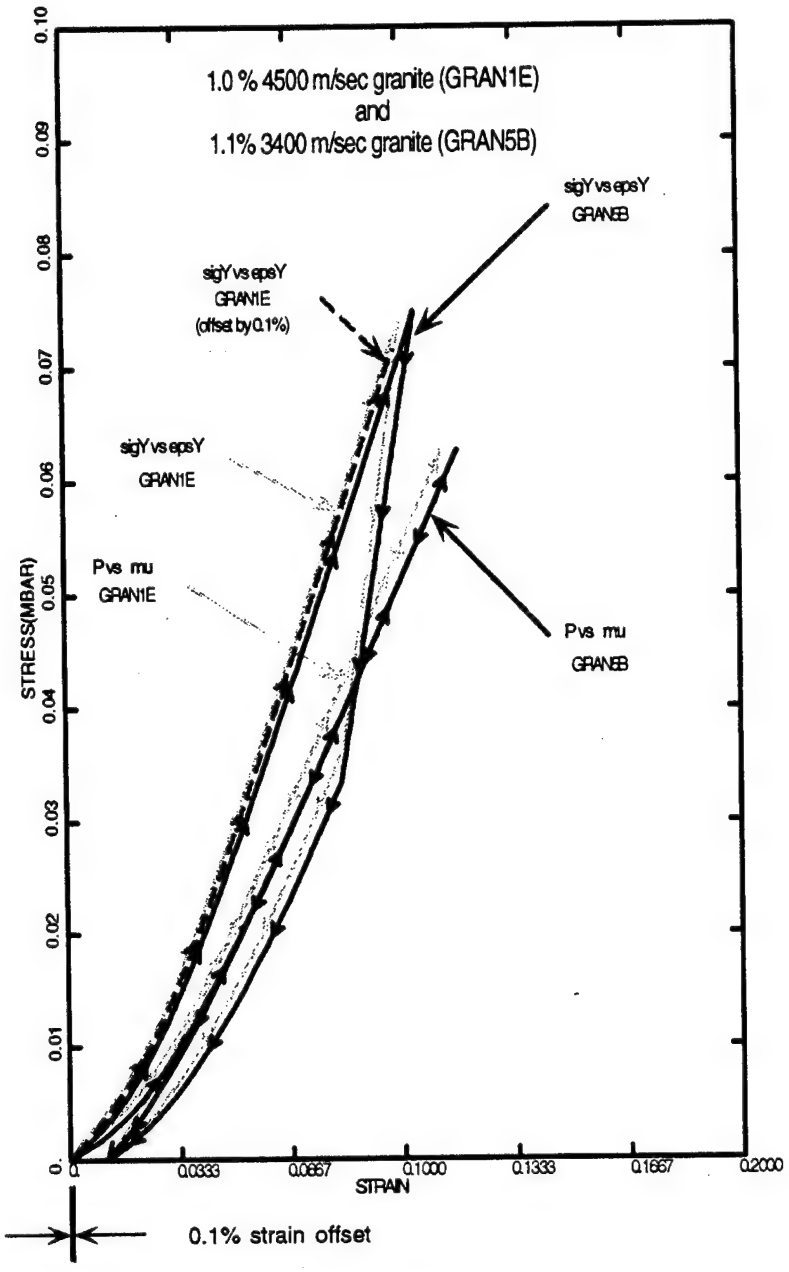


(b) stress-strain to 80 kbar

Figure 2-6. Uniaxial stress response of SHIST2 (GRAN5B) and GENERIC3 (GRAN1E). GENERIC3 is also shown with a 0.1% strain offset. (Continued)

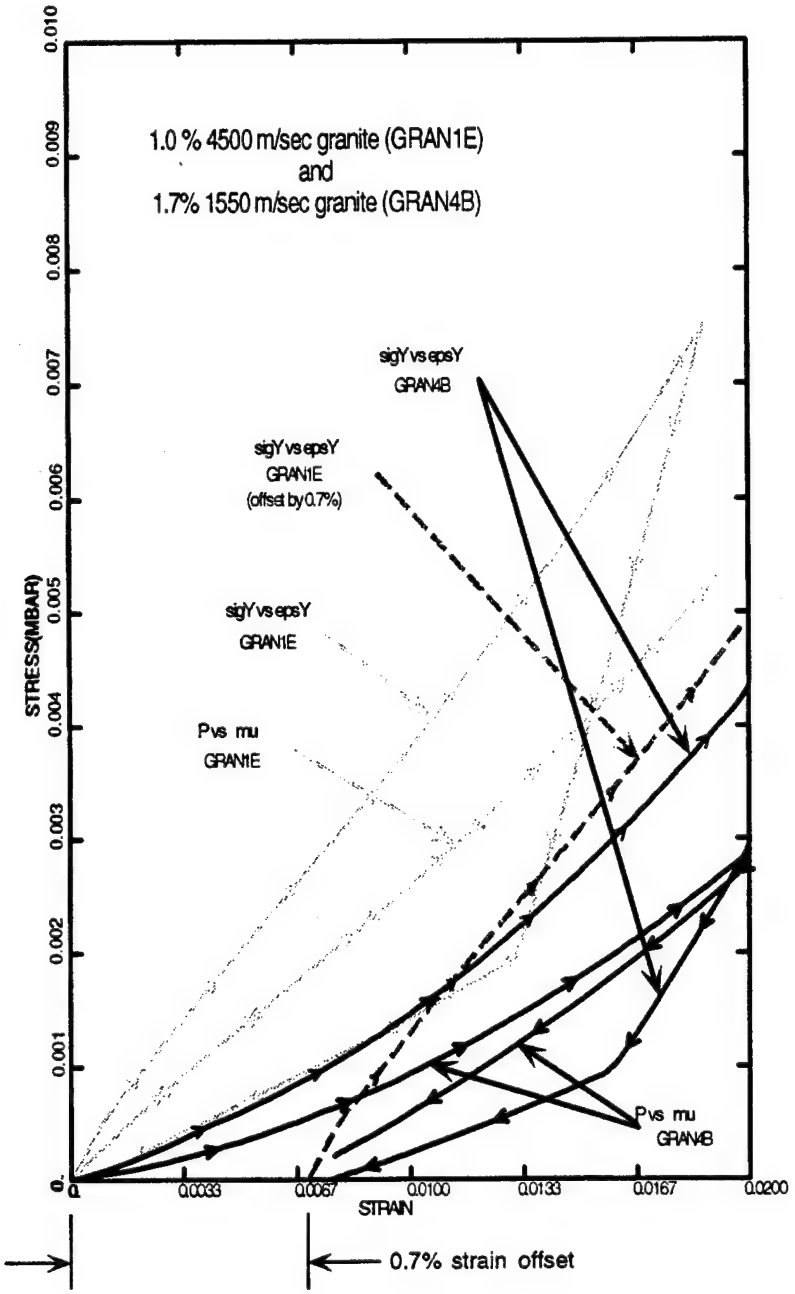


(a) stress-strain to 8 kbar

Figure 2-7. Uniaxial stress response of SHIST1 (GRAN4B) and GENERIC3 (GRAN1E). GENERIC3 is also shown with a 0.7% strain offset.

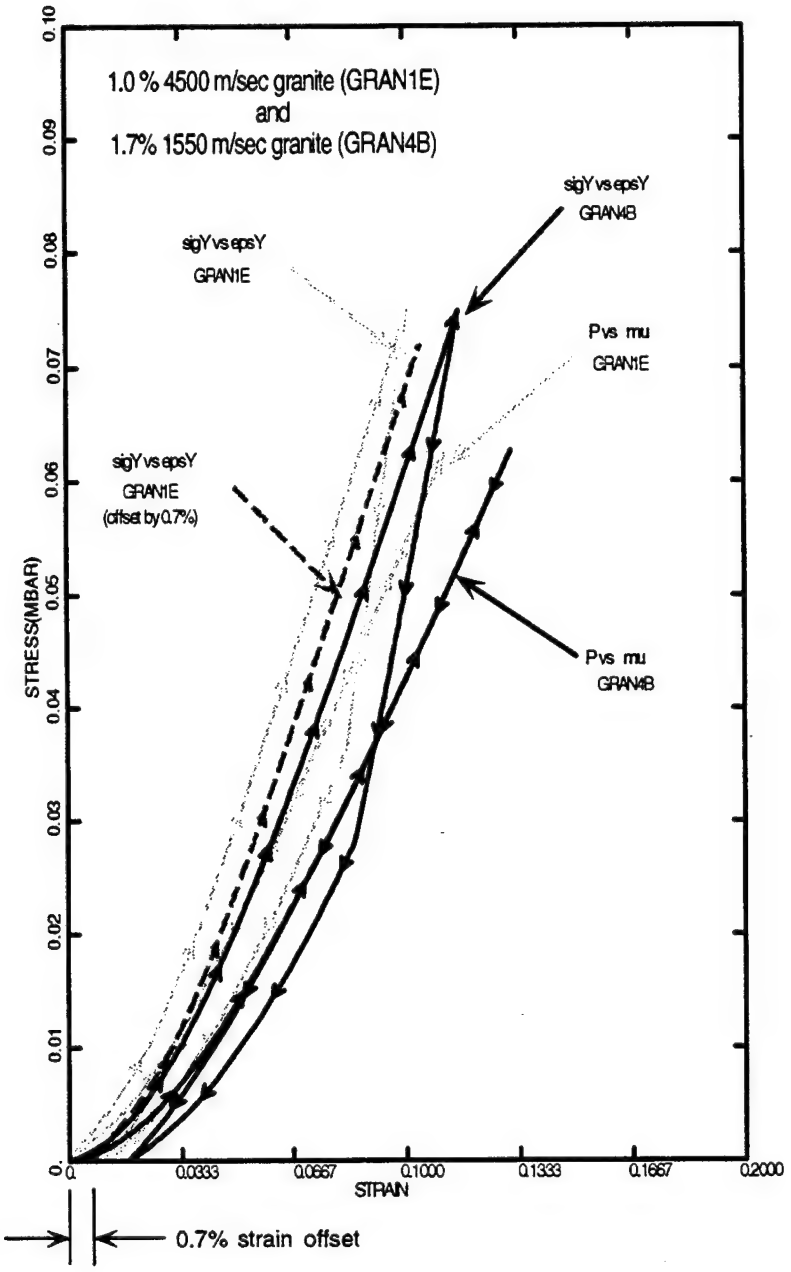


(b) stress-strain to 80 kbar

Figure 2-7. Uniaxial stress response of SHIST1 (GRAN4B) and GENERIC3(GRAN1E). GENERIC3 is also shown with a 0.7% strain offset. (Continued)

## 2.4 CONCRETE STEMMING MODEL DESCRIPTION.

The stemming material used in this study is HJC7 concrete modeled with the MCIST material model. This material model (CON5K4) has been used successfully in the past (HUSKY JAGUAR and MIGHTY NORTH) and was used here unchanged. The uniaxial stress-strain response of CON5K4 is compared to the SHIST2 (GRAN5B) granite model in Figure 2-8. It can be seen that the concrete model is similar to the SHIST model to a stress level of approximately 1 kbar, after which it is much more hysteretic. Therefore, for stresses above 1 kbar, the shock wave in the granite would be expected to outrun the shock in the concrete filled emplacement hole. This effect should be localized to the vicinity of the emplacement hole and would not be expected to influence the free field environment at the SHIST experimental gage locations. For reference, the CRALE input deck for the CON5K4 concrete model has been included in Appendix B.

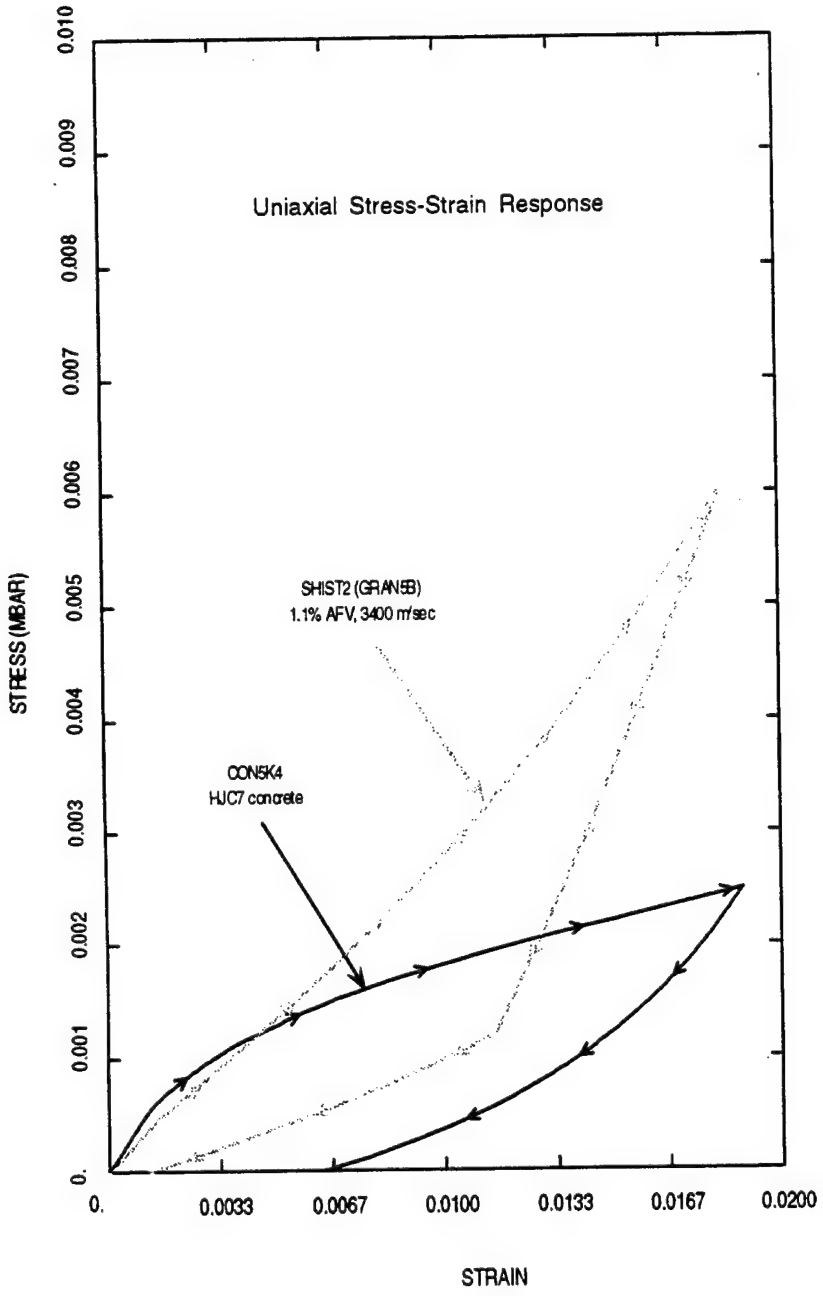


Figure 2-8. Uniaxial stress-strain response of material models CON5K4 concrete and SHIST2 (GRAN5B) jointed granite.

## SECTION 3

## PRELIMINARY FREE-FIELD ENVIRONMENT 1D CALCULATIONS FOR A 20-TON CONTAINED CHARGE

## (TASK 2)

### 3.1 1D CALCULATION SETUP.

The proposed SHIST experiment was designed specifically to generate a spherical shock wave into the free-field environment. The fully contained 20-ton QM-100/R high explosive charge was to be placed in a spherical cavity to eliminate any edge effects that may occur from a cylindrical charge configuration. The experiment therefore lends itself well to the use of 1D code calculations for examination of the ground shock phenomenology.

To evaluate the shock propagation from the charge, a number of 1-D CRALE calculations were performed. A JWL detonation model for QM-100/R was used in all the 1D (and 2D) calculations. This model was developed by LLNL, having an initial density of 1.509 g/cc and Chapman-Jouget detonation pressure of 200 kbar. For reference, the input deck for the QM-100/R HE EOS used in the CRALE code has been included in Appendix B.

The CRALE 1-D calculations were run with an average zone size of 20 cm in the granite and with 20 cells in the HE sphere (radius of 1.42 m). The CRALE HE burn model was used to create the initial shock wave into the surrounding media. Two series of calculations were run, one using the SHIST1 and SHIST2 material models for jointed granite described in Section 2, and a second using the GENERIC2 and GENERIC3 granite material models to evaluate potential perturbations due to material model uncertainties.

## 3.2 1D CALCULATIONS USING SHIST1 AND SHIST2 JOINTED GRANITE MATERIAL MODELS.

Two 1D calculations were run with the SHIST1 (GRAN4B, 1,550 m/s, 1.7% AFV) and SHIST2 (GRAN5B, 3,400 m/s, 1.1% AFV) "jointed" granite material models described in Section 2.3 above. These calculations were run with an average zone size of 20 cm in the granite and with 20 cells in the QM-100/R HE sphere (radius of 1.42 m). Figures 3-1 through 3-3 show the peak stress, velocity, and displacement vs. range attenuation curves calculated for the two SHIST material models. The calculated stress, velocity and displacement waveforms for SHIST1 and SHIST2 are plotted at ranges between 2 and 100 meters in Figures 3-4 through 3-6.

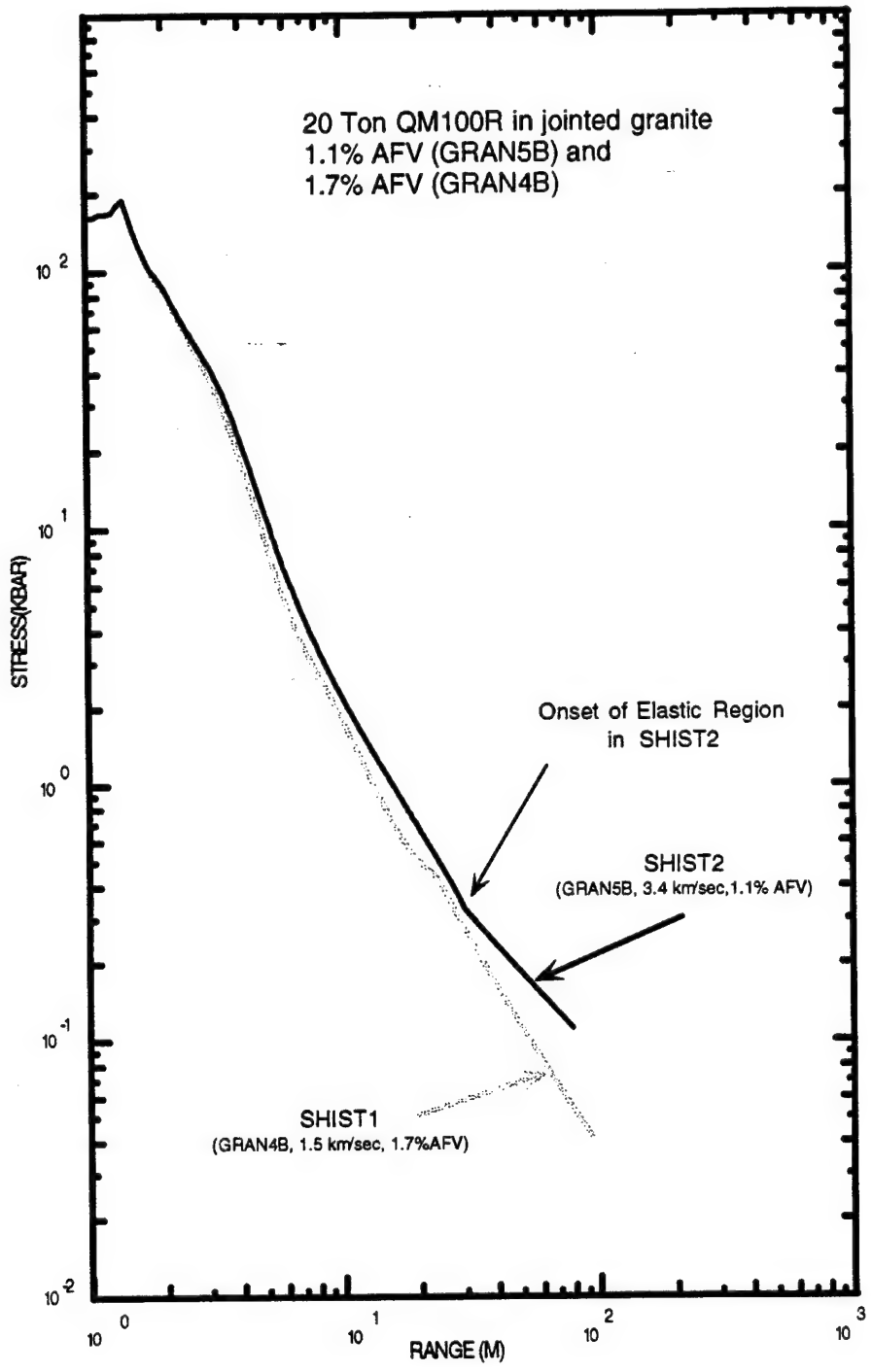


Figure 3-1. Calculated 1D peak stress vs. range for a 20-ton QM-100/R charge in SHIST1 (GRAN4B, 1,550 m/s, 1.7% AFV and SHIST2 (GRAN5B, 3,400 m/s, 1.1% AFV) jointed granite.

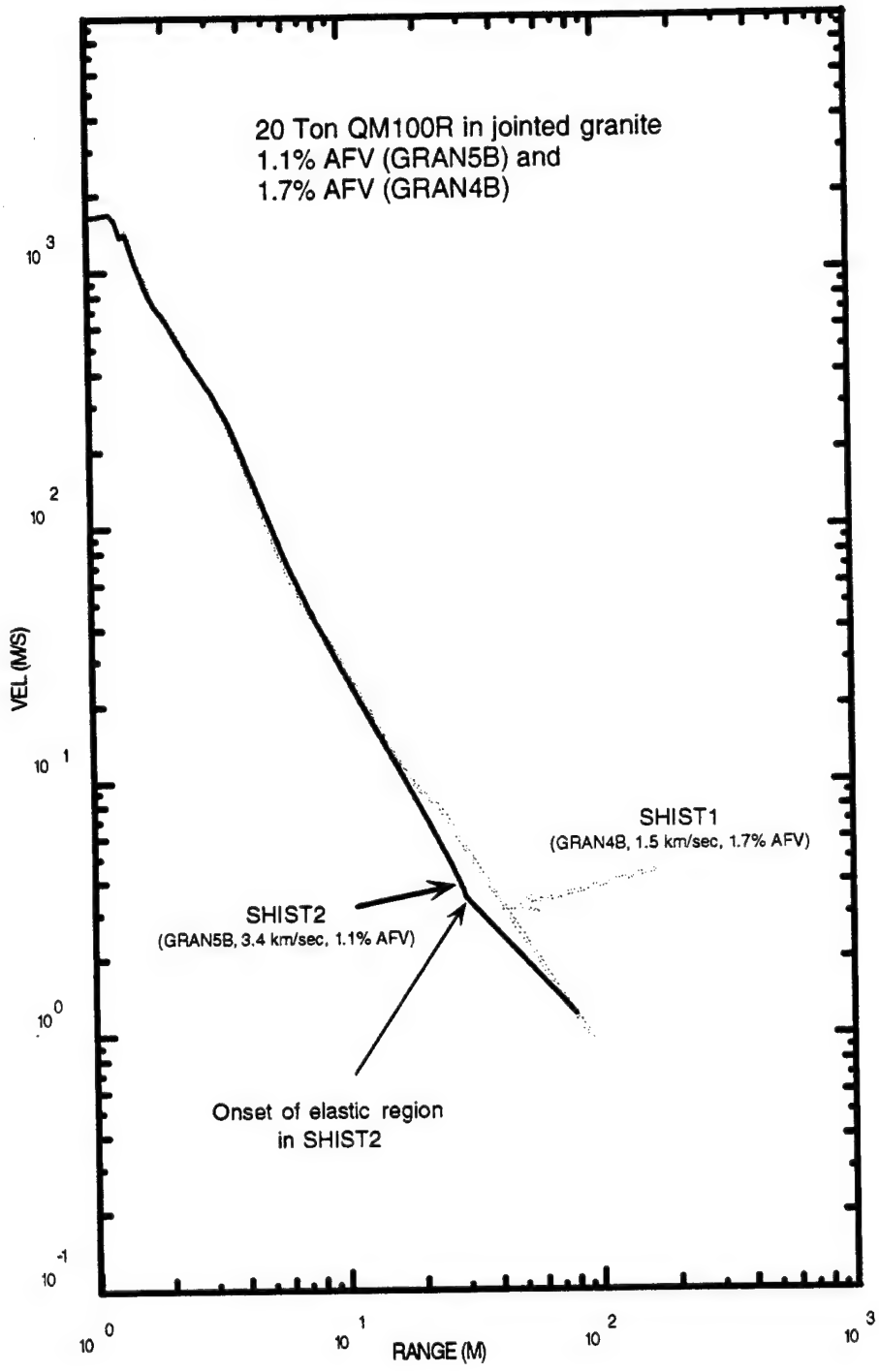


Figure 3-2. Calculated 1D peak velocity vs. range for a 20-ton QM-100/R charge in SHIST1 (GRAN4B, 1,550 m/s, 1.7% AFV and SHIST2 (GRAN5B, 3,400 m/s, 1.1% AFV) jointed granite.

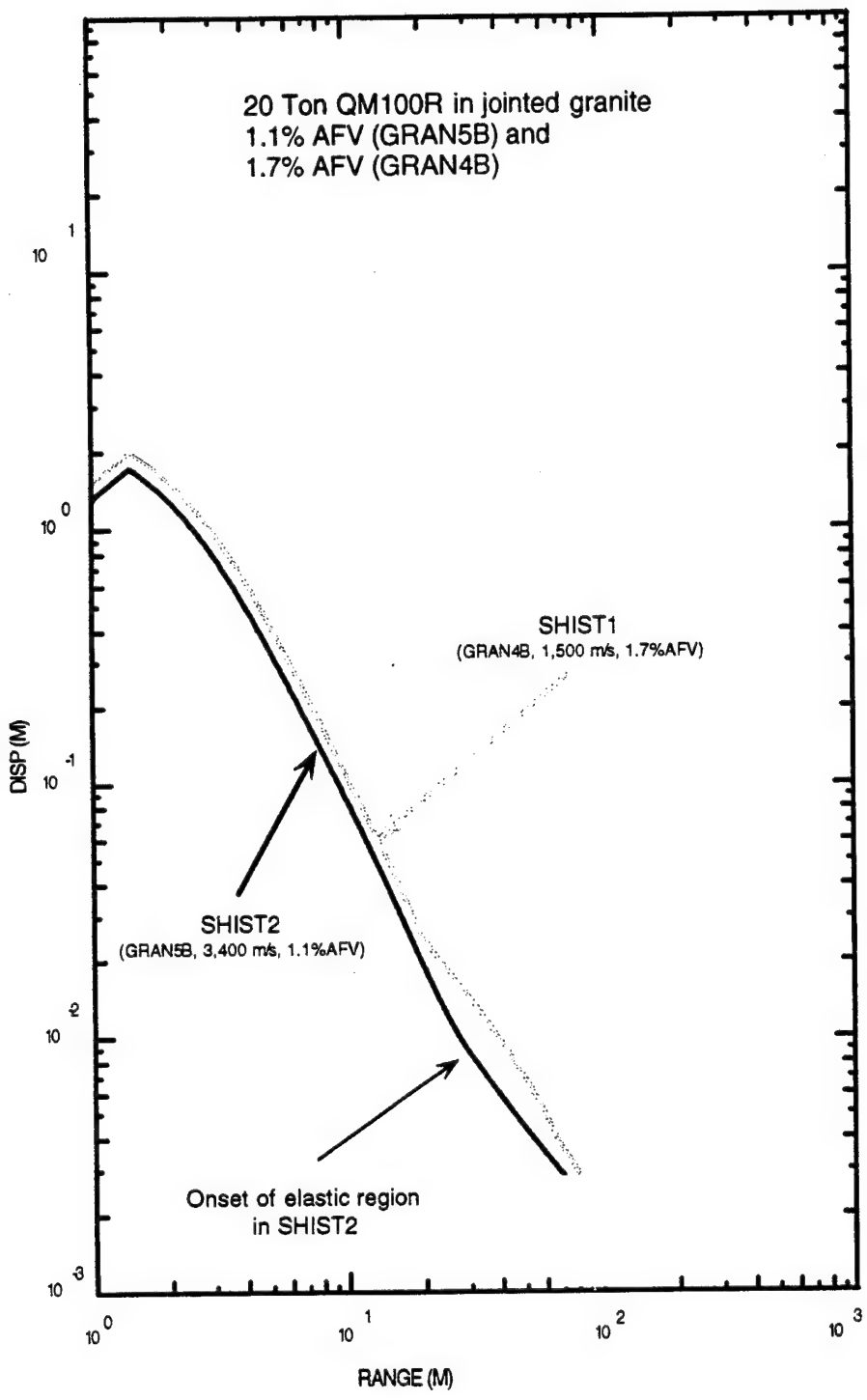


Figure 3-3. Calculated 1D peak displacement vs. range for a 20-ton QM-100/R charge in SHIST1 (GRAN4B, 1,550 m/s, 1.7% AFV and SHIST2 (GRAN5B, 3,400 m/s, 1.1% AFV) jointed granite.

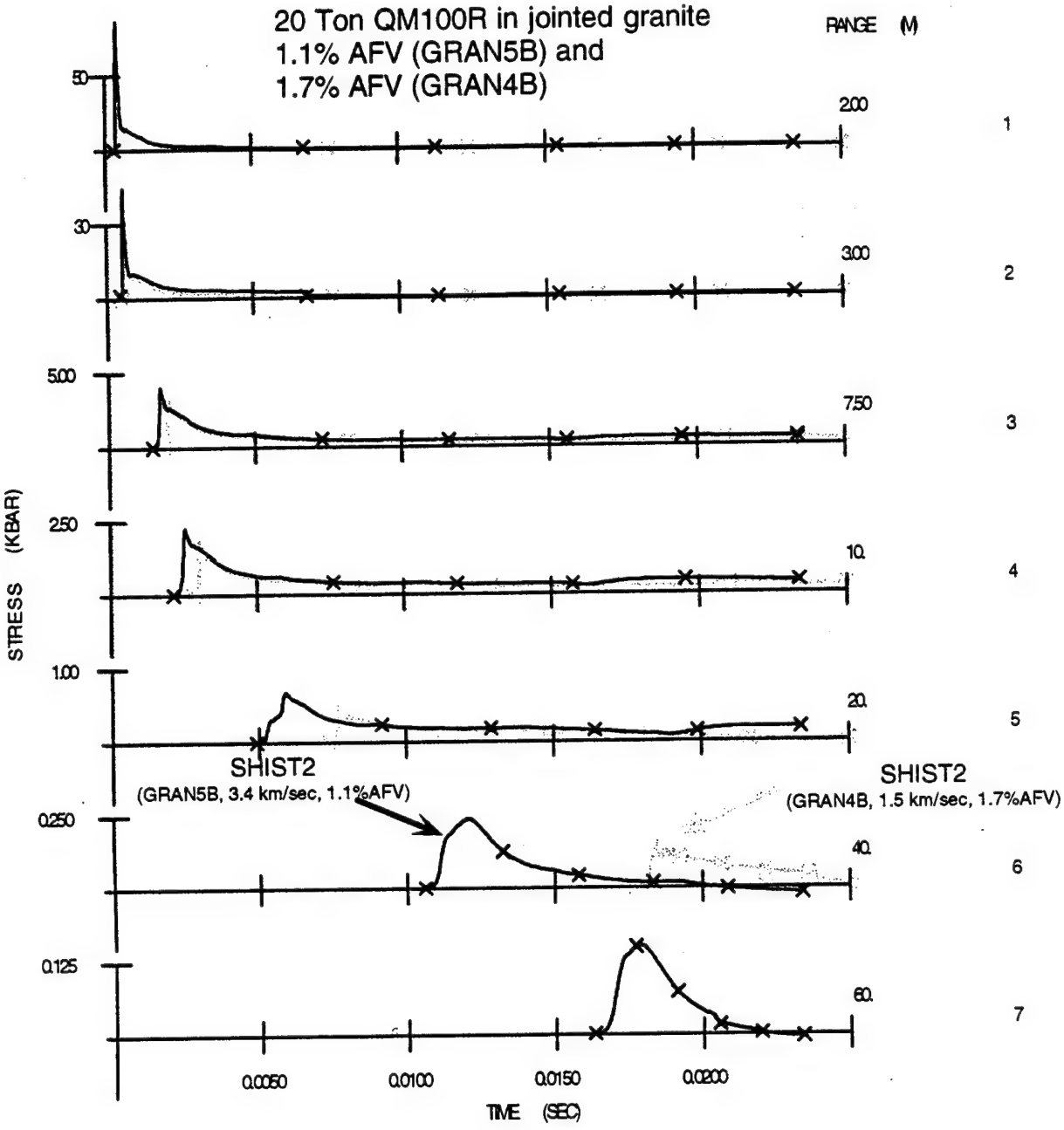


Figure 3-4. Calculated 1D stress waveforms for a 20-ton QM-100/R charge in SHIST1 (GRAN4B, 1,550 m/s, 1.7% AFV and SHIST2 (GRAN5B, 3,400 m/s, 1.1% AFV) jointed granite.

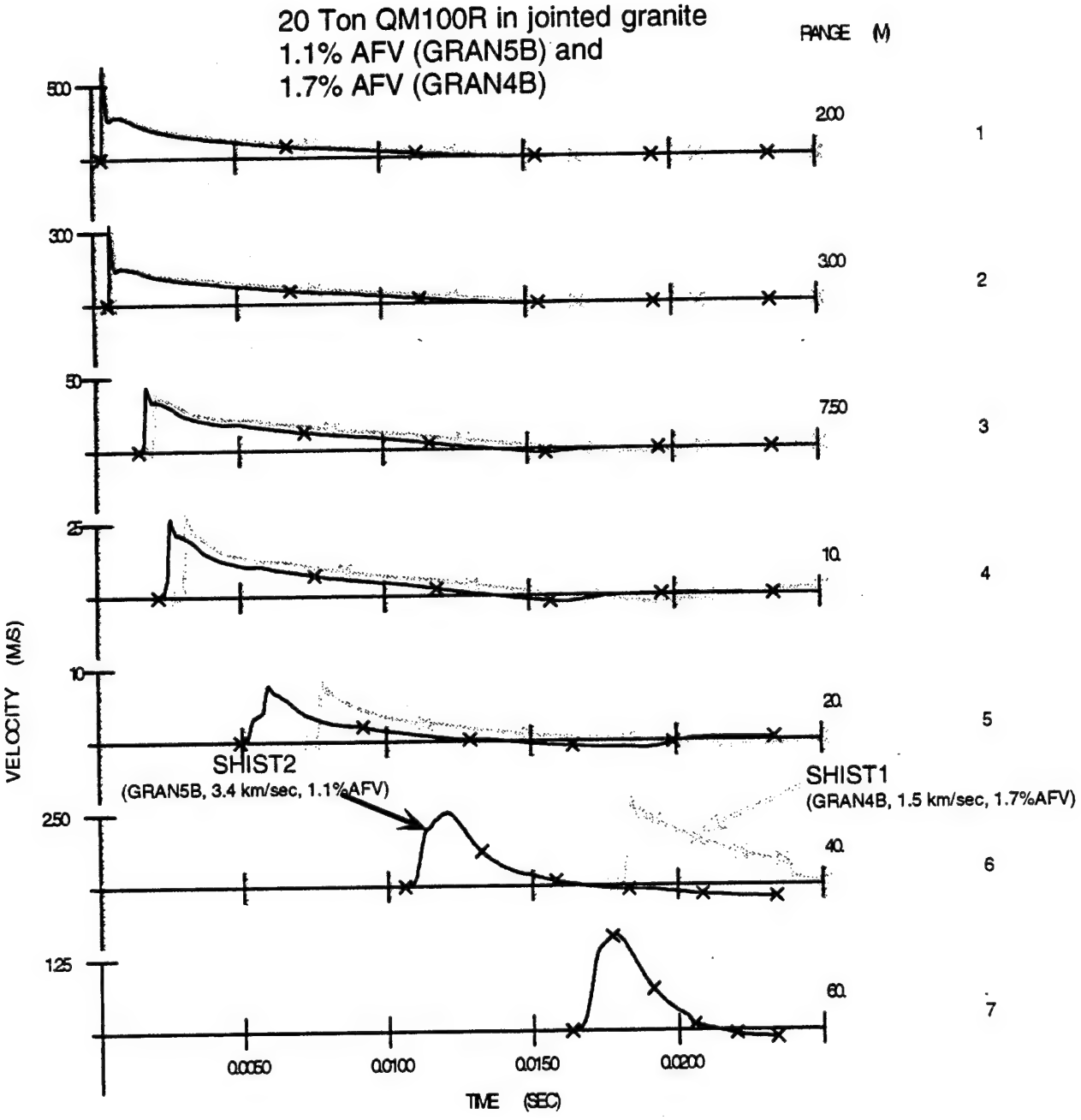


Figure 3-5. Calculated 1D velocity waveforms for a 20-ton QM-100/R charge in SHIST1 (GRAN4B, 1,550 m/s, 1.7% AFV and SHIST2 (GRAN5B, 3,400 m/s, 1.1% AFV) jointed granite.

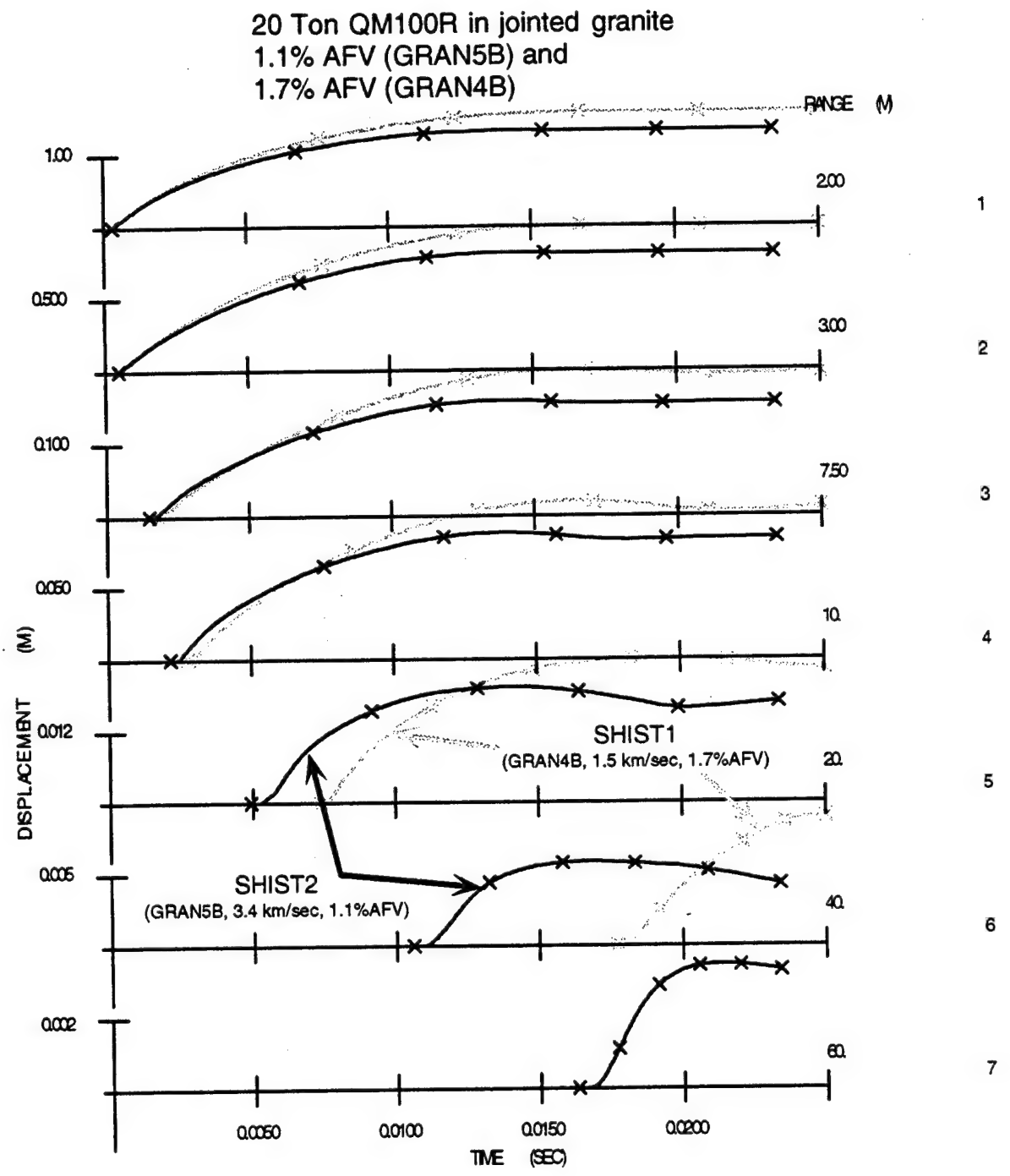


Figure 3-6. Calculated 1D displacement waveforms for a 20-ton QM-100/R charge in SHIST1 (GRAN4B, 1,550 m/s, 1.7% AFV and SHIST2 (GRAN5B, 3,400 m/s, 1.1% AFV) jointed granite.

As can be seen in the figures above, the 1-D calculation for material model SHIST2 (GRAN5B, 3,400 m/s, 1.1% AFV) shows a distinct range at which the onset of the "elastic" attenuation regime begins, approximately 30 meters from the charge center at a stress level of 0.3 kbar. This onset occurs at the point where the peak stress and velocity attenuation rates approach a slope of 1 (the theoretical spherical attenuation of a purely elastic wave). As can be seen in Figures 3-1 and 3-2 above, the SHIST2 plastic wave has a plastic stress wave attenuation on the order of $R^{-1.7}$, a plastic velocity wave attenuation on the order of $R^{-1.8}$, and an elastic wave attenuation of $R^{-1.1}$. Since most of the experimental gages will be placed within the SHIST2 layer (depth > 15 m), these 1D attenuations can be used to assist in gage placement. Potential surface rarefaction will be examined in the 2-D calculations reported in Section 4 below.

The 1-D results using material model SHIST1 (GRAN4B, 1,550 m/s, 1.7% AFV) does not show a distinct range at which the shock attenuates as an elastic wave. SHIST2 is has a lower seismic velocity and is more hysteretic than SHIST1 which causes the shock to attenuate more rapidly. An "elastic" regime is not predicted by the calculation within a range of 100 meters, Figures 3-1 and 3-2. Since this material model is a oversimplification of the weathered rock, it may be an overestimate of the jointing effects of the upper layer but without experimental data, this is difficult to confirm.

### 3.3 1D CALCULATIONS USING GENERIC2 AND GENERIC3 GRANITE MATERIAL MODELS.

Figures 3-7 through 3-9 show the peak stress, velocity, and displacement vs. range attenuation curves calculated for the GENERIC2 (GRAN1C, 4,500 m/s, 1% AFV) and GENERIC3 (GRAN1E, 4,500 m/s, 1% AFV) granite material models. These calculations were included to examine material properties excursions to the SHIST site. Since accurate in-situ data is not currently available for the SHIST site, the degree of weathering in uncertain and it is not known at what stress level the joints will close. The GENERIC2,3 models are a higher quality granite than the SHIST1,2 models and was felt their predicted attenuations could assist in future test gage planning. As can be

seen, the onset of the "elastic" attenuation regime for the GENERIC models occurs at a slightly greater range than predicted for SHIST1, approximately 40 meters from the charge center at a stress level of 0.3 kbar. The calculated stress, velocity and displacement waveforms for GENERIC2 and GENERIC3 are plotted at ranges between 2 and 100 meters in Figures 3-10 through 3-12. The GENERIC2,3 models predict a plastic stress wave attenuation on the order of $R^{-1.8}$, a plastic velocity wave attenuation on the order of $R^{-1.7}$, and an elastic wave attenuation of $R^{-1.1}$.

The two GENERIC 1% AFV granite models can be seen to give virtually identical shock attenuations. Slight differences can be seen due to variations in the strength characteristics of the two materials (linear DP/VM yield surface vs. exponential surface). GENERIC3 gives slightly smaller displacements than GENERIC2 but times of arrival are identical in both materials, with the elastic wave running at 4,500 m/s.

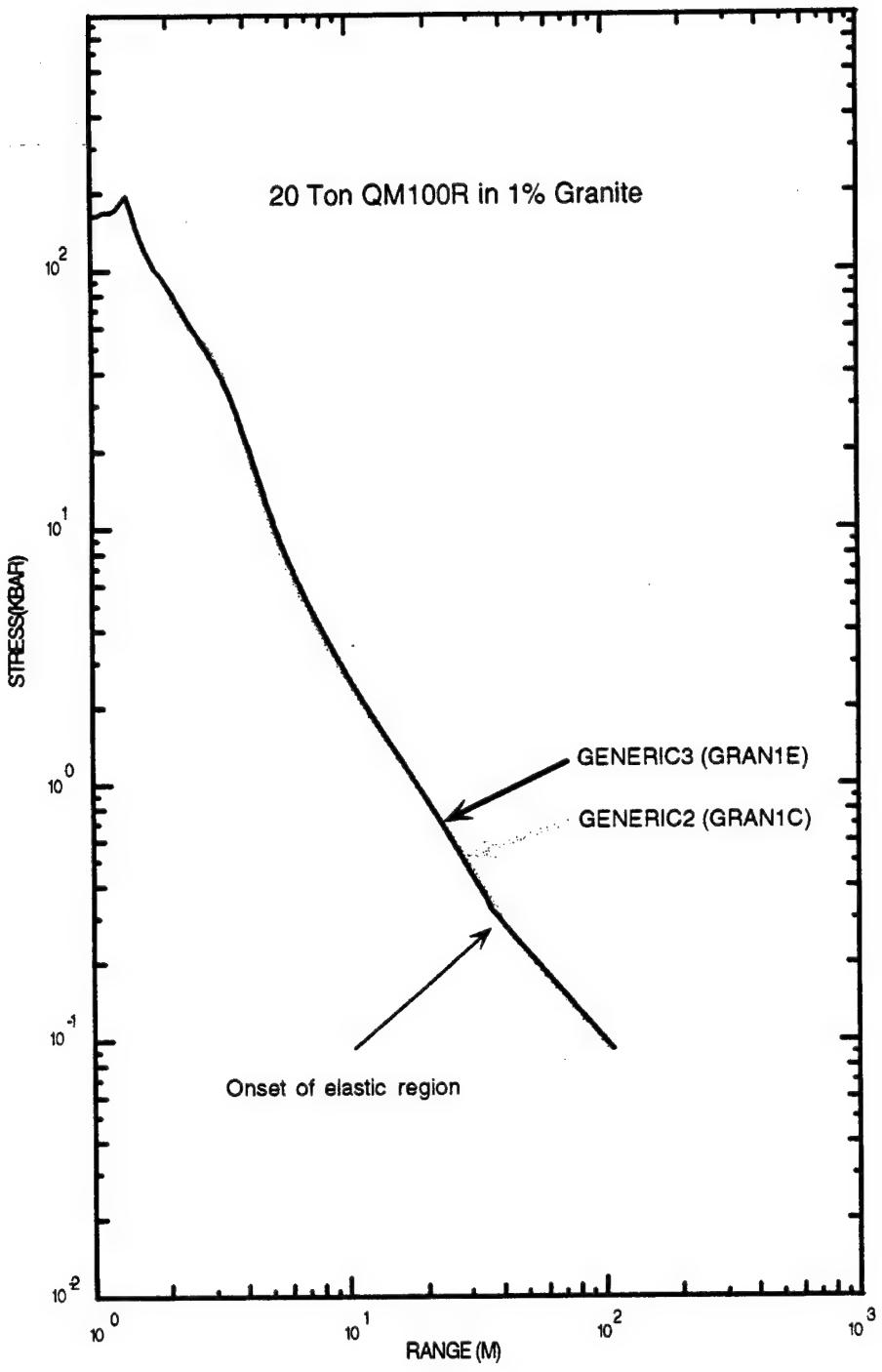


Figure 3-7. Calculated 1D peak stress vs. range for a 20-ton QM-100/R charge in 4,500 m/s, 1% AFV granite using GENERIC2 (GRAN1C) and GENERIC3 (GRAN1E) material models.

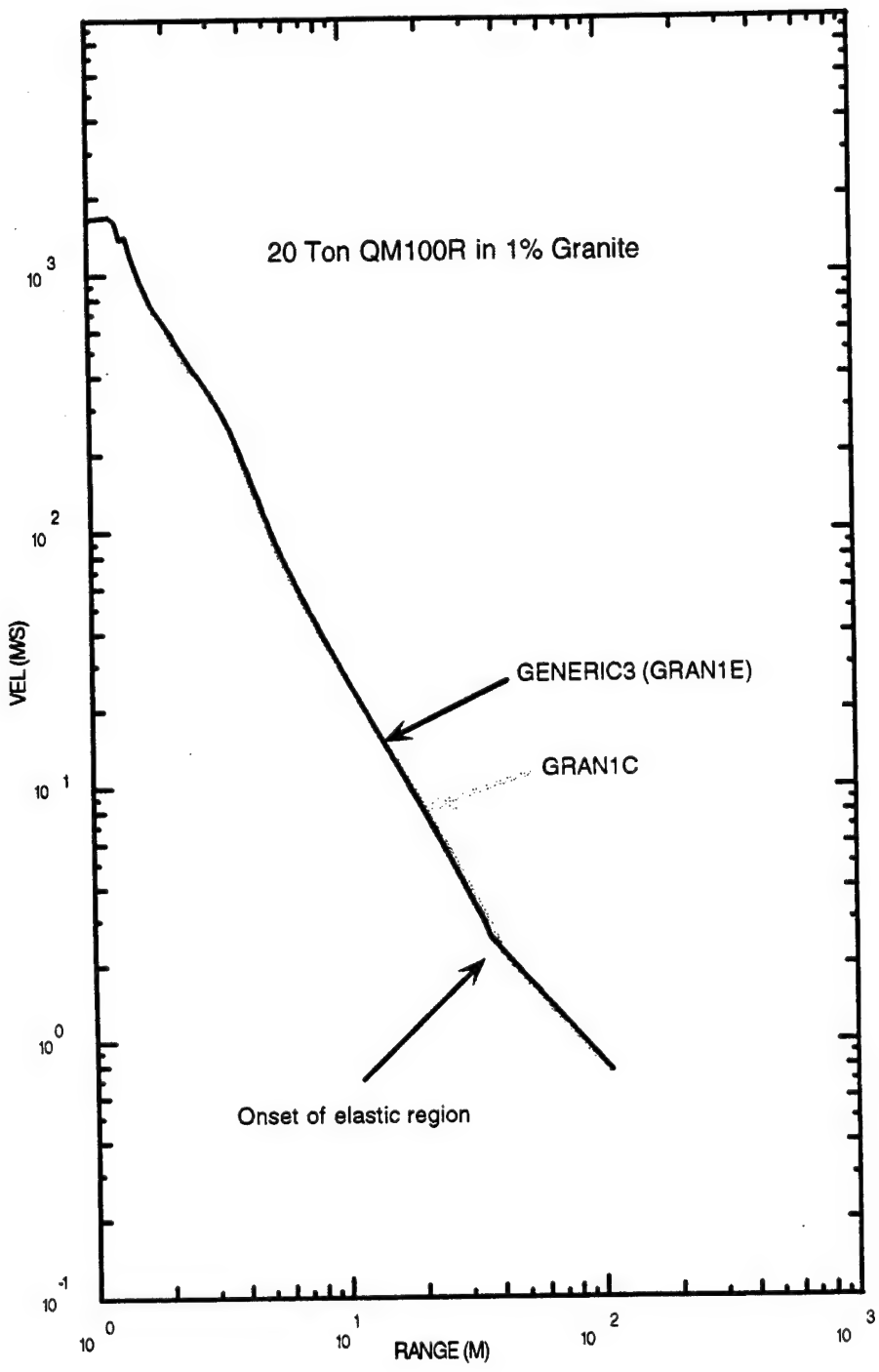


Figure 3-8. Calculated 1D peak velocity vs. range for a 20-ton QM-100/R charge in 4,500 m/s, 1% AFV granite using GENERIC2 (GRAN1C) and GENERIC3 (GRAN1E) material models.

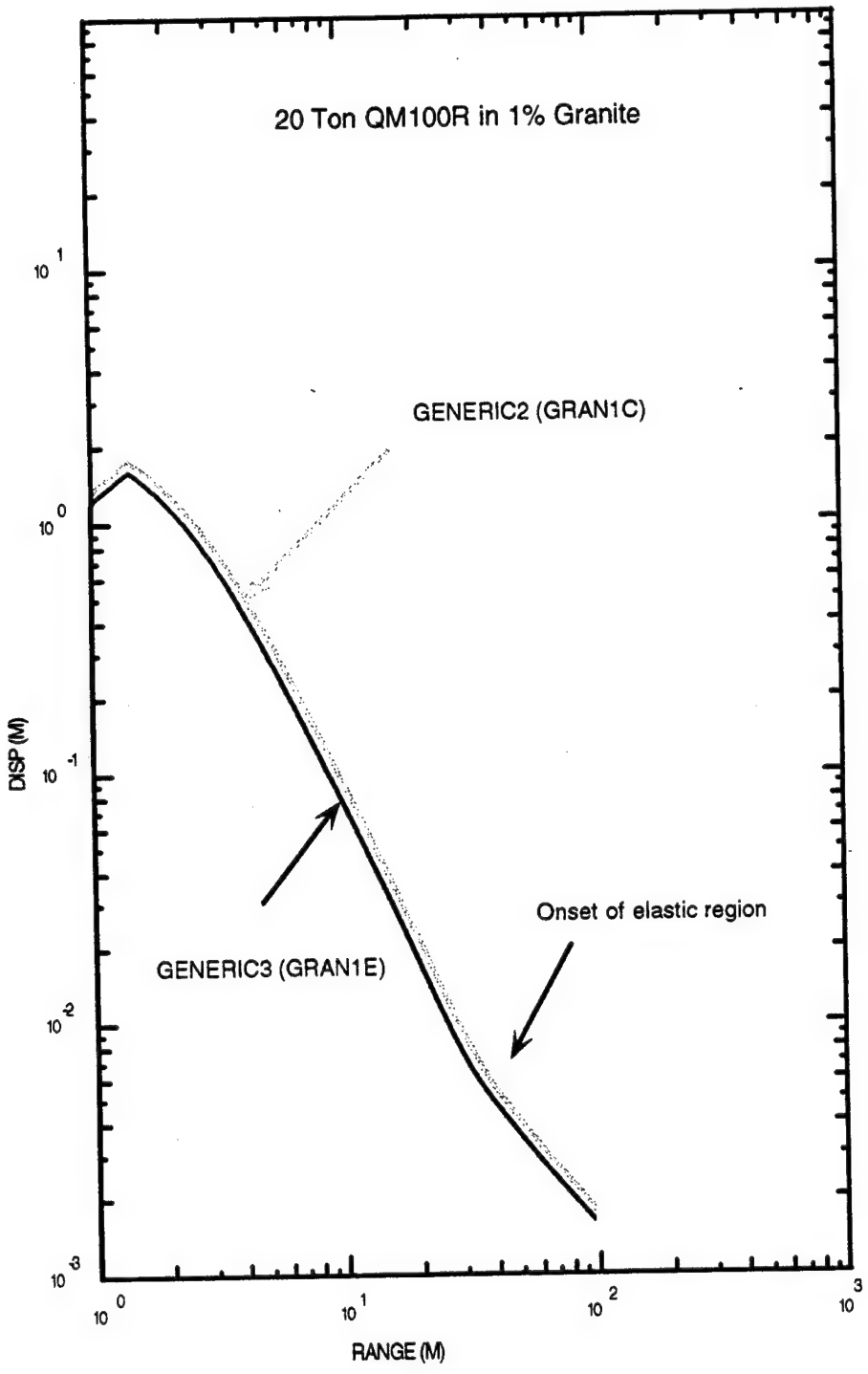


Figure 3-9. Calculated 1D peak displacement vs. range for a 20-ton QM-100/R charge in 4,500 m/s, 1% AFV granite using GENERIC2 (GRAN1C) and GENERIC3 (GRAN1E) material models.

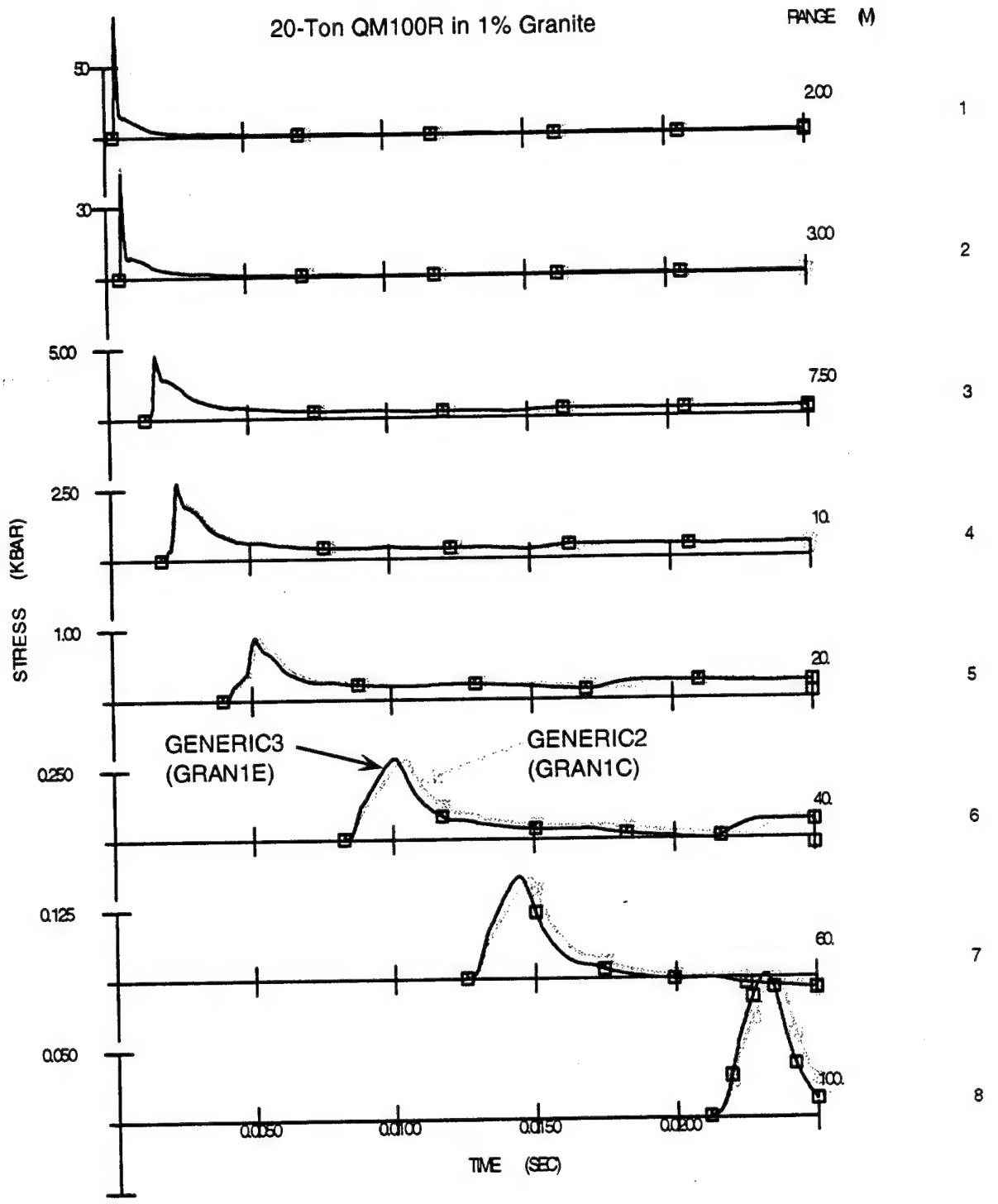


Figure 3-10. Calculated 1D stress waveforms range for a 20-ton QM-100/R charge in 4,500 m/s, 1% AFV granite using GENERIC2 (GRAN1C) and GENERIC3 (GRAN1E) material models.

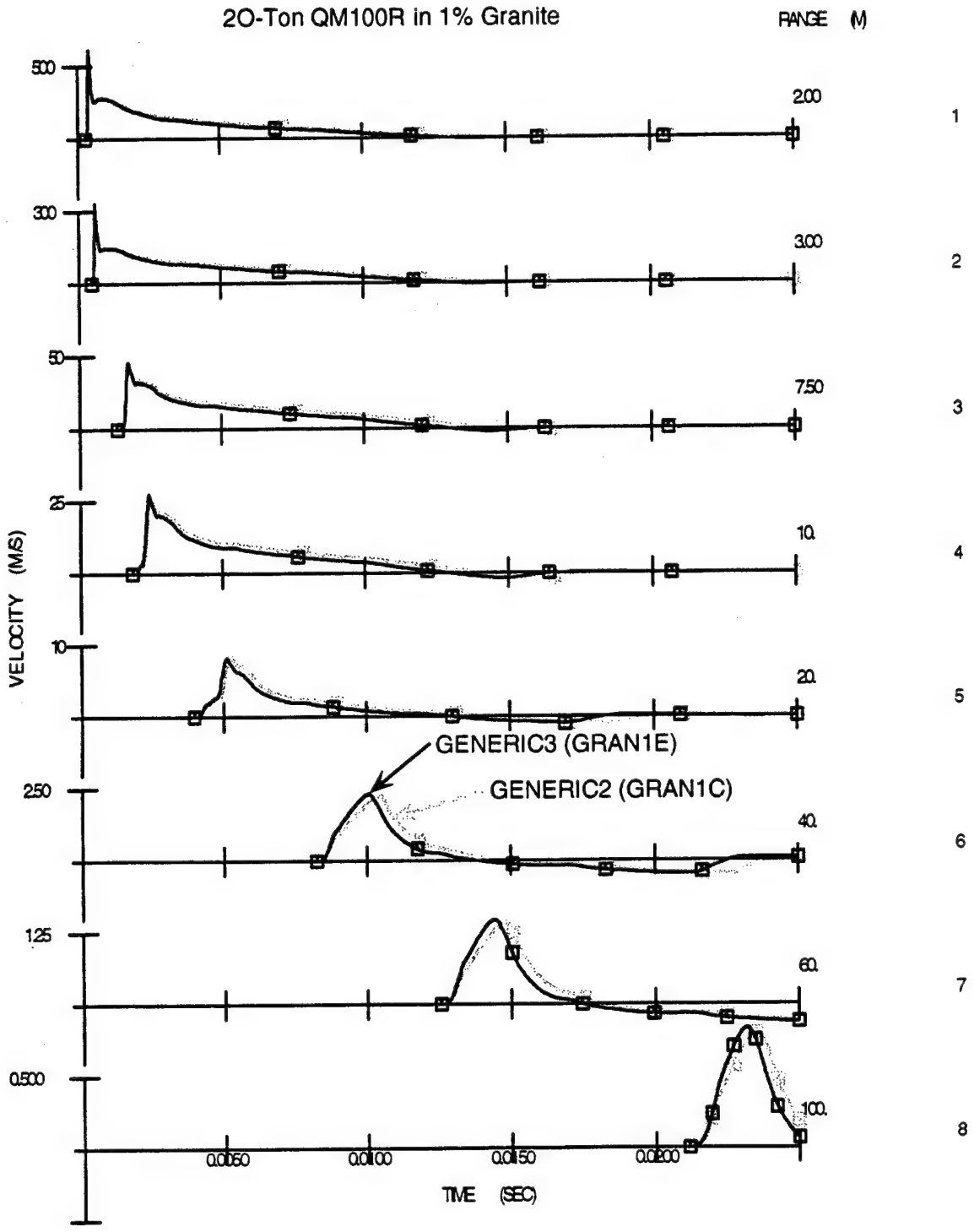


Figure 3-11. Calculated 1D velocity waveforms range for a 20-ton QM-100/R charge in 4,500 m/s, 1% AFV granite using GENERIC2 (GRAN1C) and GENERIC3 (GRAN1E) material models.

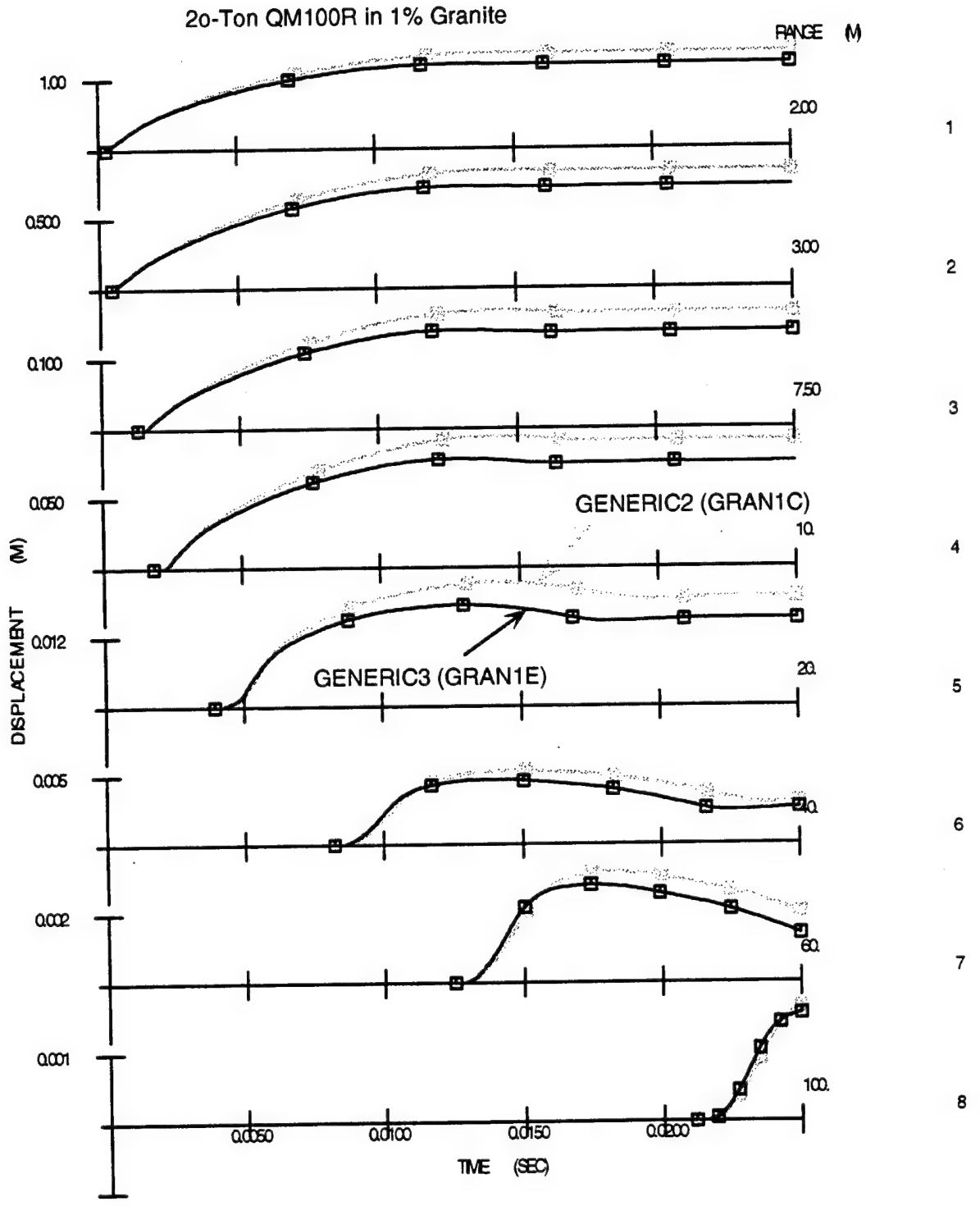


Figure 3-12. Calculated 1D displacement waveforms range for a 20-ton QM-100/R charge in 4,500 m/s, 1% AFV granite using GENERIC2 (GRAN1C) and GENERIC3 (GRAN1E) material models.

# SECTION 4

# 2D SCOPING CALCULATIONS FOR SHIST (TASK 3)

## 4.1 2D CALCULATION SETUP.

The material models discussed in the sections above were implemented in the CRALE 2-D code and used to investigate the details of the interaction of the explosively-driven shock with the surrounding concrete stemming materials and granite. We used the latest proposed charge and stemming configuration provided to us by DNAFC. This plan called for a 20 ton sphere of QM-100/R with a diameter of 2.896 meter (9.5 ft) to be placed at a shot depth of 35 meters. A 1.066 meter (42 inch) diameter downhole stem extends vertically from the surface to approximately 15 meters below charge (50 meter depth). The downhole was to be filled with HJC7 concrete for which an existing CRALE material model exists (CON5K4 using the MCIST EOS).

Three 2D calculations were performed in this study to examine the shock propagation in the granite materials discussed in the sections above, and to evaluate potential perturbations due to the material model uncertainties of the SHIST site. Each calculation was run to a maximum time of 20 msec to capture the peak displacements at the experimental gage locations. The first calculation, designated 2DSHIST03 and discussed in Section 4.2, consisted of a top layer of SHIST1 (GRAN4B, 1,550 m/s, 1.7% AFV) jointed granite to a depth of 15 meters below which was an infinite layer of SHIST2 (GRAN5B, 3,400 m/s, 1.1% AFV) jointed granite. This calculation is currently our best representation for the SHIST experiment. The second calculation, designated 2DSHIST02 and discussed in Section 4.3, consisted of a homogeneous layer of SHIST2 jointed granite. This calculation could be used in conjunction with 2DSHIST03 to help evaluate the potential layering effects on the free field waveforms. The third calculation, designated 2DSHIST01 and discussed in Section 4.4, consisted of a top layer of GENERIC2 (GRAN1C, 4,500 m/s, 1% AFV) granite below which was an infinite layer of

GENERIC3 (GRAN1E, 4,500 m/s, 1% AFV) granite. This calculation was used as a second material model excursion and 2D zoning study to be compared to the 1D calculations discussed in Section 3.

Due to zoning constraints of the 2D code, the calculations were started with an initial zone size of approximately 10 cm in the vicinity of the HE charge. The initial 2D calculation grid is shown in Figure 4-1. The HE was modeled as a spherical charge with 20 cells in the radial direction and the CRALE 2D burn logic was used to calculate its detonation. After the HE was complete and the shock wave entered the surrounding media, at a time 0.4 msec, the grid was dezoned to an average zone size of 40 cm. This zone size was then maintained throughout the remainder of the calculation, roughly twice that used in the 1D calculations reported in Section 3.

An array of 197 target points were placed in the 2D calculations to a range and depth of 100 meters. Included in this array were target points placed at the latest experimental gage locations that you provided us. Figure 4-2 shows the target point array, with the experimental gages bolded.

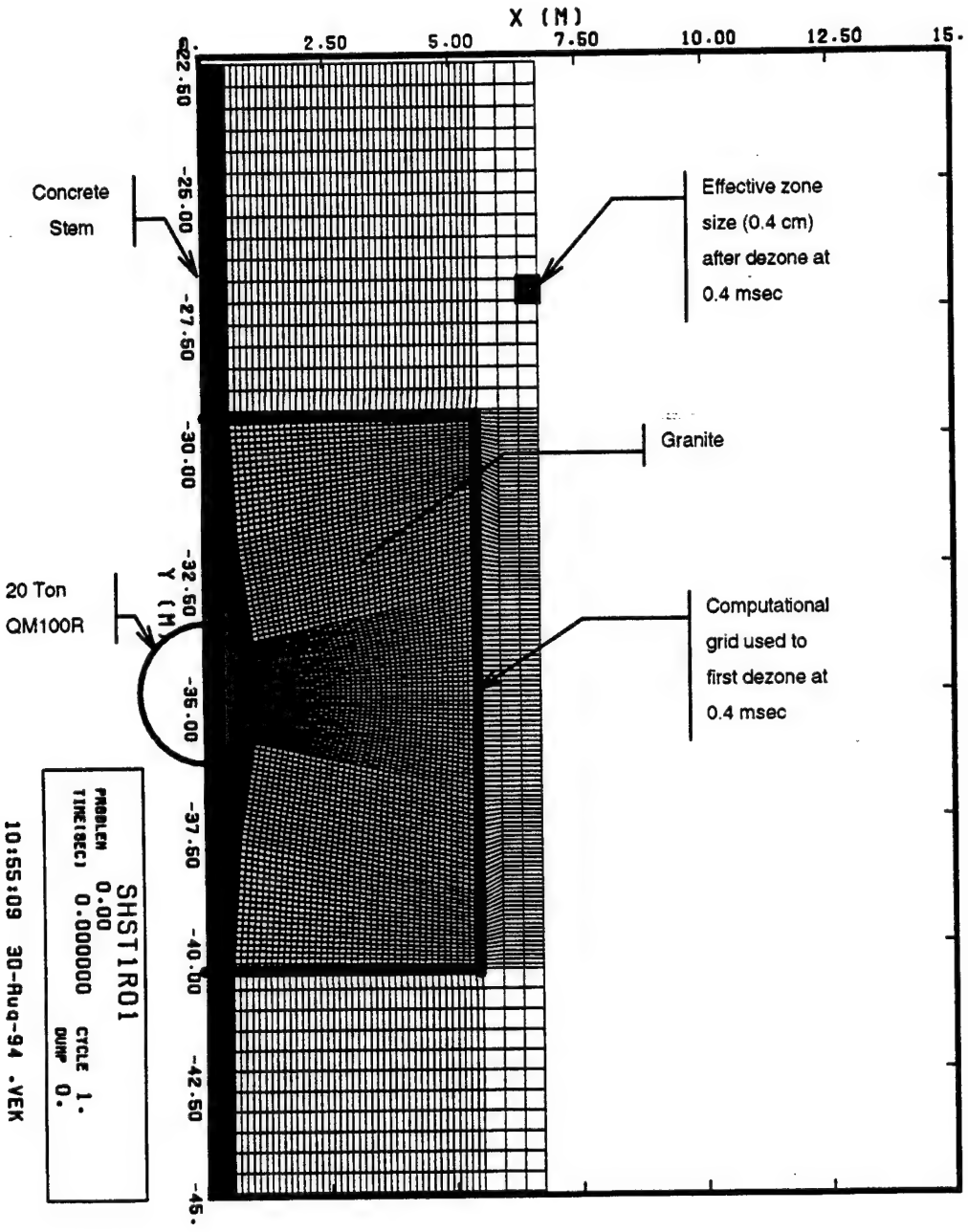


Figure 4-1. Initial grid used in 2D CRALE SHIST scoping calculations.

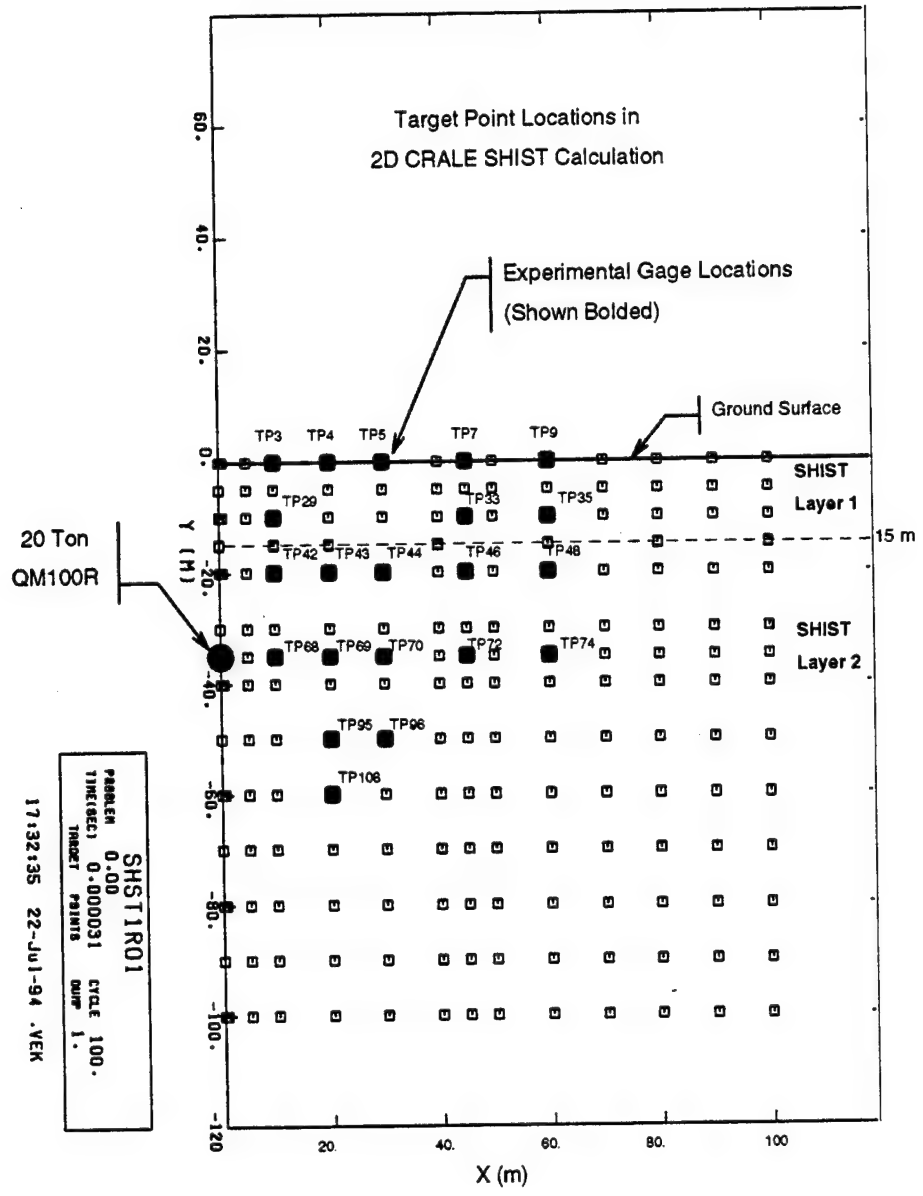


Figure 4-2. Target point locations and site layering for 2D CRALE SHIST scoping calculations.

## 4.2 CRALE 2D CALCULATION 2DSHIST03.

**SHIST1 (GRAN4B, 1,550 m/s, 1.1% AFV) 0 to 15 meter**
**SHIST2 (GRAN5B, 3,400 m/s) depth > 15 meters**

The first calculation of this study, 2DSHIST03, was run on the DNA Field Command Silicon Graphics Crimson workstation. CRALE has been successfully ported to this platform and the code is fully operational there (the current version of CRALE is CRALEPL3). The 2DSHIST03 calculation examined the 2D shock wave propagation through a layered, highly weathered and jointed granite site. The calculation consisted of material model SHIST1 (GRAN4B, 1,550 m/s, 1.7% AFV) to a depth of 15 meters with model SHIST2 (GRAN5B, 3,400 m/s, 1.1% AFV) for depths greater than 15 meters. In this calculation, the shock in layer SHIST2 can be considered spherical (1D) up to the time it hits the 15 meter deep layer interface. The presence of the concrete filled emplacement hole does not appear to affect the behavior of the free-field environment in the region of the experimental gages. Once the shock enters the SHIST1 layer, it begins to propagate at a slower velocity through the upper layer. This results in the formation of a downward directed relief wave into the SHIST2 layer. A second surface rarefaction wave results when the shock reaches the ground surface. Figures 4-3 through 4-5 show velocity vector fields from the calculation at 8, 16, and 22 msec respectively in which the surface relief as well as relief from the 15 meter interface can be observed. The vertical and horizontal stress, velocity, and displacement waveforms for the target points at the experimental gage locations are included as Figures 4-6 through 4-25. The peak stress contours for the 2DSHIST03 calculation are shown in Figure 4-26.

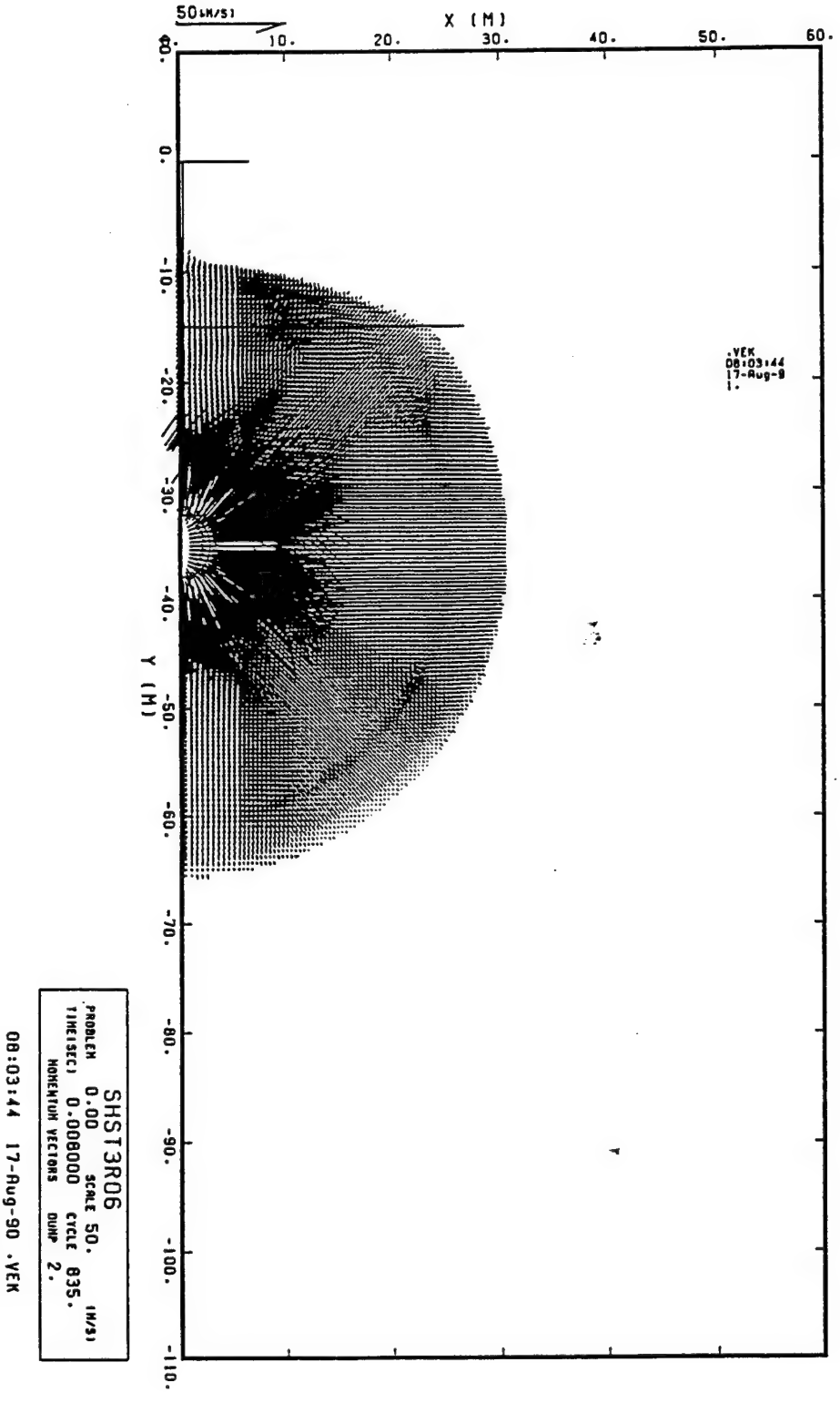


Figure 4-3. Velocity vector field at 8 msec for 2DSHIST03 CRALE calculation.

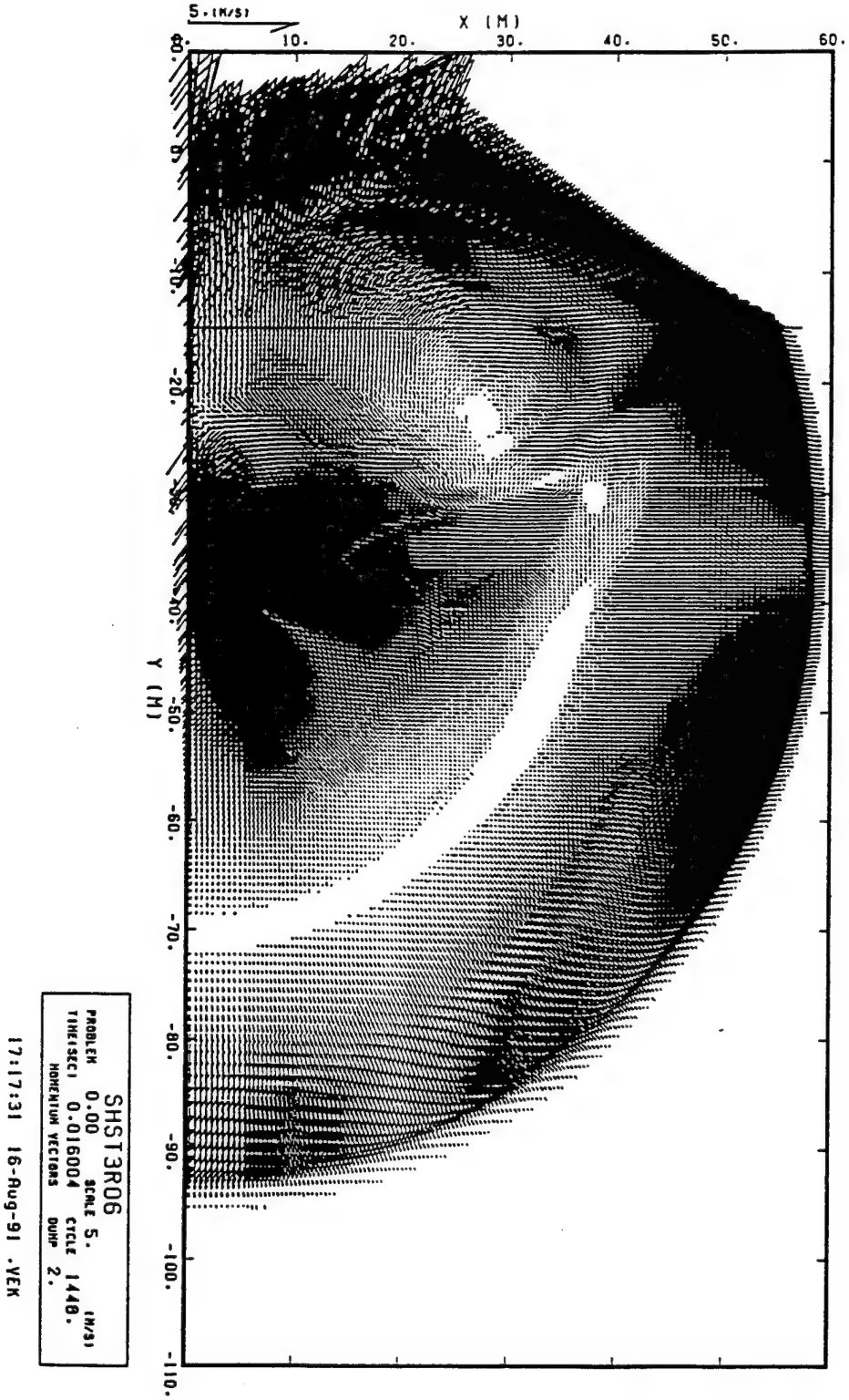


Figure 4-4. Velocity vector field at 16 msec for 2DSHIST03 CRALE calculation.

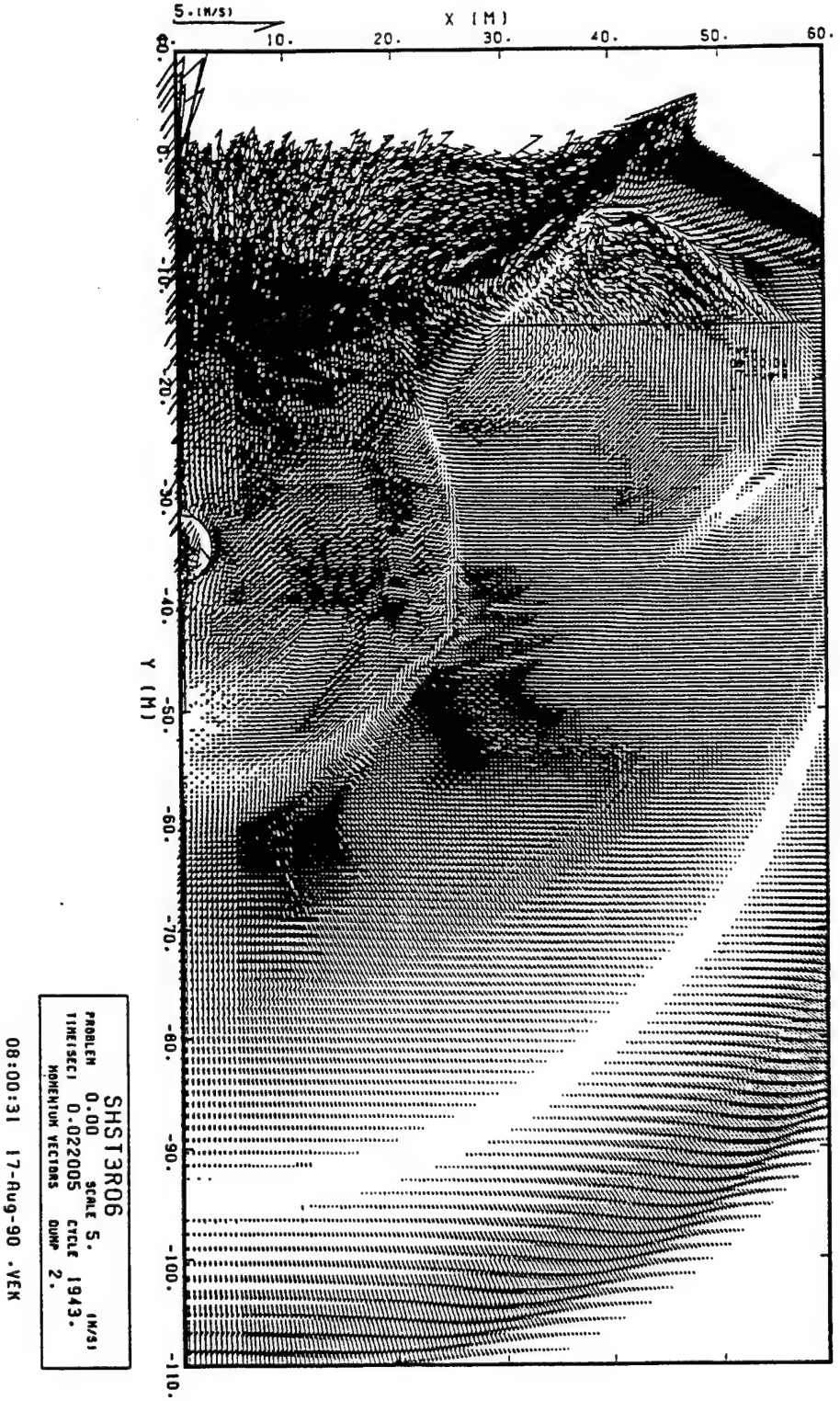


Figure 4-5. Velocity vector field at 22 msec for 2DSHIST03 CRALE calculation.

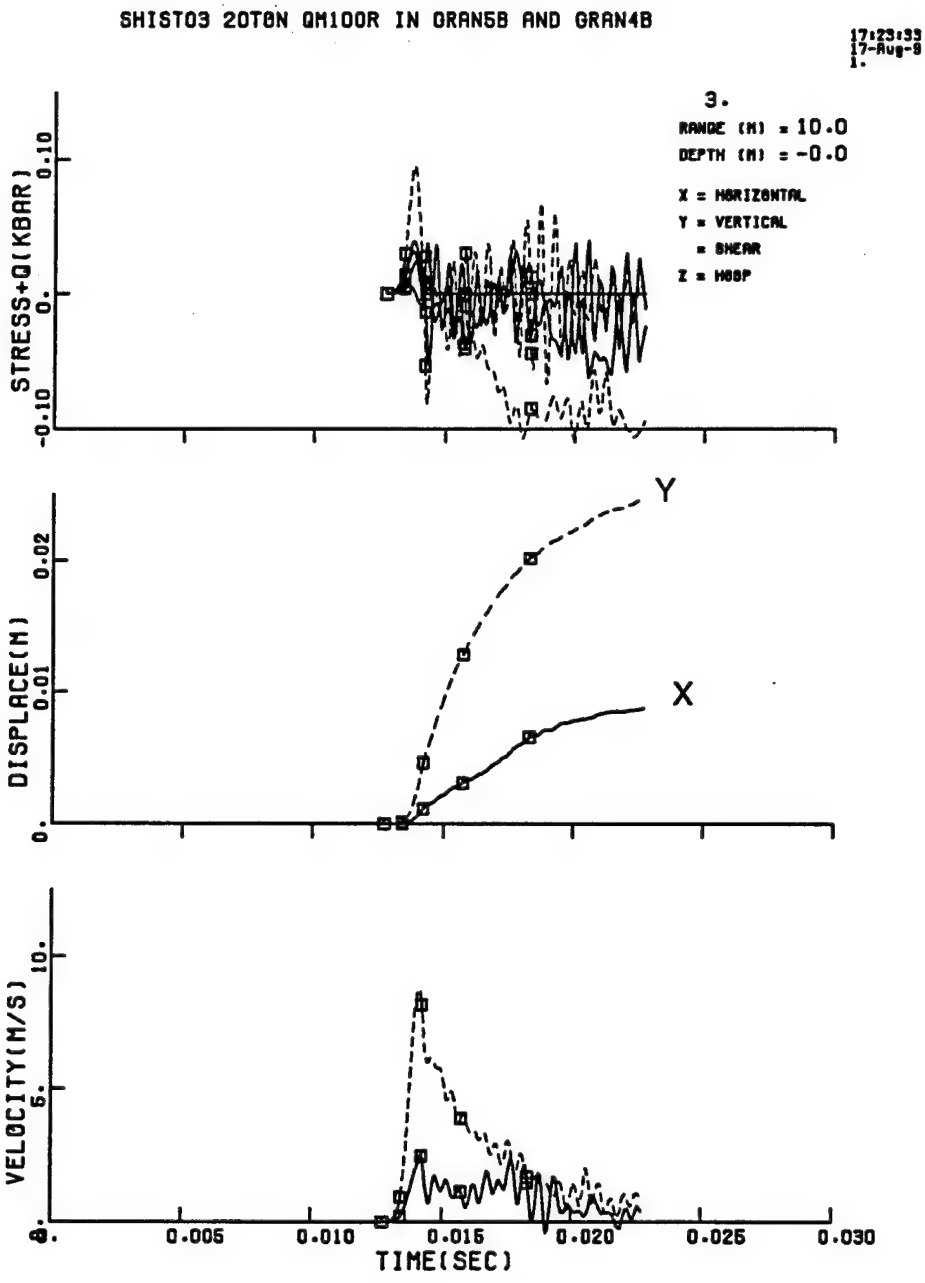


Figure 4-6. Target point 3 time history for 2DSHIST03 CRALE calculation.

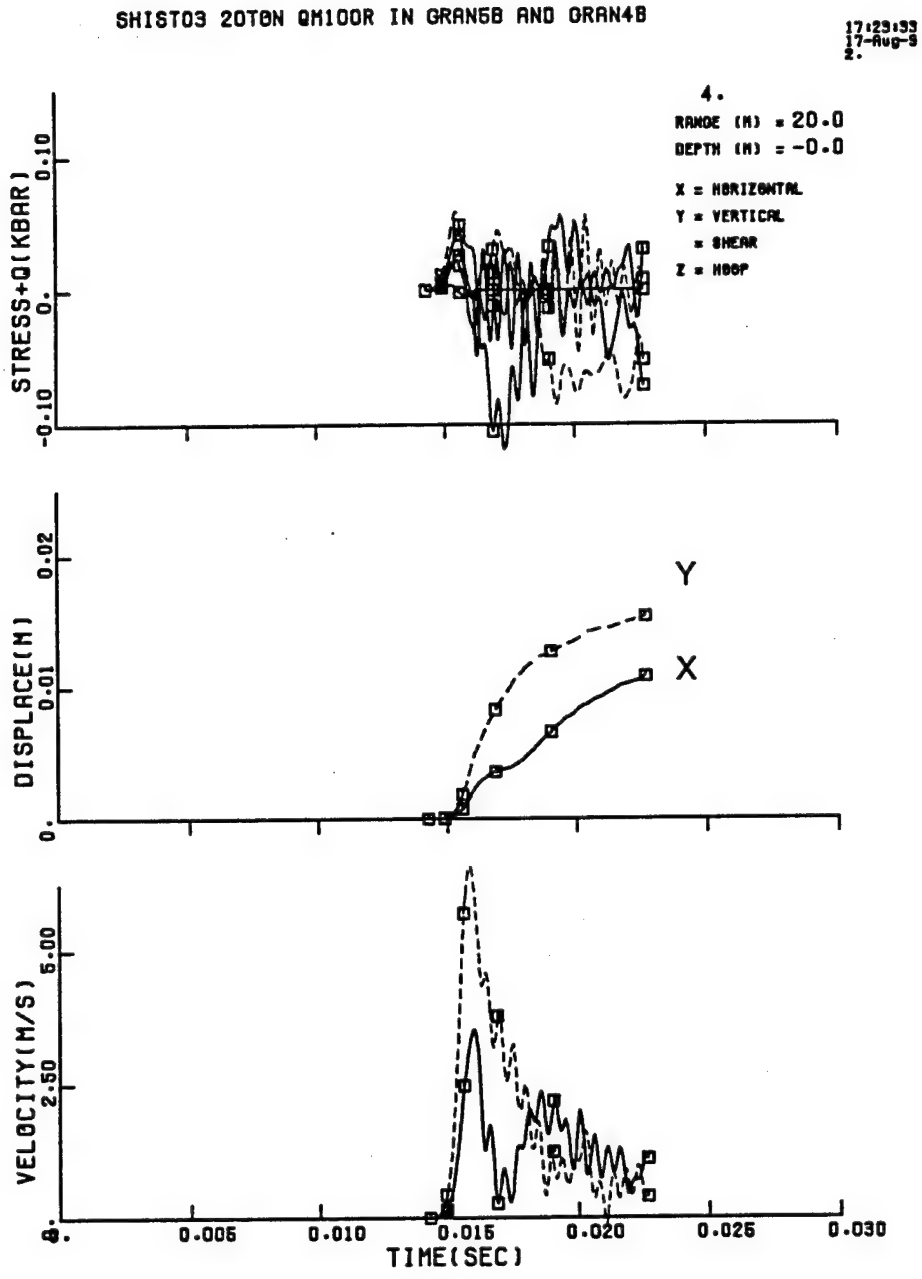


Figure 4-7. Target point 4 time history for 2DSHIST03 CRALE calculation.

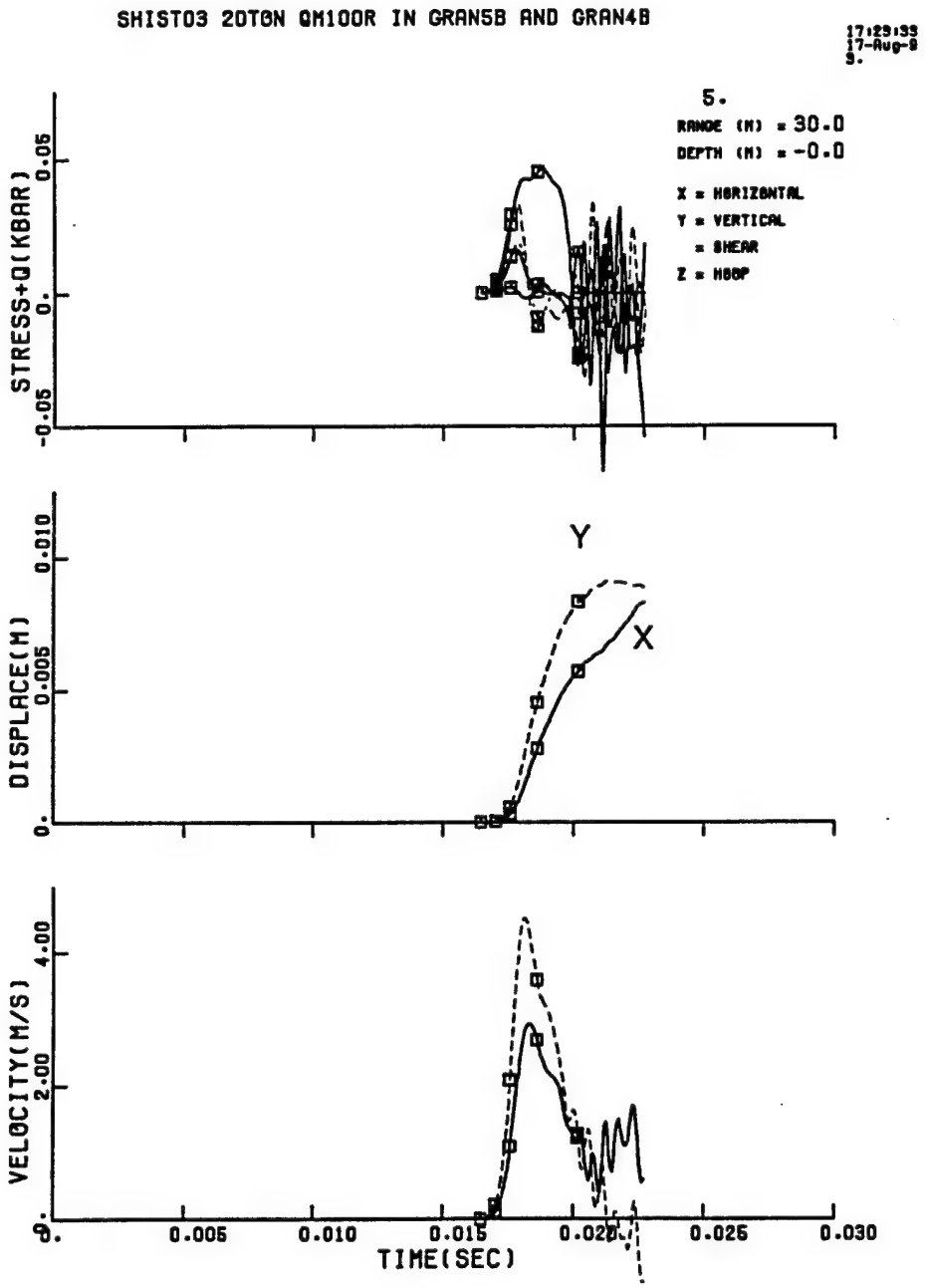


Figure 4-8. Target point 5 time history for 2DSHIST03 CRALE calculation.

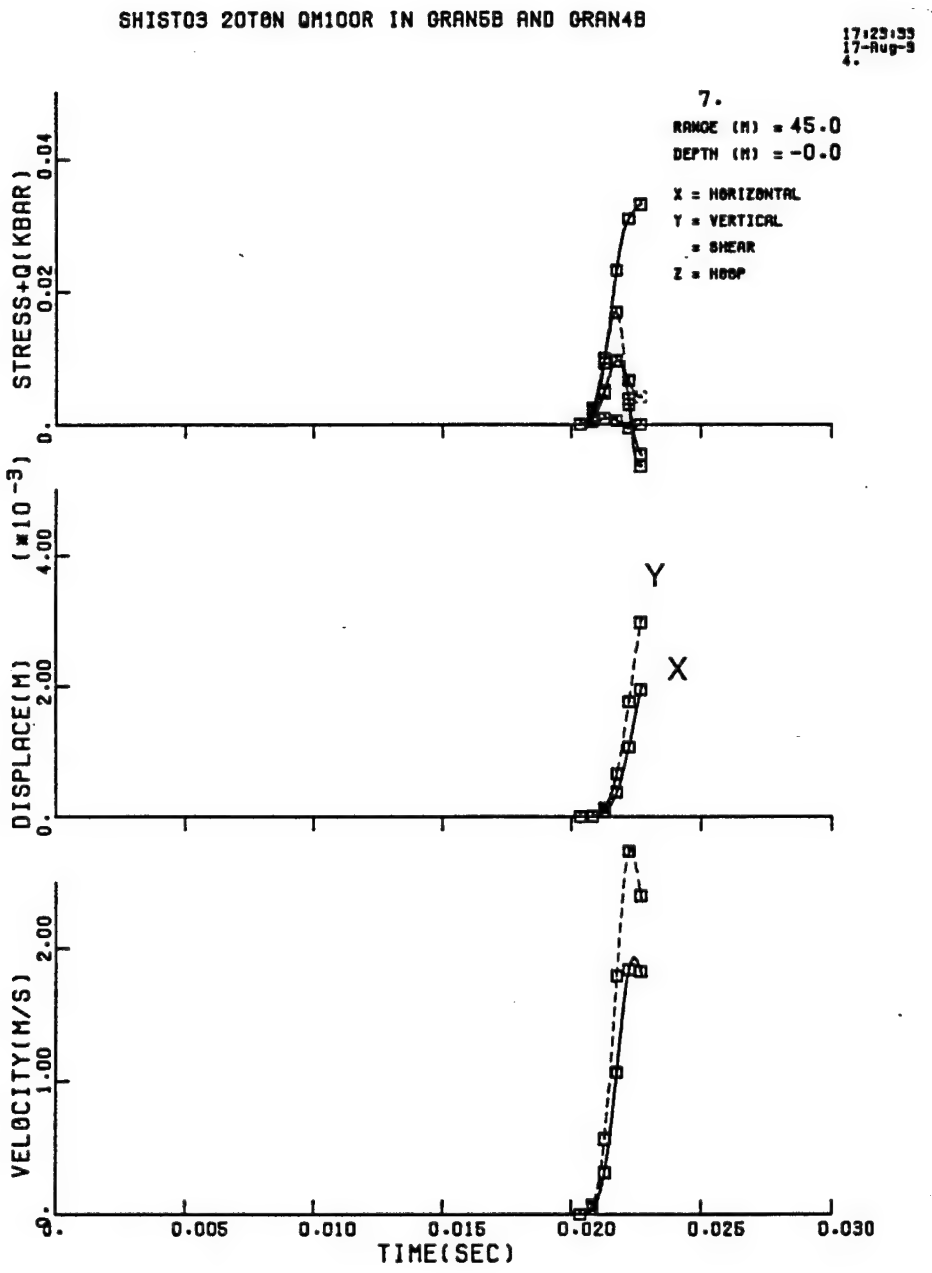


Figure 4-9. Target point 7 time history for 2DSHIST03 CRALE calculation.

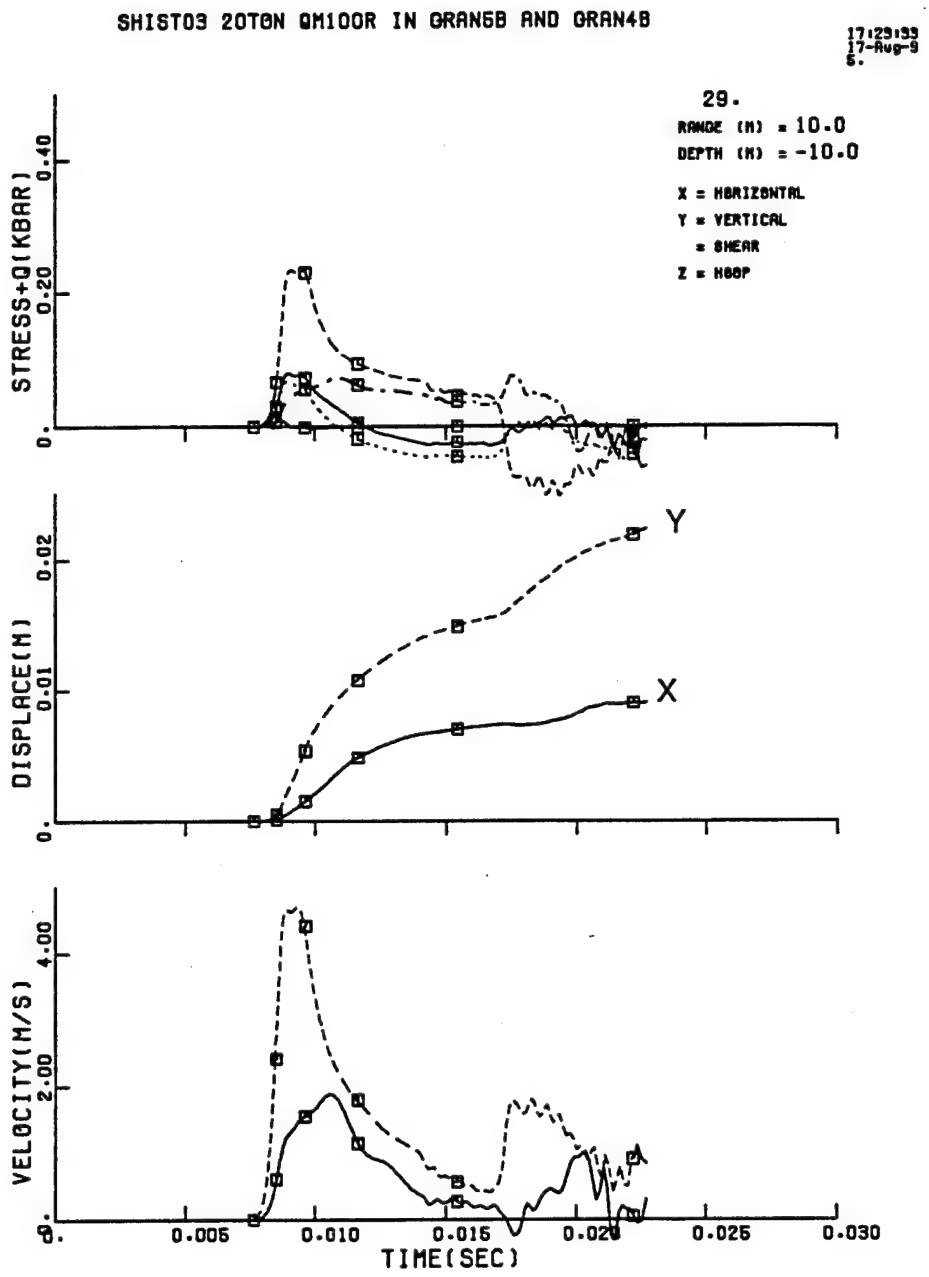


Figure 4-10. Target point 29 time history for 2DSHIST03 CRALE calculation.

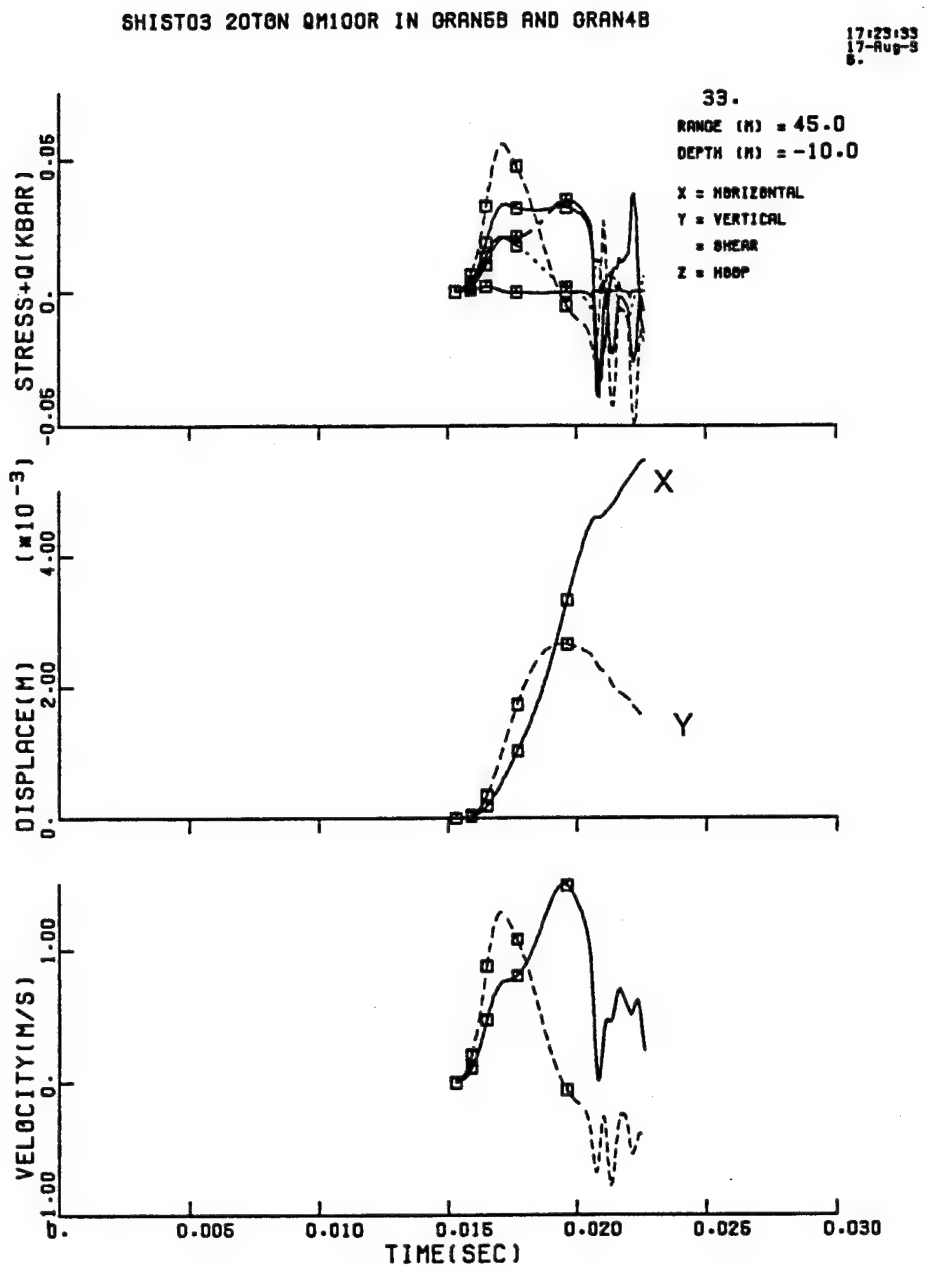


Figure 4-11. Target point 33 time history for 2DSHIST03 CRALE calculation.

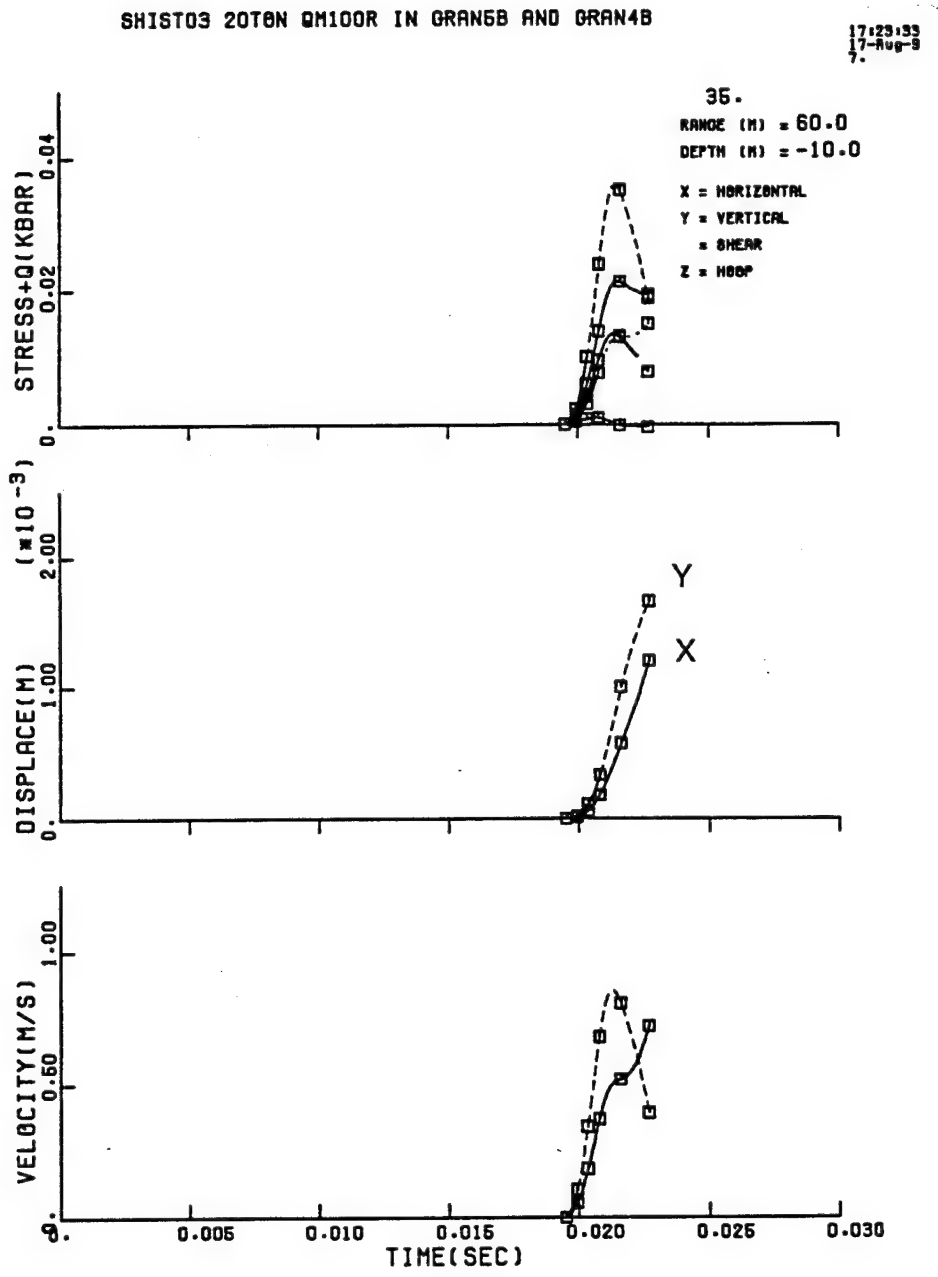


Figure 4-12. Target point 35 time history for 2DSHIST03 CRALE calculation.

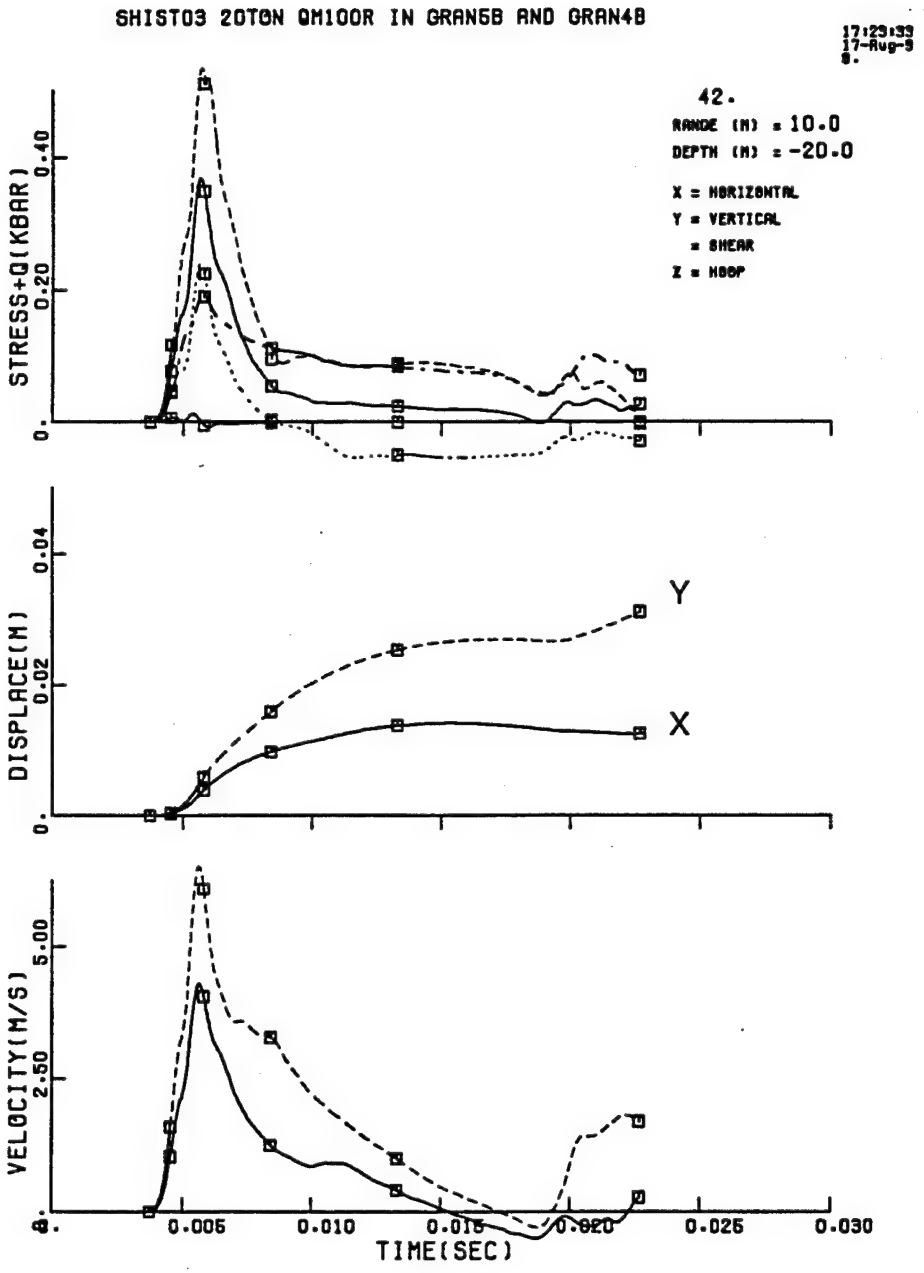


Figure 4-13. Target point 42 time history for 2DSHIST03 CRALE calculation.

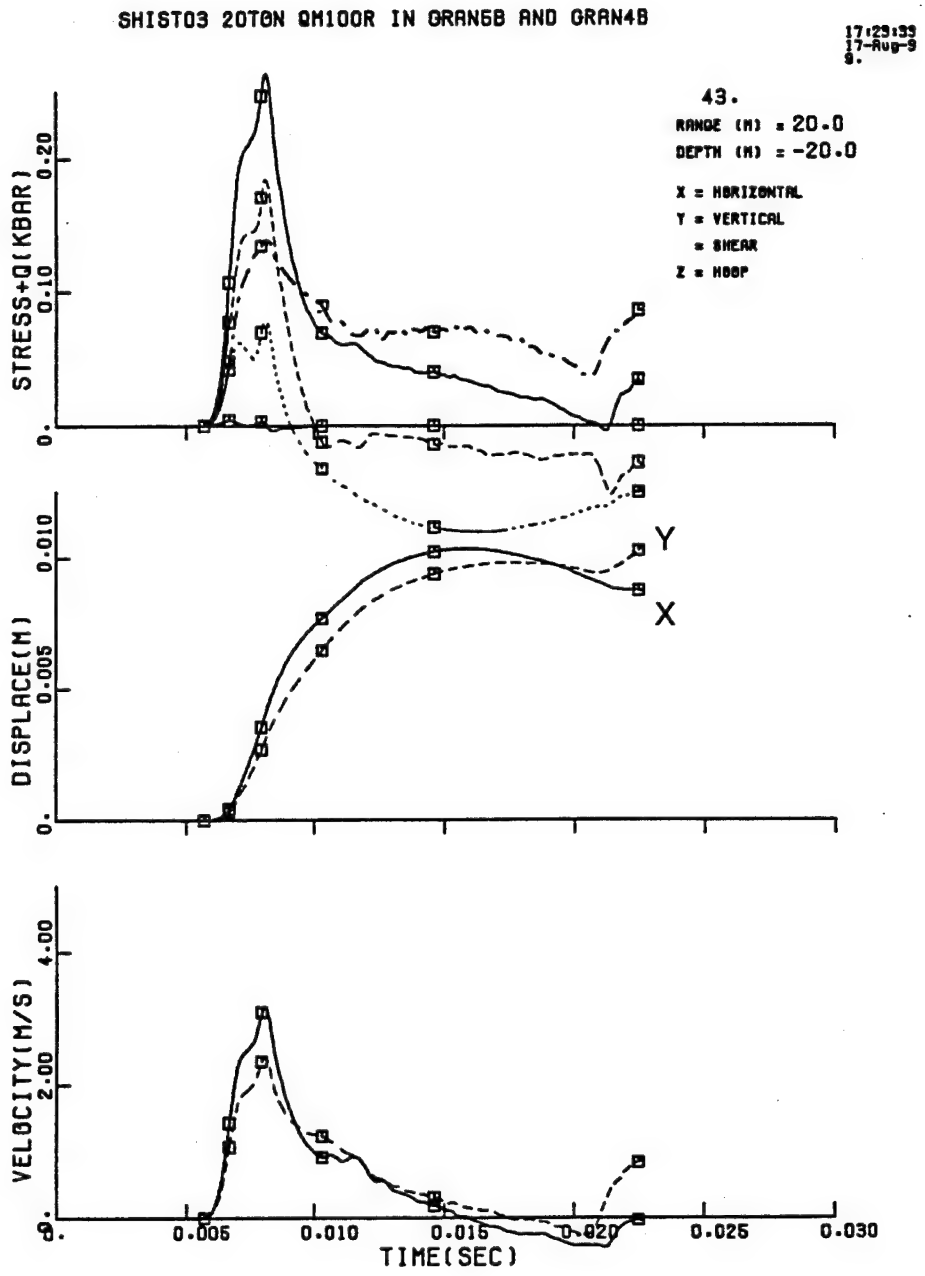


Figure 4-14. Target point 43 time history for 2DSHIST03 CRALE calculation.

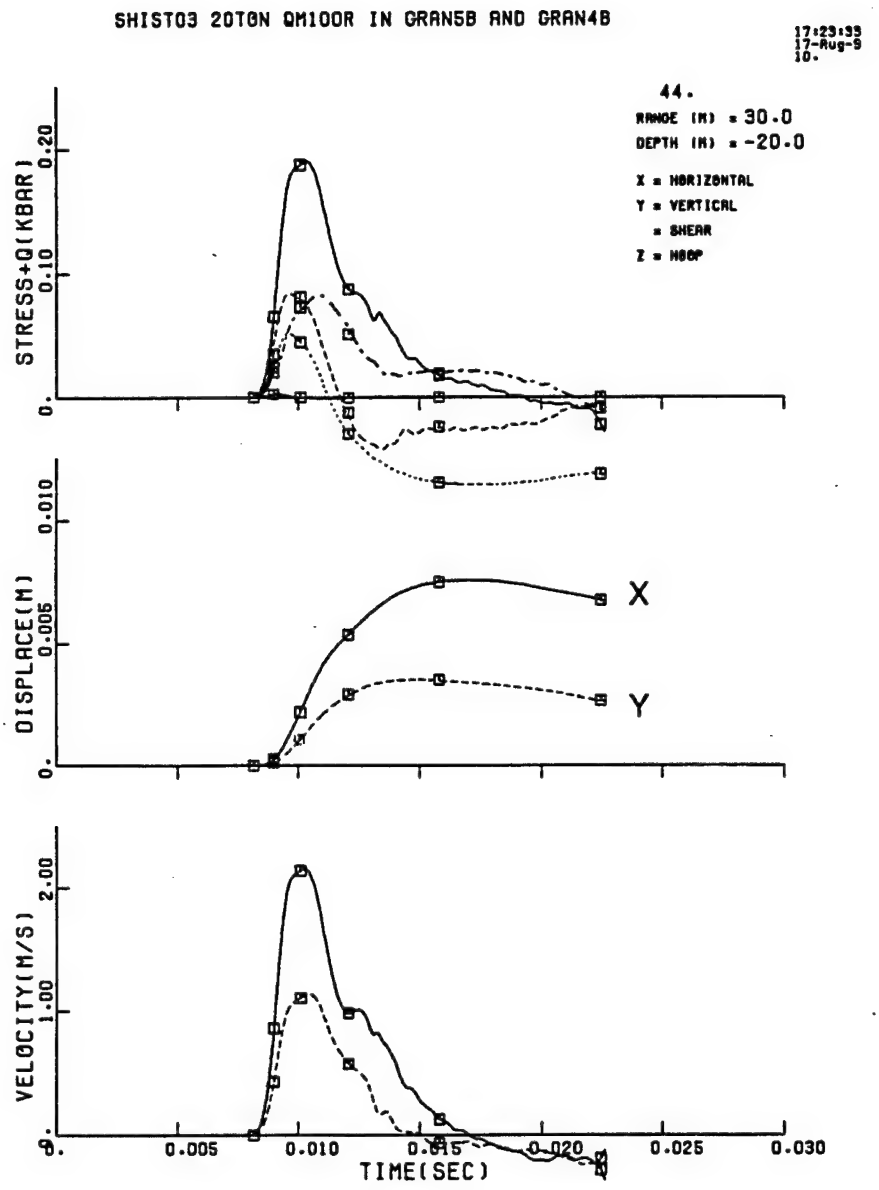


Figure 4-15. Target point 44 time history for 2DSHIST03 CRALE calculation.

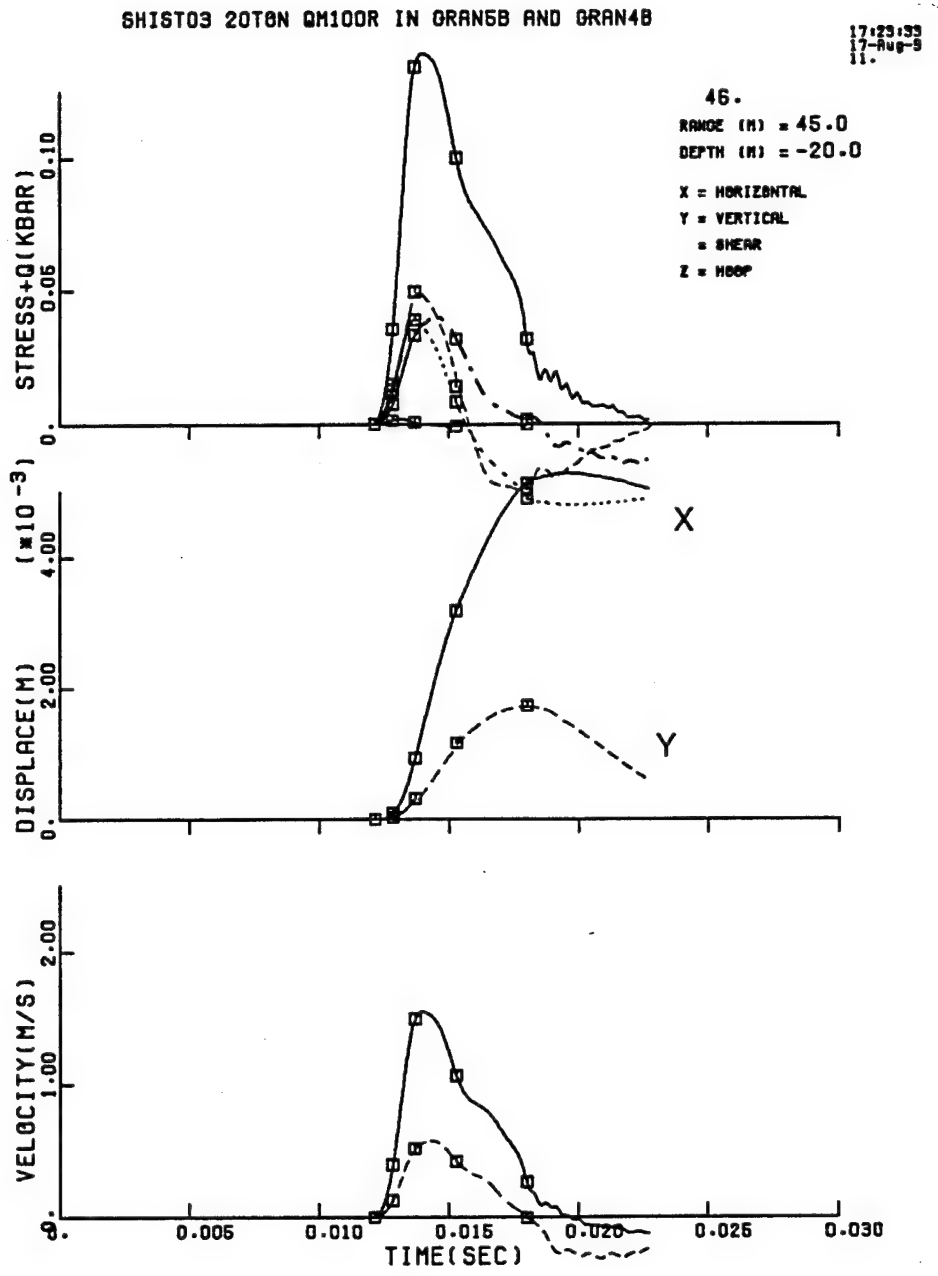


Figure 4-16. Target point 46 time history for 2DSHIST03 CRALE calculation.

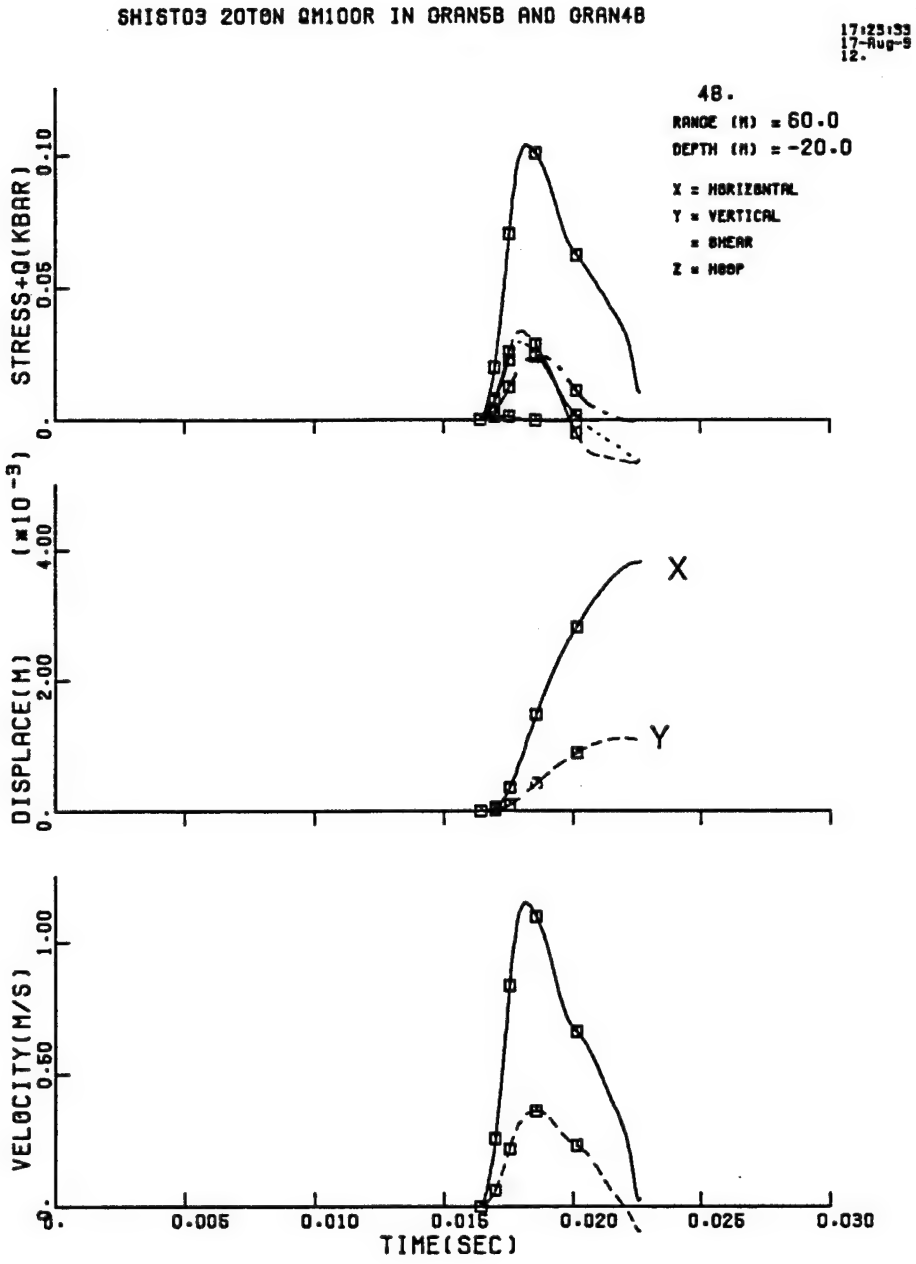


Figure 4-17. Target point 48 time history for 2DSHIST03 CRALE calculation.

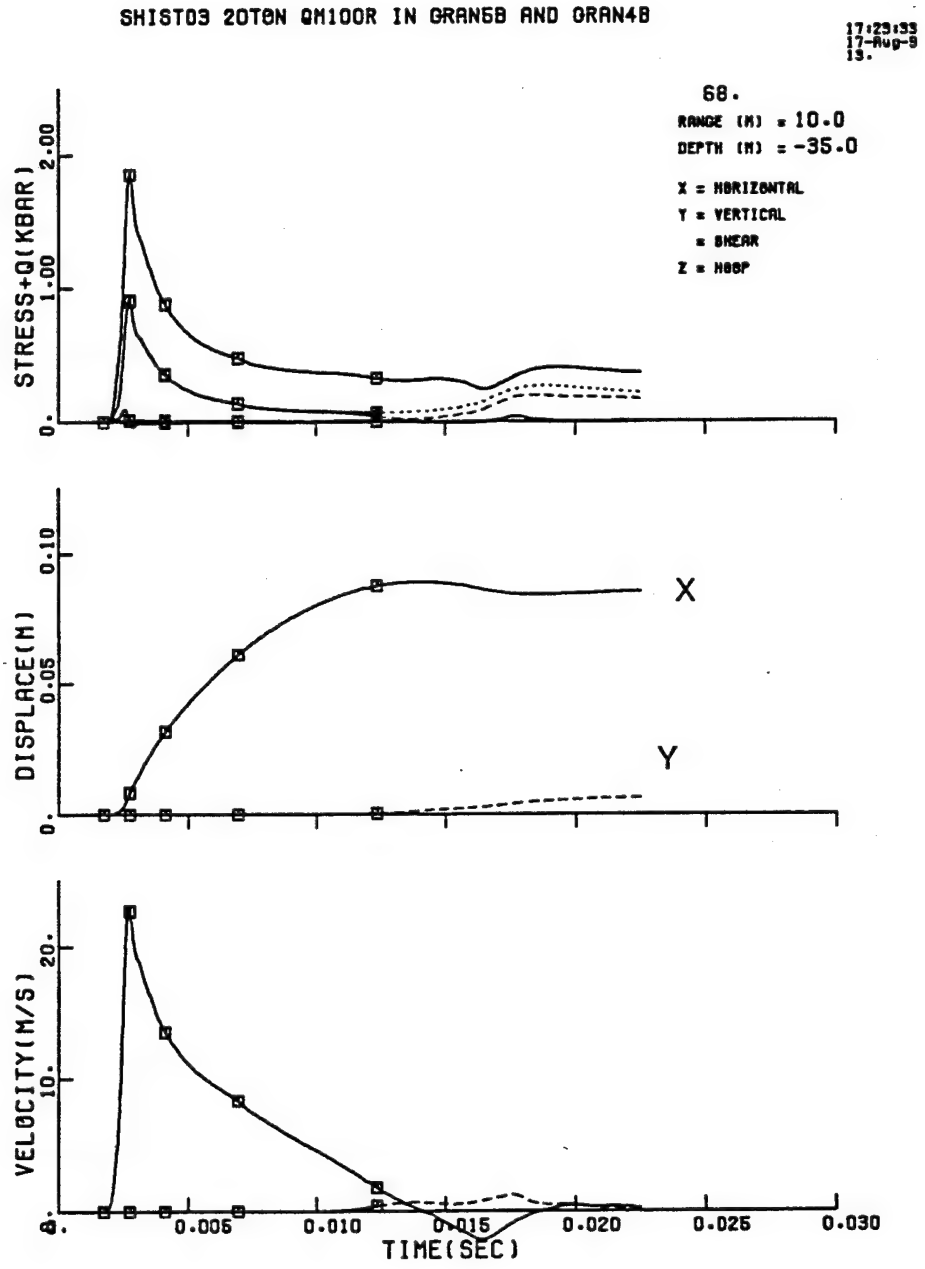


Figure 4-18. Target point 68 time history for 2DSHIST03 CRALE calculation.

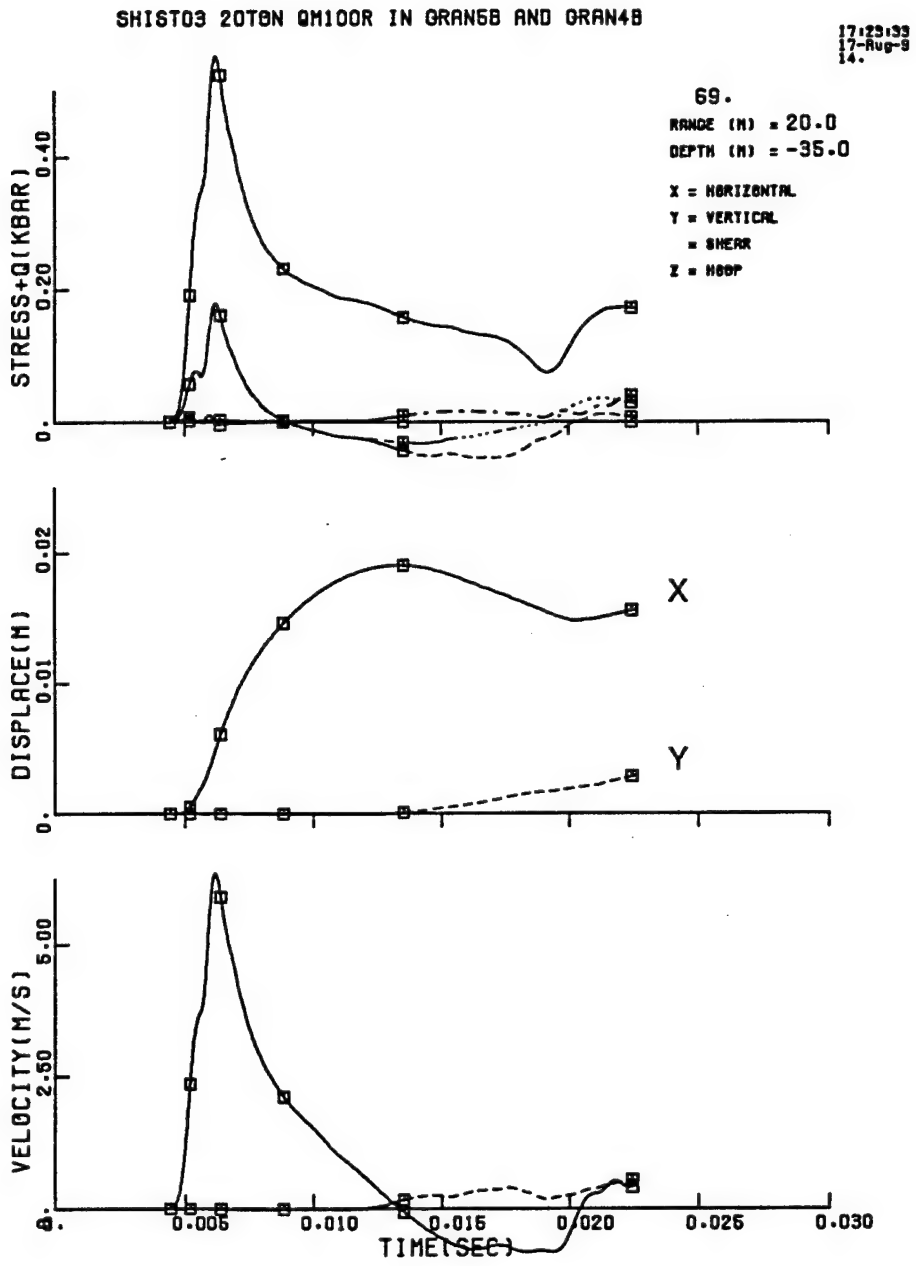


Figure 4-19. Target point 69 time history for 2DSHIST03 CRALE calculation.

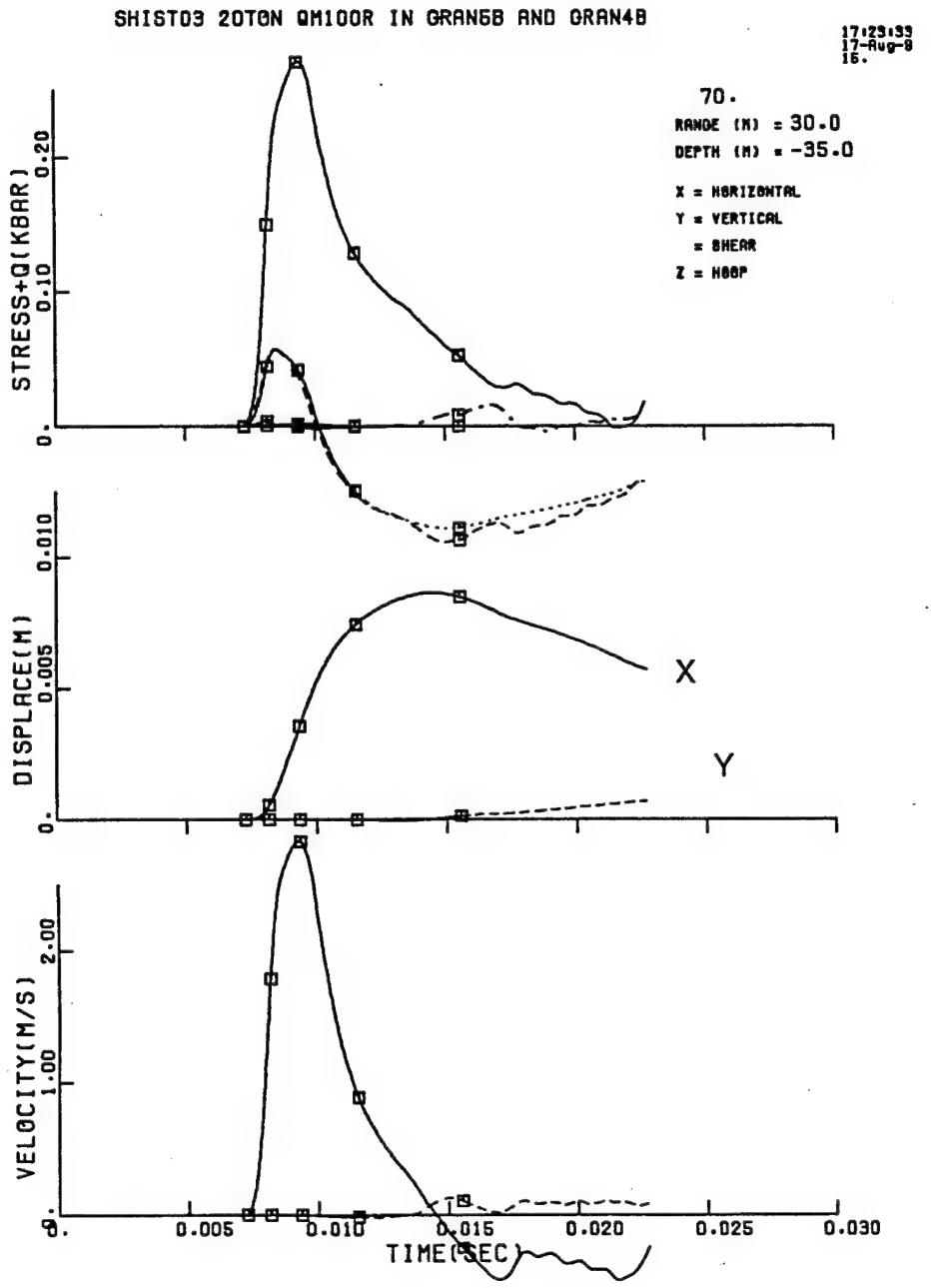


Figure 4-20. Target point 70 time history for 2DSHIST03 CRALE calculation.

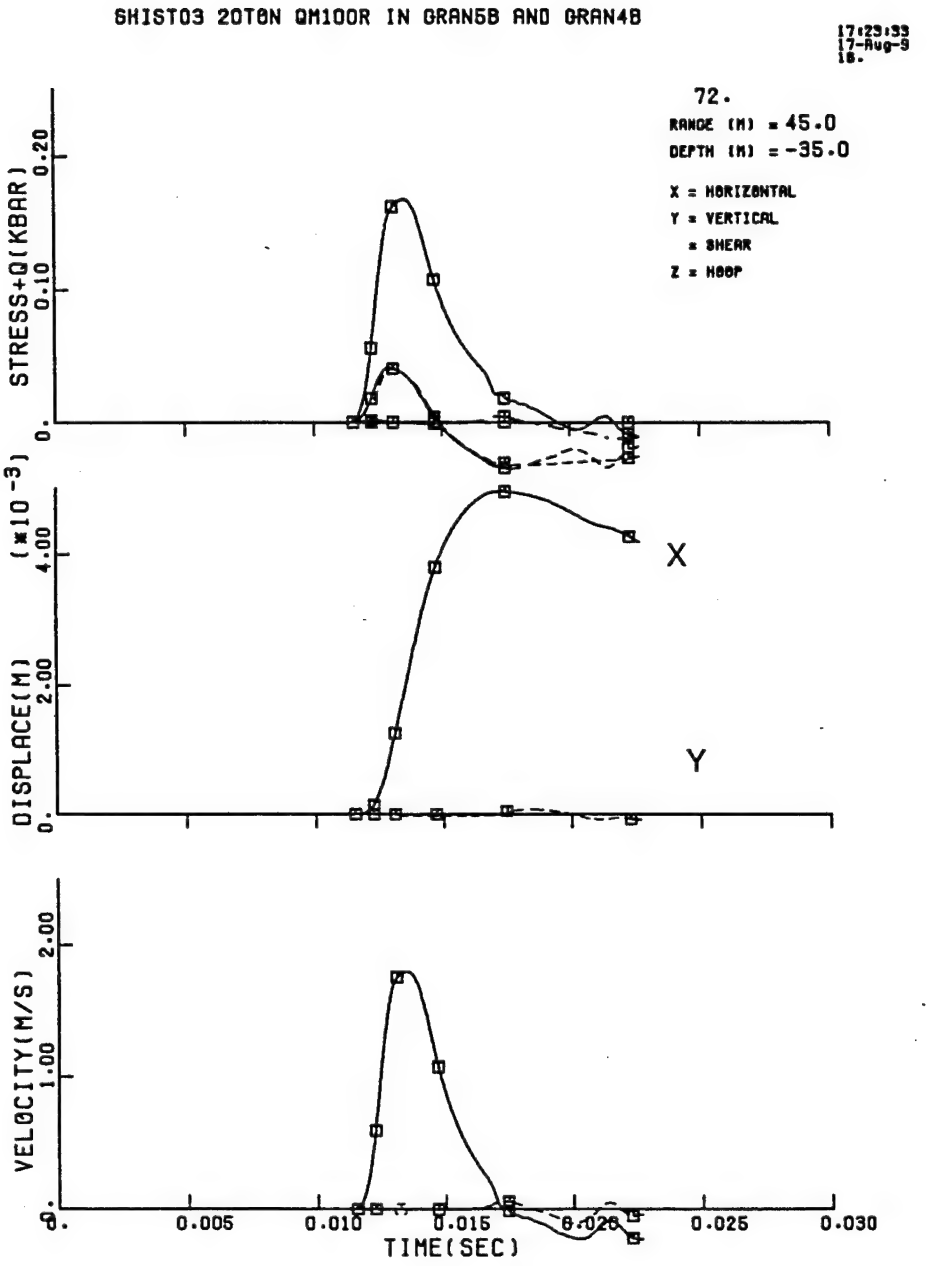


Figure 4-21. Target point 72 time history for 2DSHIST03 CRALE calculation.

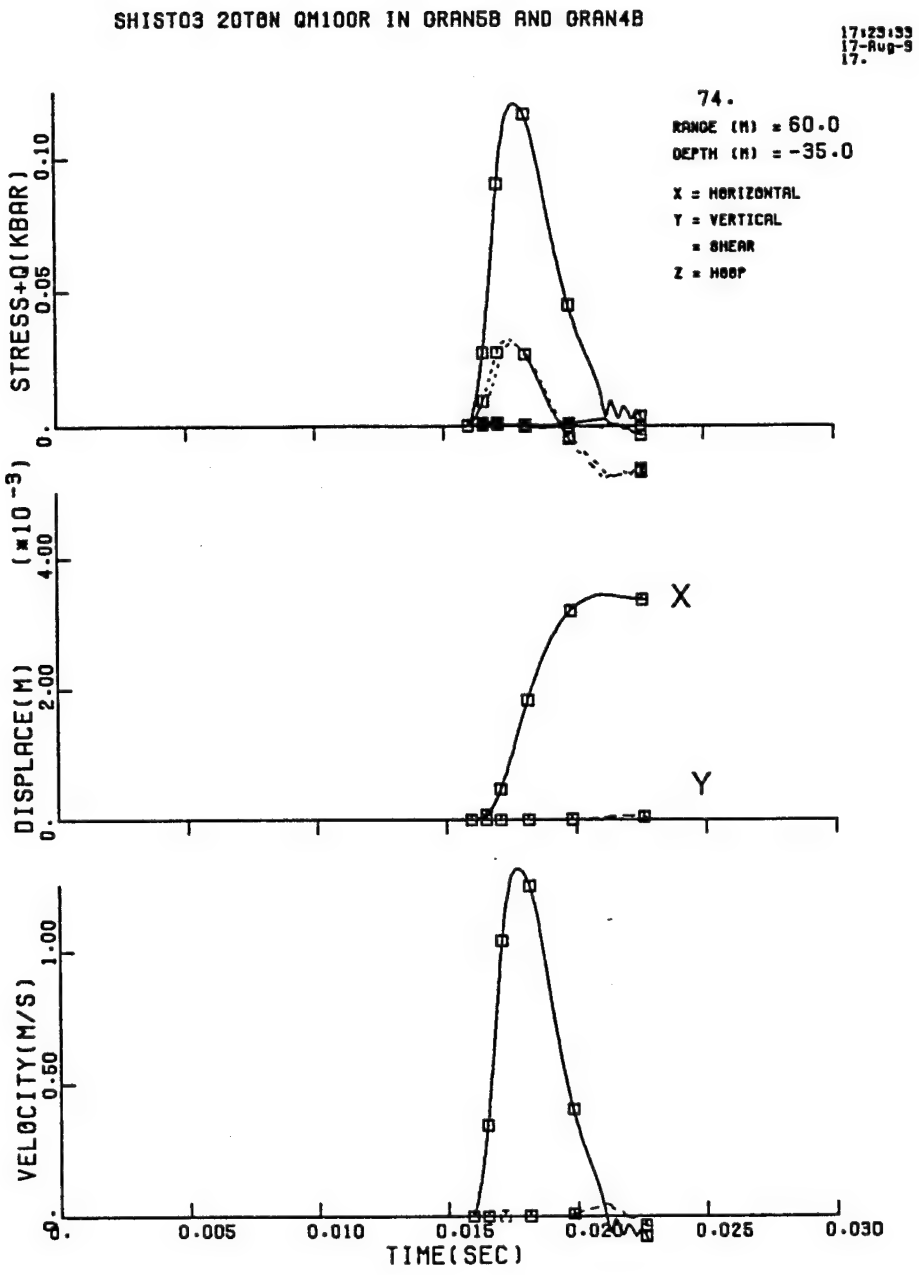


Figure 4-22. Target point 74 time history for 2DSHIST03 CRALE calculation.

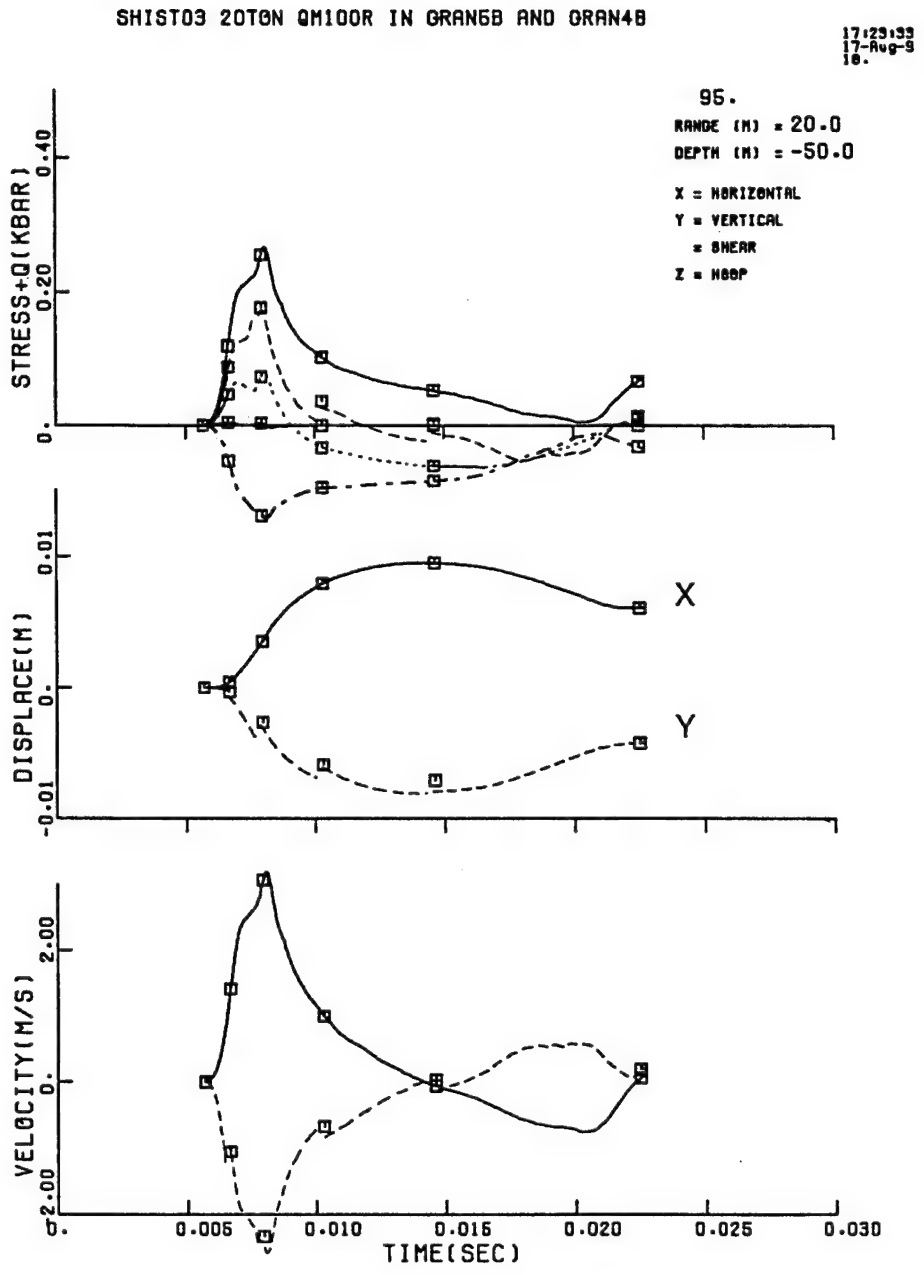


Figure 4-23. Target point 95 time history for 2DSHIST03 CRALE calculation.

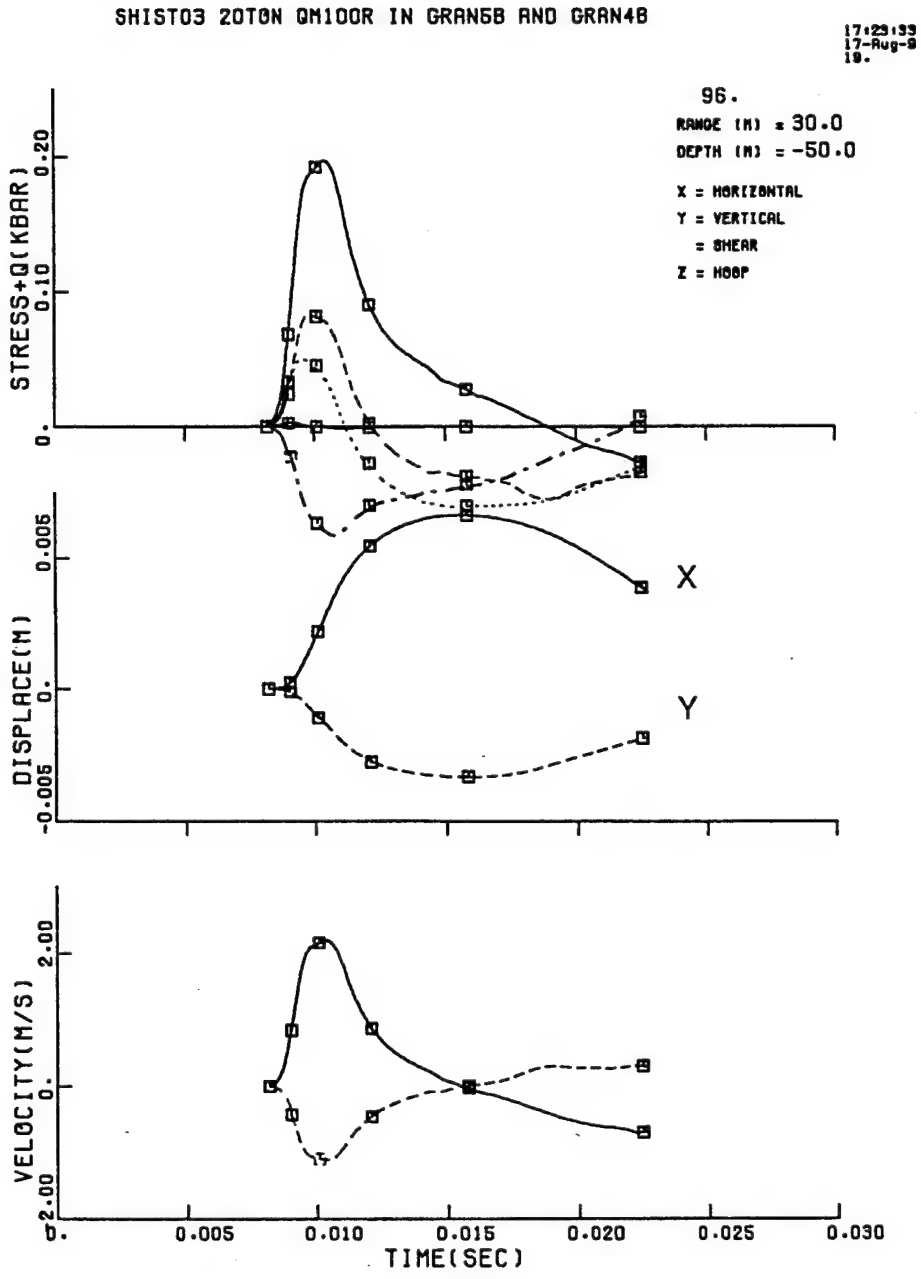


Figure 4-24. Target point 96 time history for 2DSHIST03 CRALE calculation.

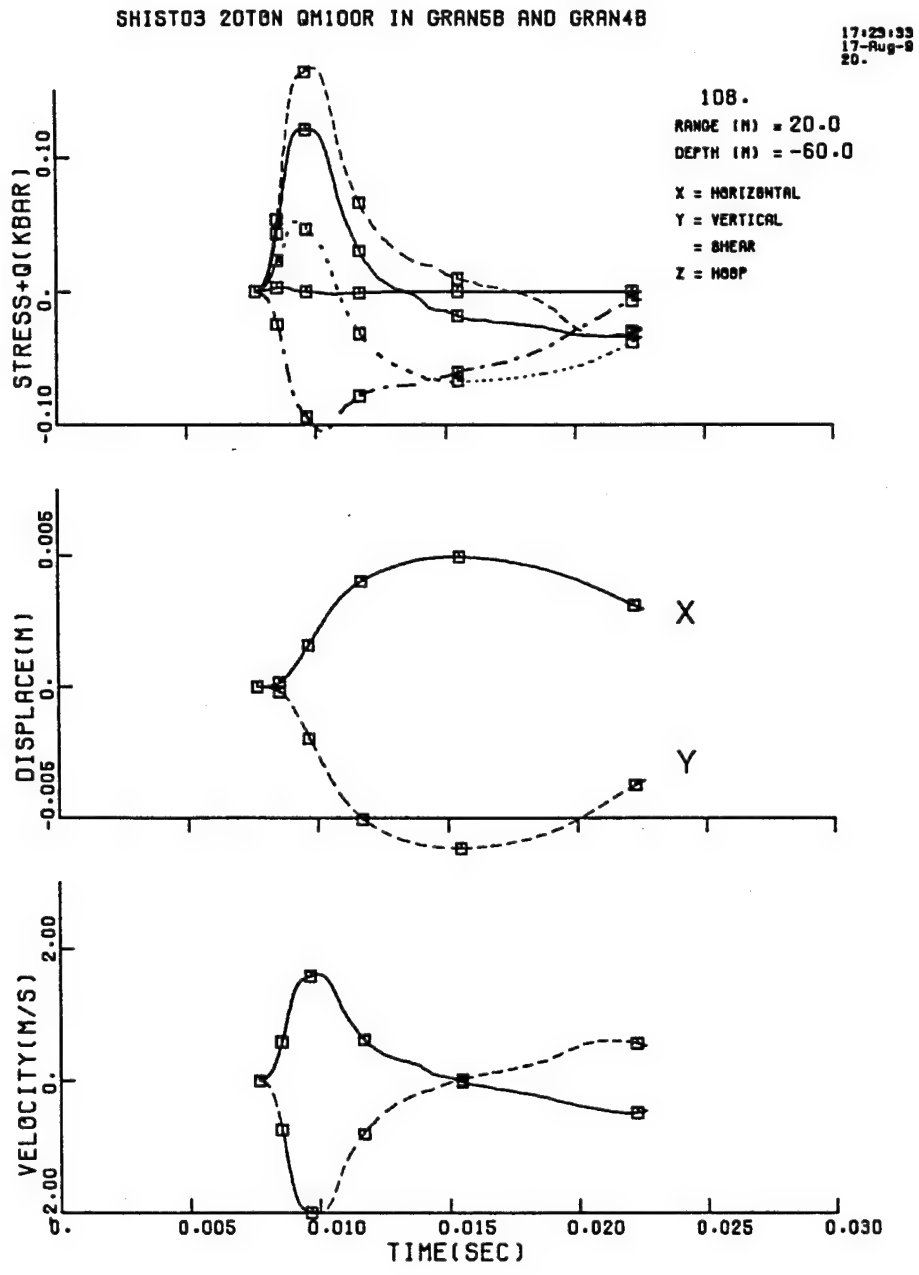


Figure 4-25. Target point 108 time history for 2DSHIST03 CRALE calculation.

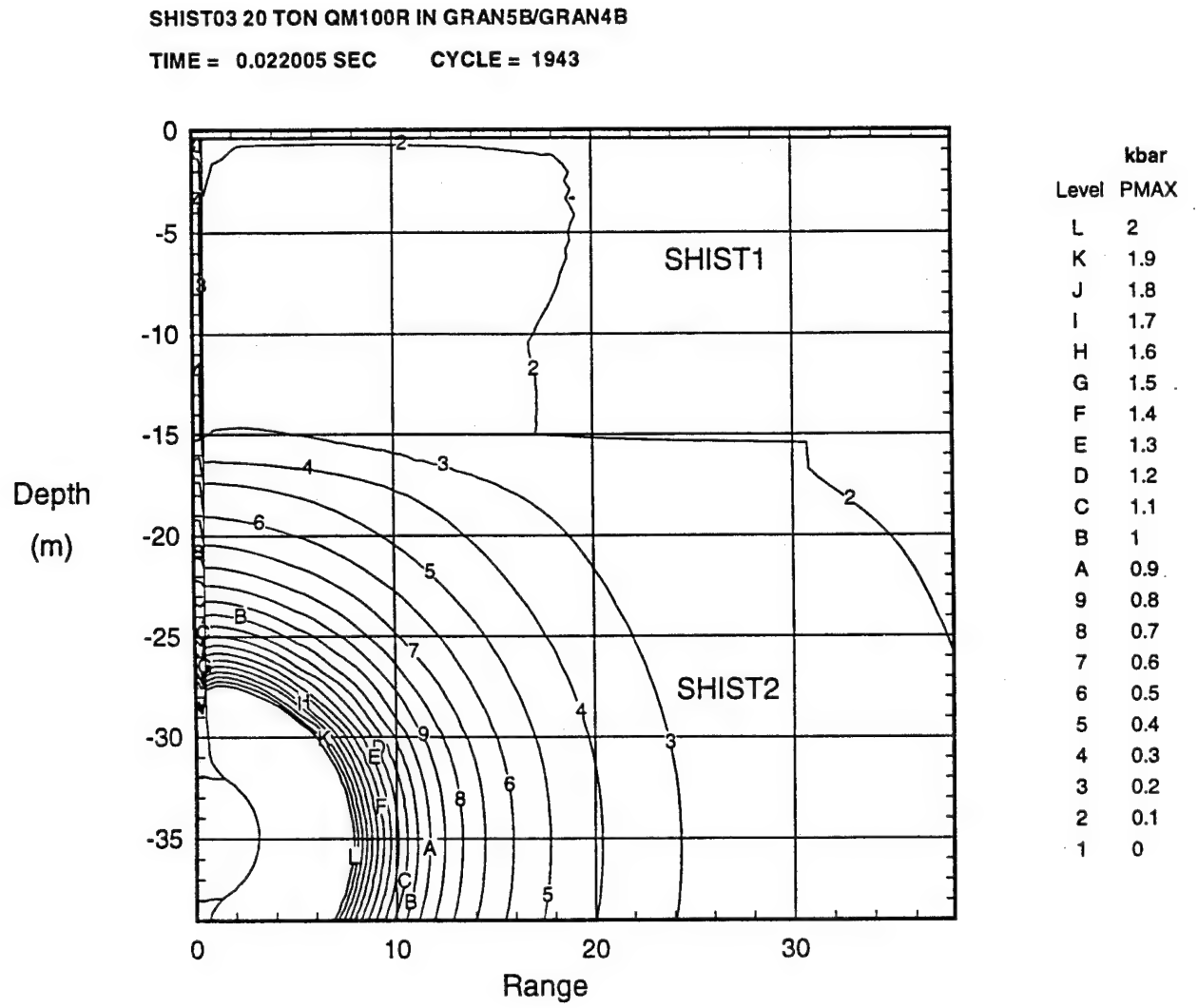


Figure 4-26. Peak stress contours for the 2DSHIST03 CRALE calculation SHIST1 (GRAN4B, 1,550m/s, 1.7%AFV) to 15 meter depth with SHIST2 (GRAN5B, 3,400m/s, 1.1%AFV) below.

## 4.3 CRALE 2D CALCULATION 2DSHIST02.

### HOMOGENEOUS SHIST2 (GRAN5B, 3,400 M/S, 1.1% AFV)

The second calculation of this study, 2DSHIST02, consisted of a homogeneous site of SHIST2 (GRAN5B, 3,400 m/s, 1.1% AFV). The shock propagation in this calculation is spherical until it hits the free surface, at which time a relief wave propagates back into the ground. Figures 4-27 through 4-29 show velocity vector fields from the calculation at 8, 16, and 22 msec respectively in which the surface relief can be observed. The vertical and horizontal stress, velocity, and displacement waveforms for the target points at the experimental gage locations are included as Figures 4-30 through 4-50. The peak stress contours for the 2DSHIST02 calculation are shown in Figure 4-51.

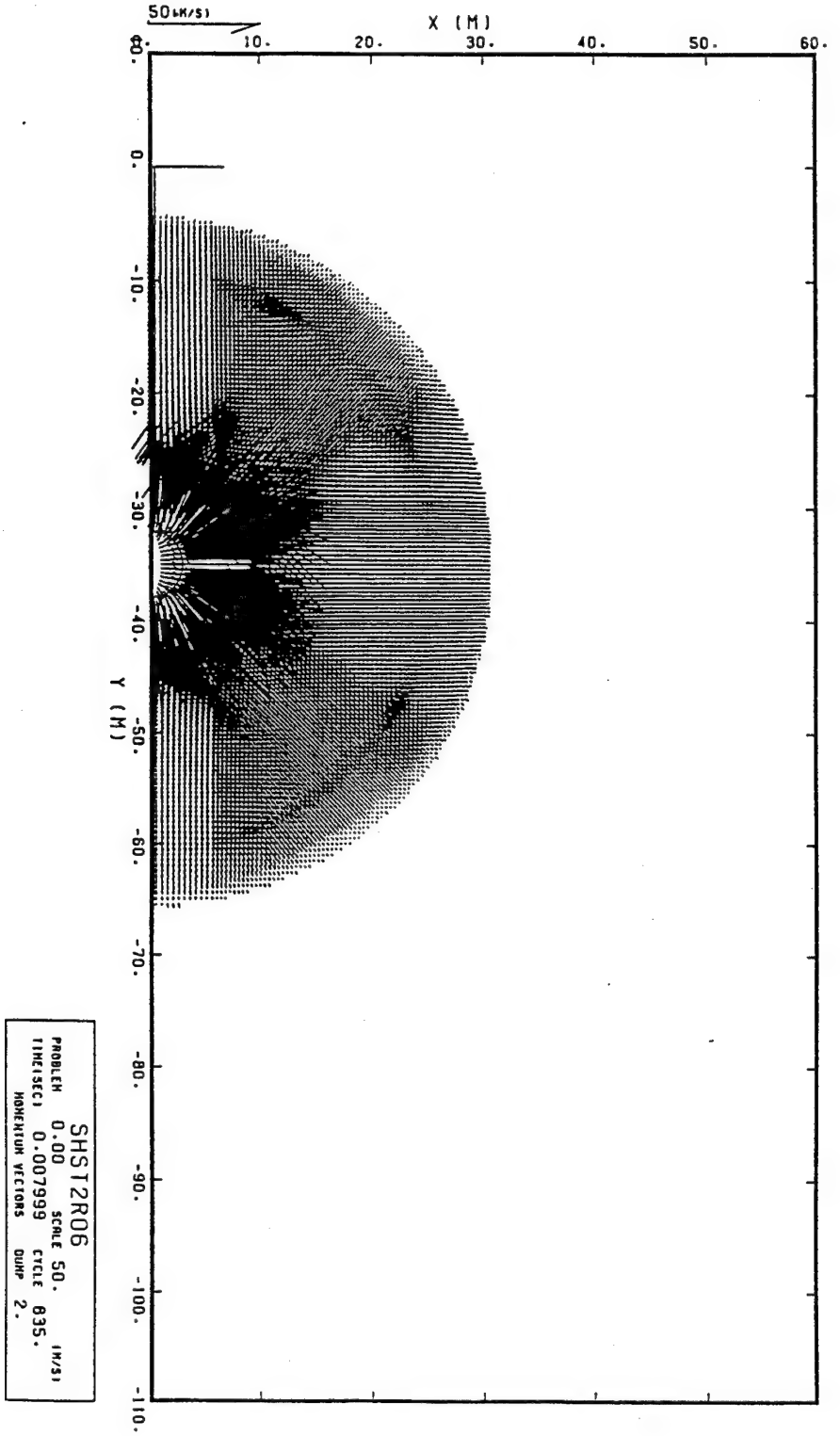


Figure 4-27. Velocity vector field at 8 msec for 2DSHIST02 CRALE calculation.

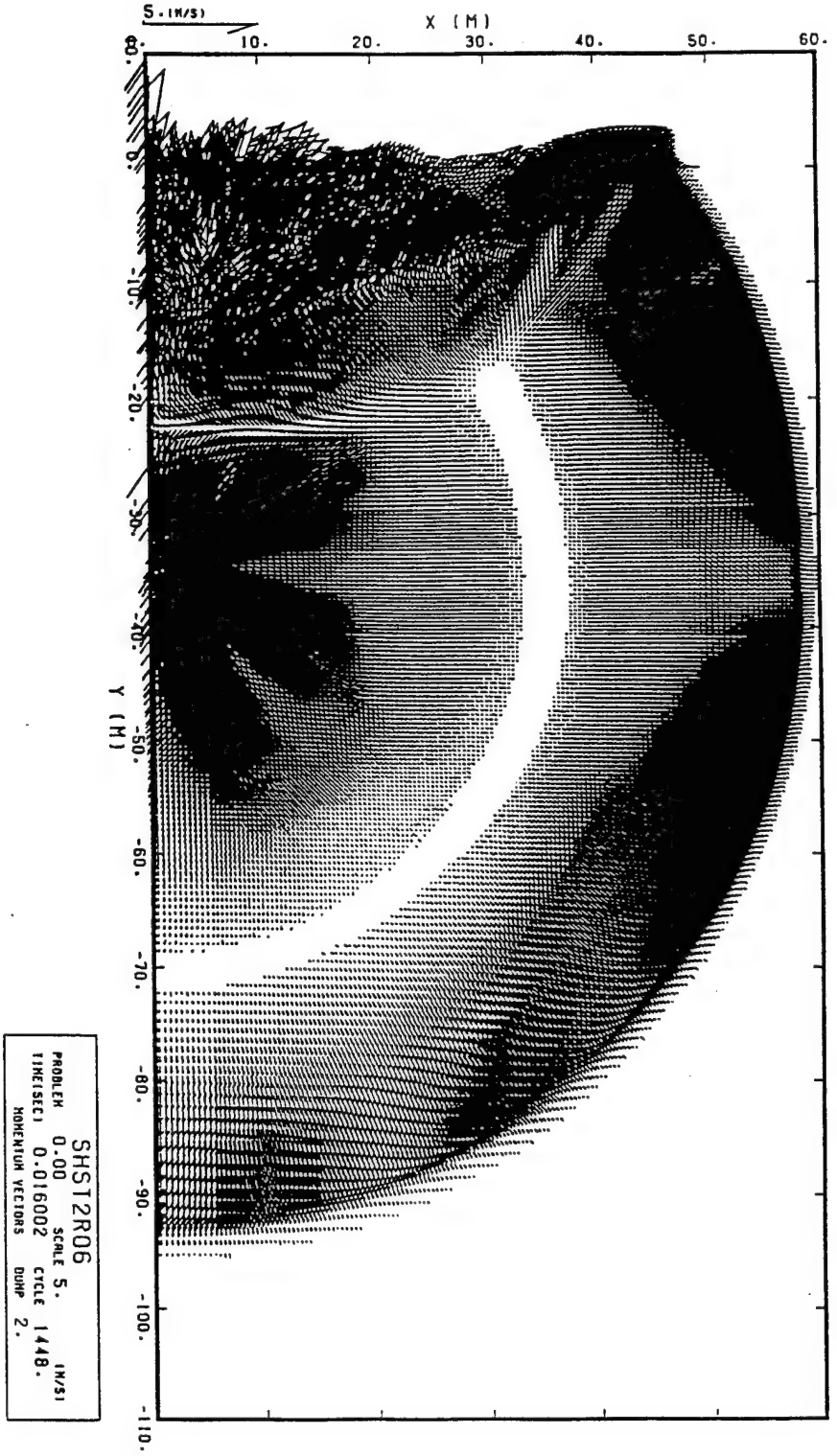


Figure 4-28. Velocity vector field at 16 msec for 2DSHIST02 CRALE calculation.

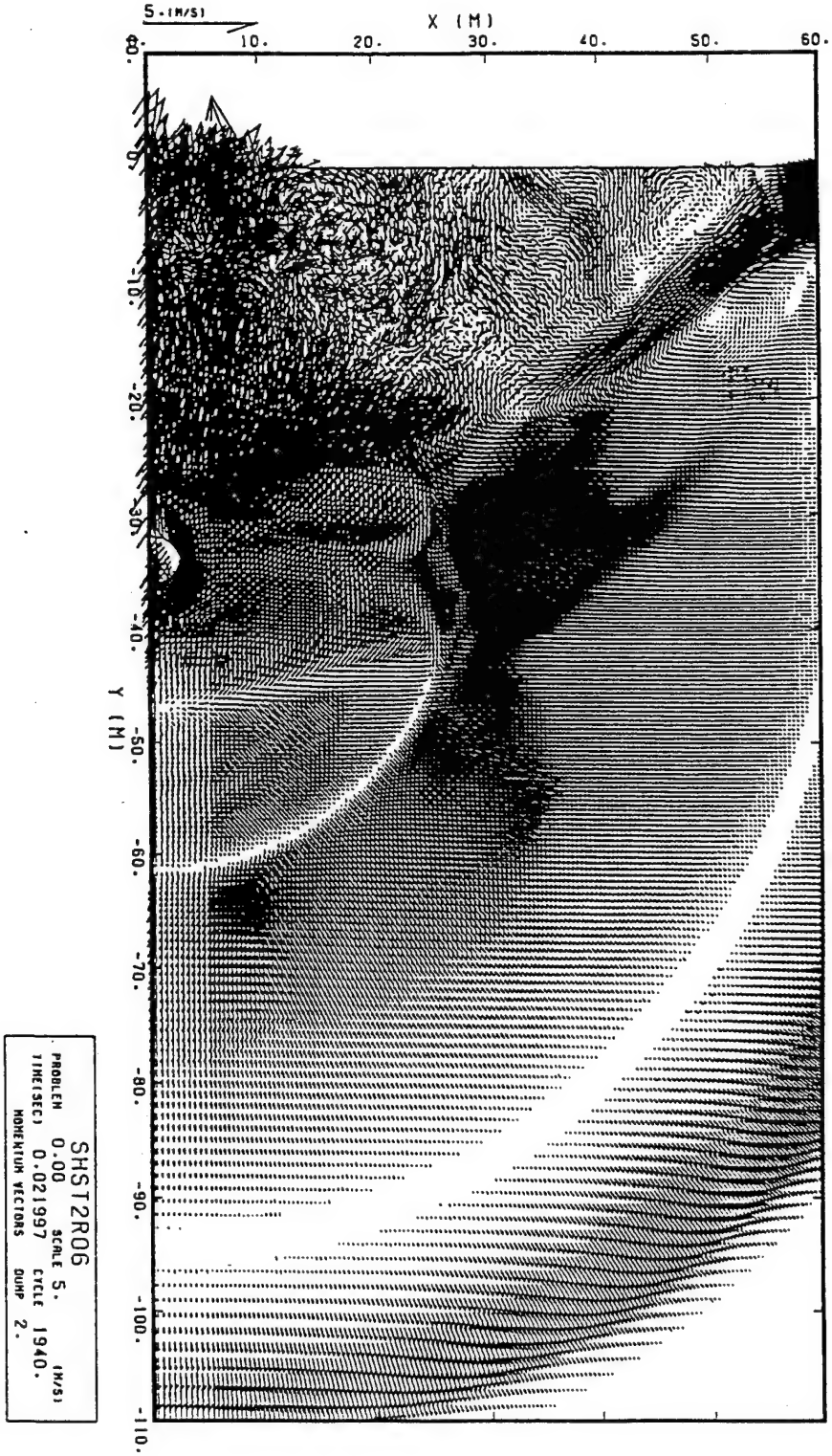


Figure 4-29. Velocity vector field at 22 msec for 2DSHIST02 CRALE calculation.

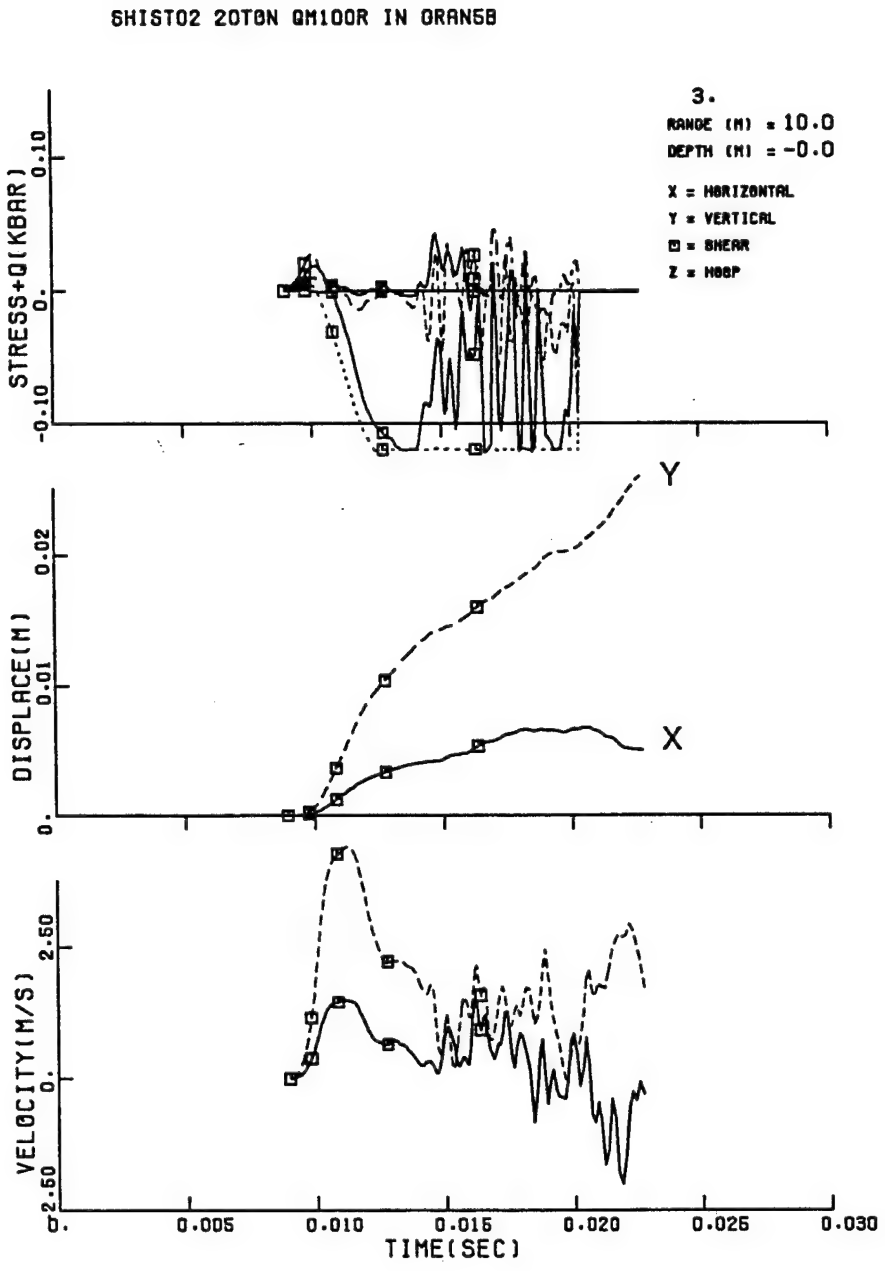


Figure 4-30. Target point 3 time history for 2DSHIST02 CRALE calculation.

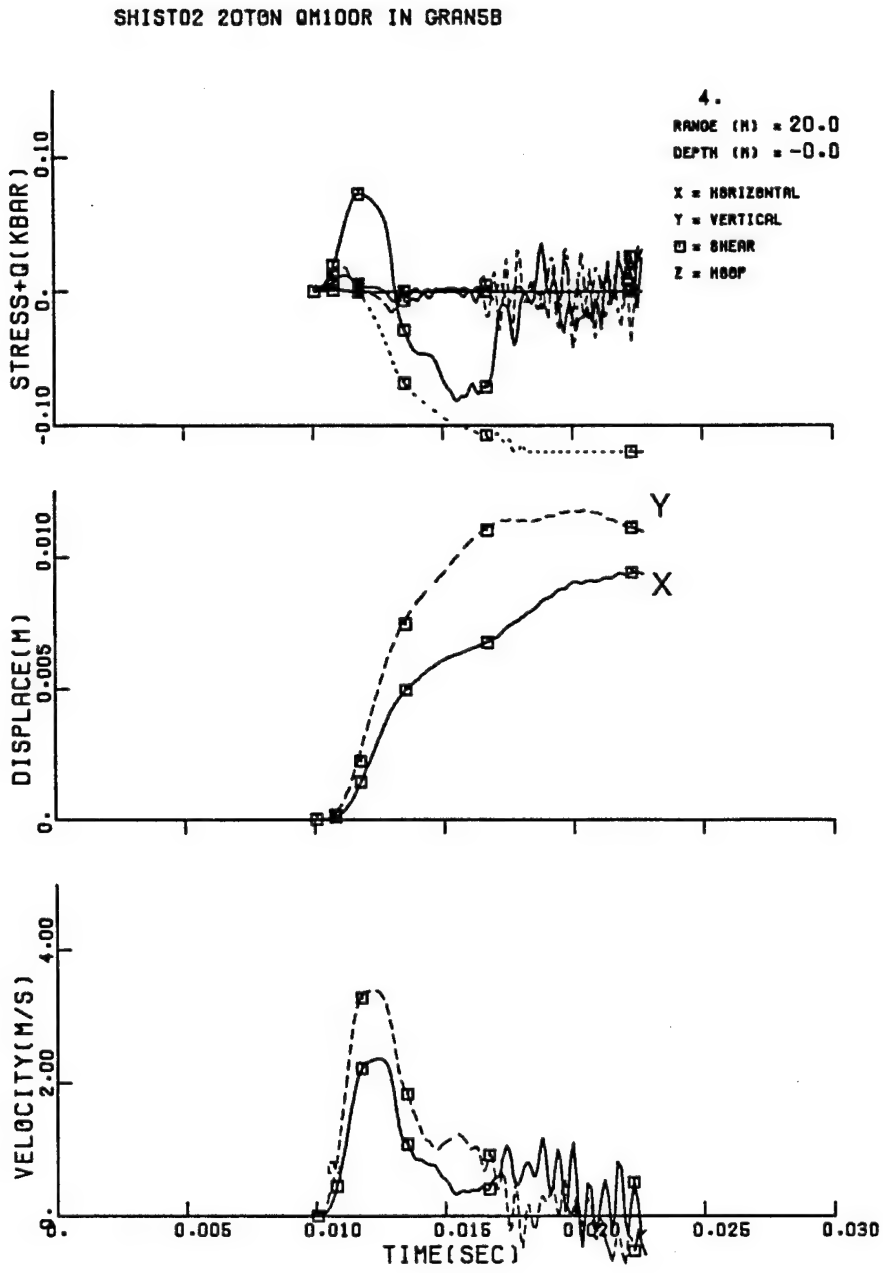


Figure 4-31. Target point 4 time history for 2DSHIST02 CRALE calculation.

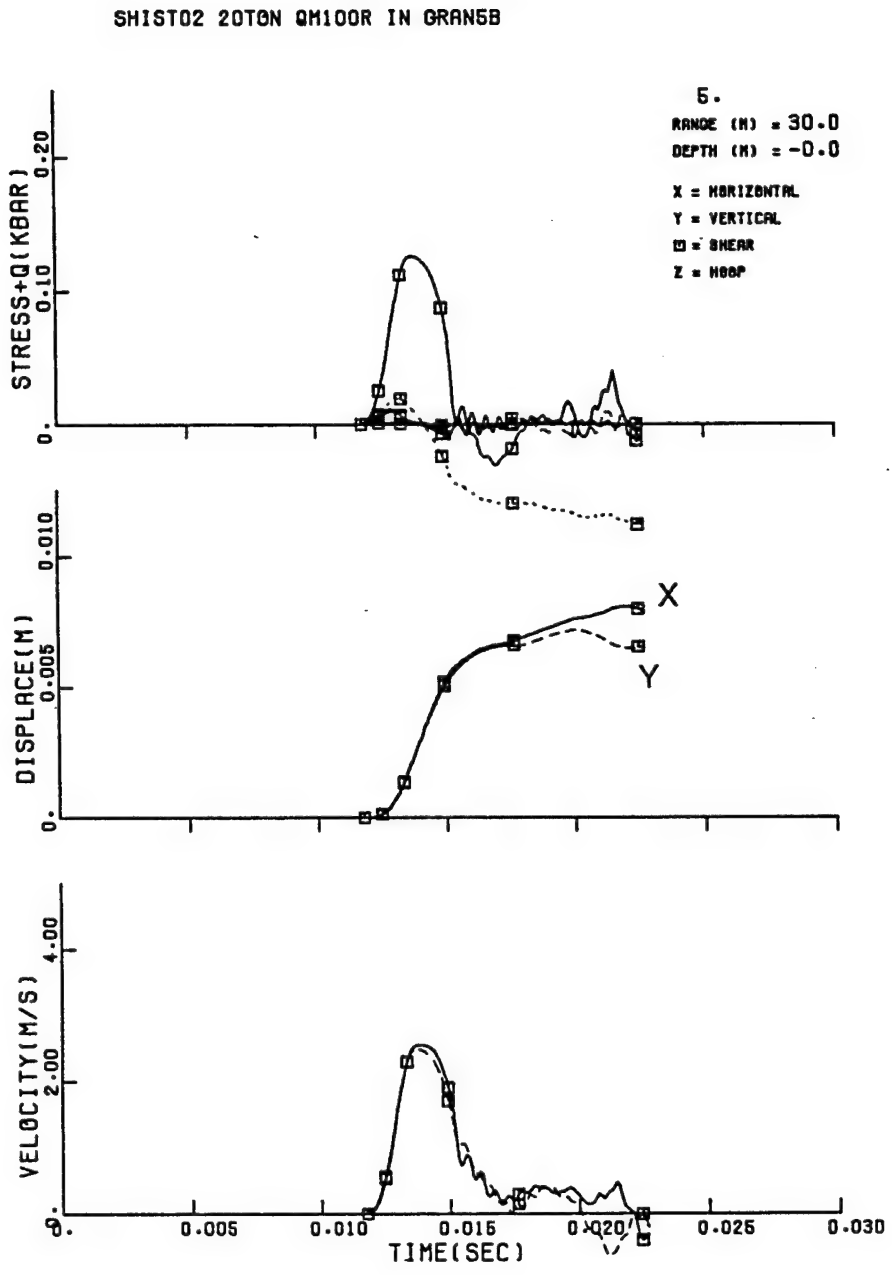


Figure 4-32. Target point 5 time history for 2DSHIST02 CRALE calculation.

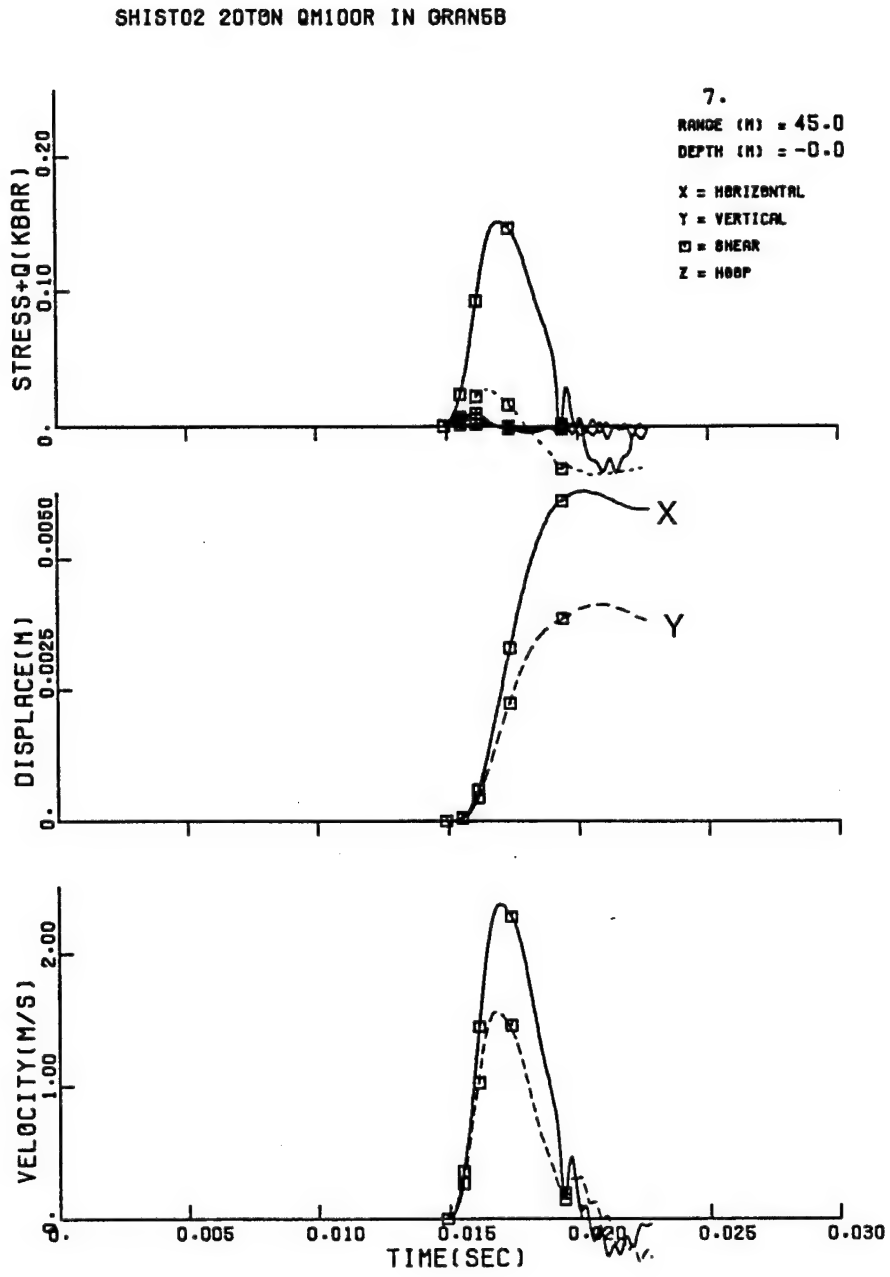


Figure 4-33. Target point 7 time history for 2DSHIST02 CRALE calculation.

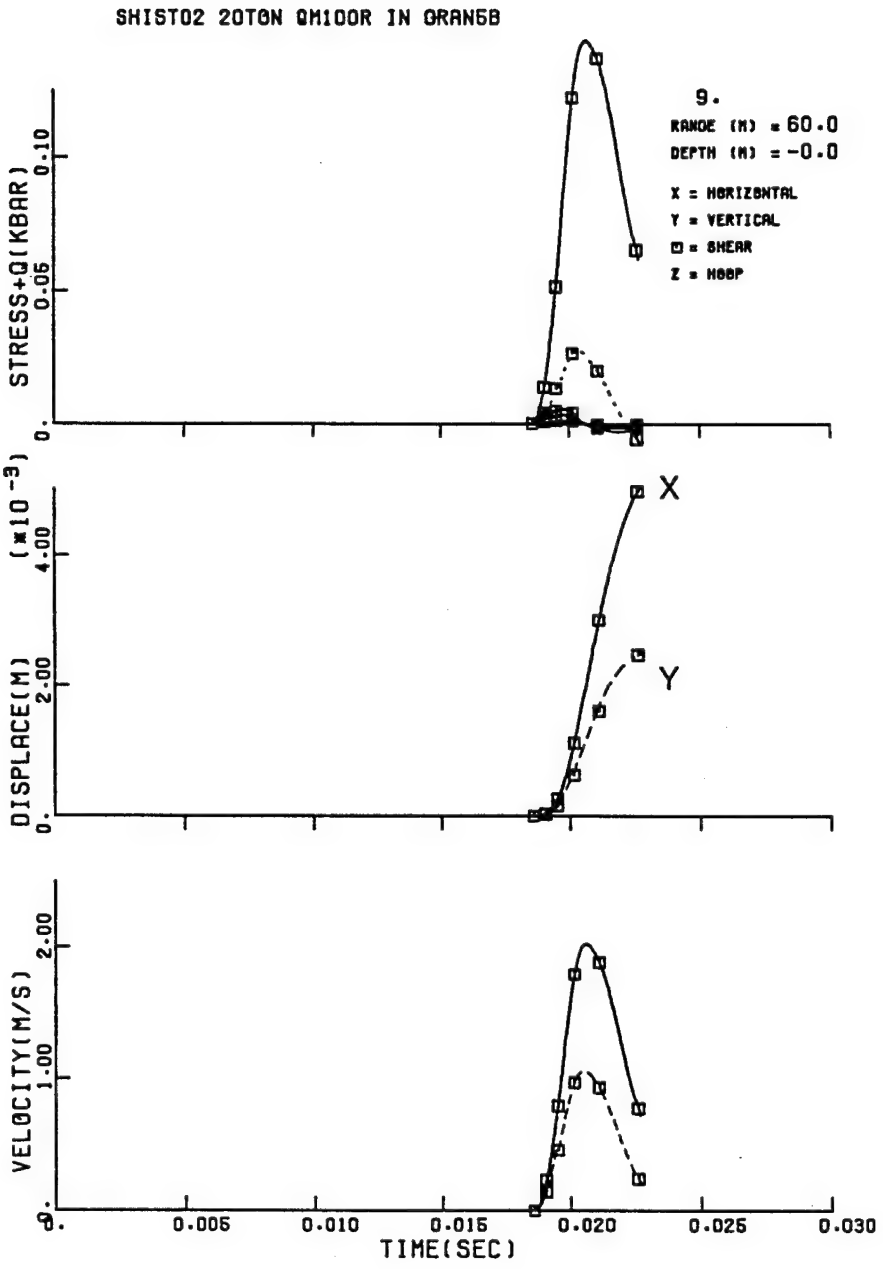


Figure 4-34. Target point 9 time history for 2DSHIST02 CRALE calculation.

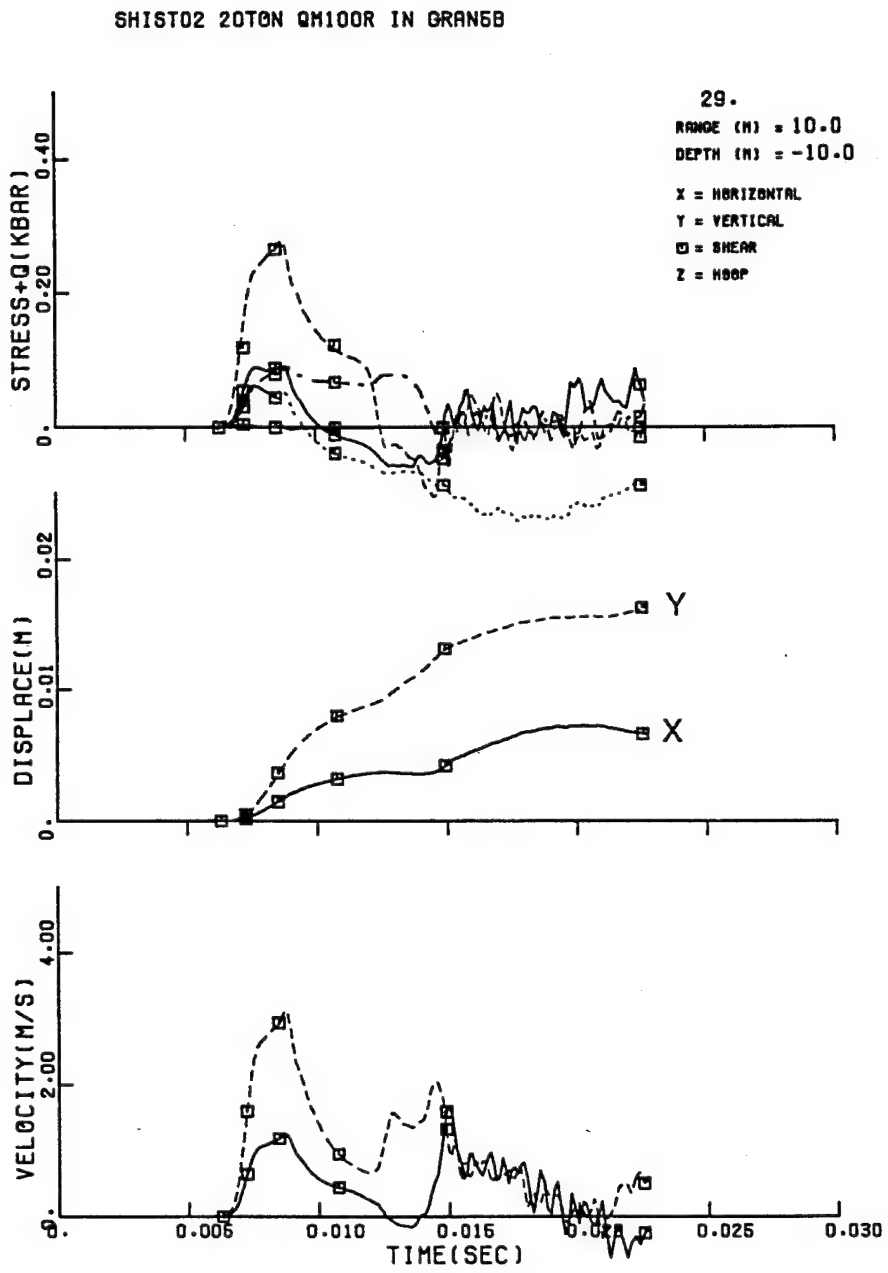


Figure 4-35. Target point 29 time history for 2DSHIST02 CRALE calculation.

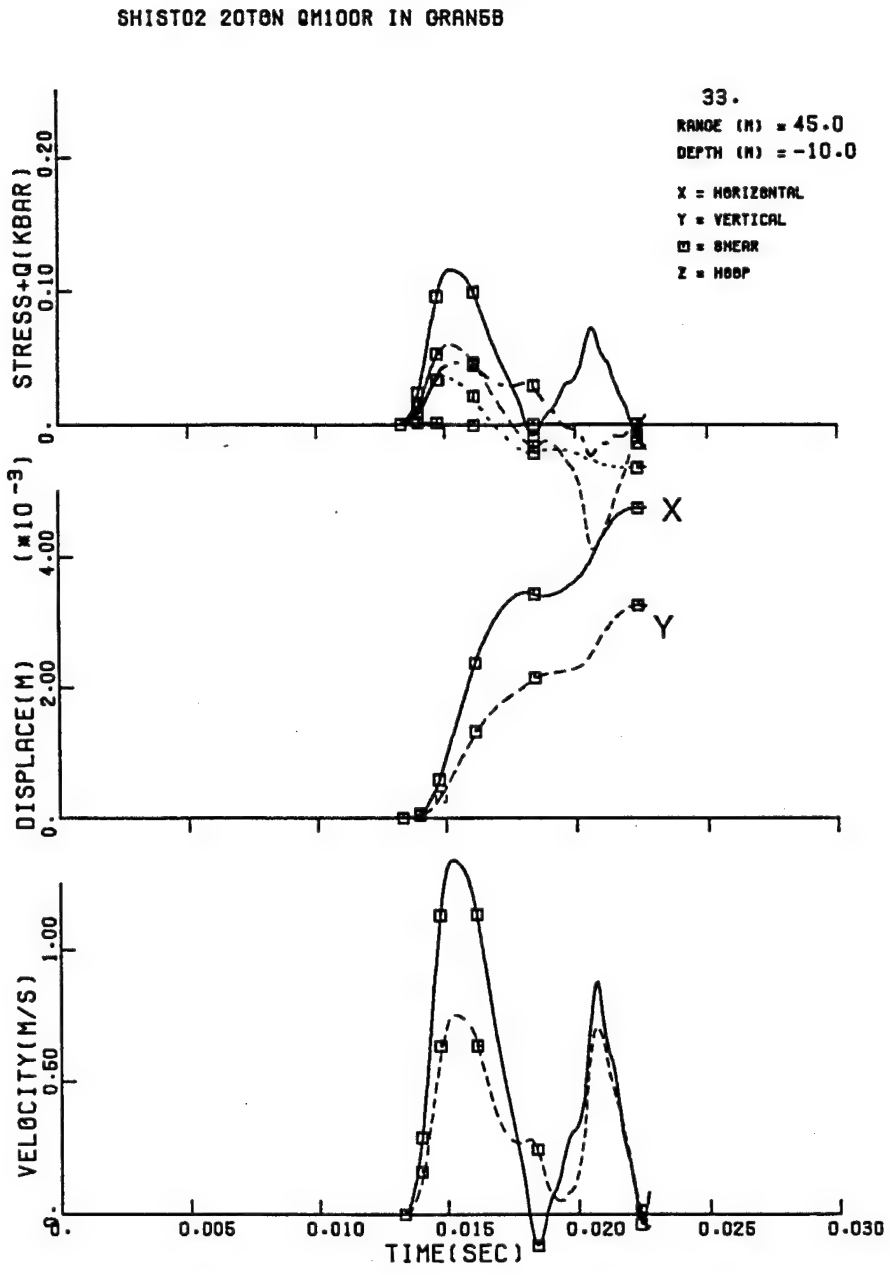


Figure 4-36. Target point 33 time history for 2DSHIST02 CRALE calculation.

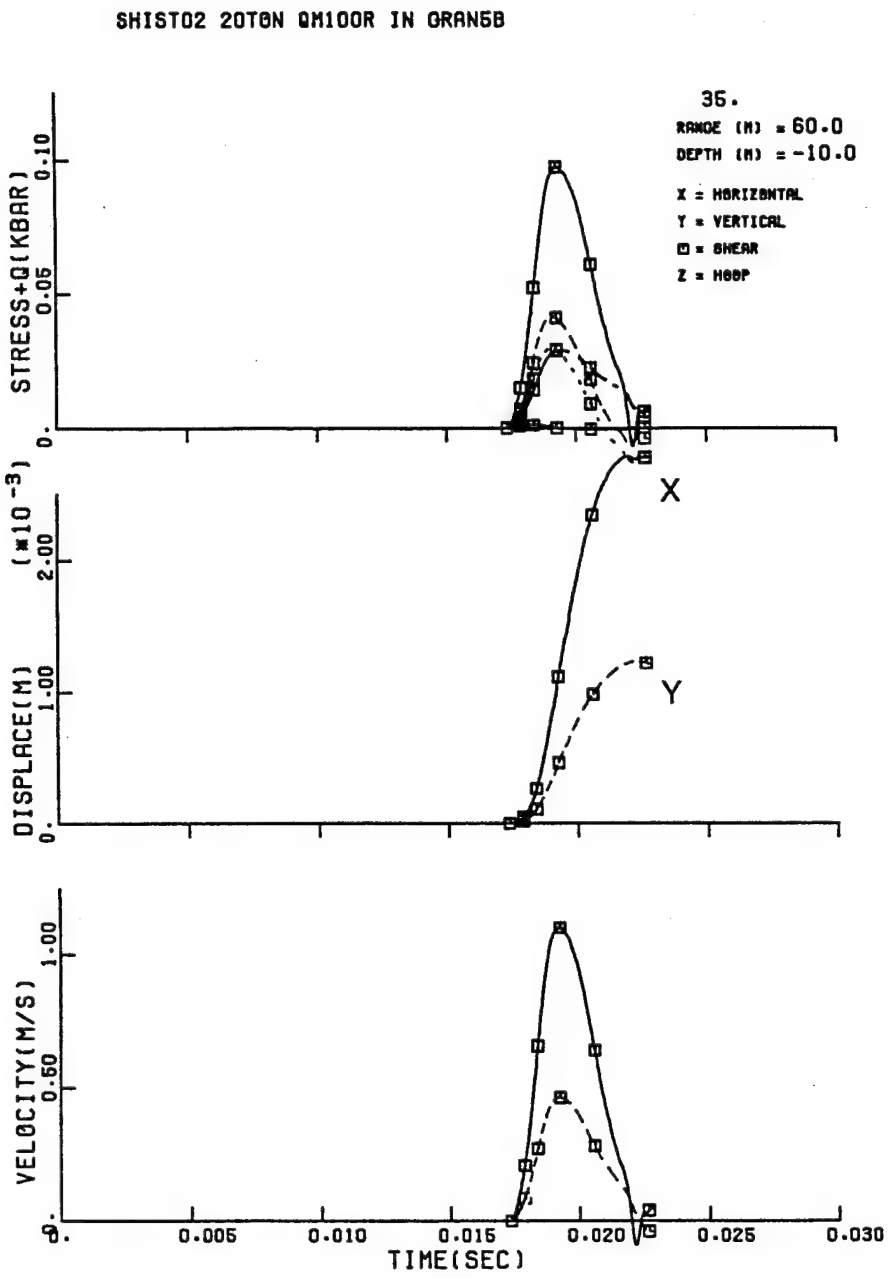


Figure 4-37. Target point 35 time history for 2DSHIST02 CRALE calculation.

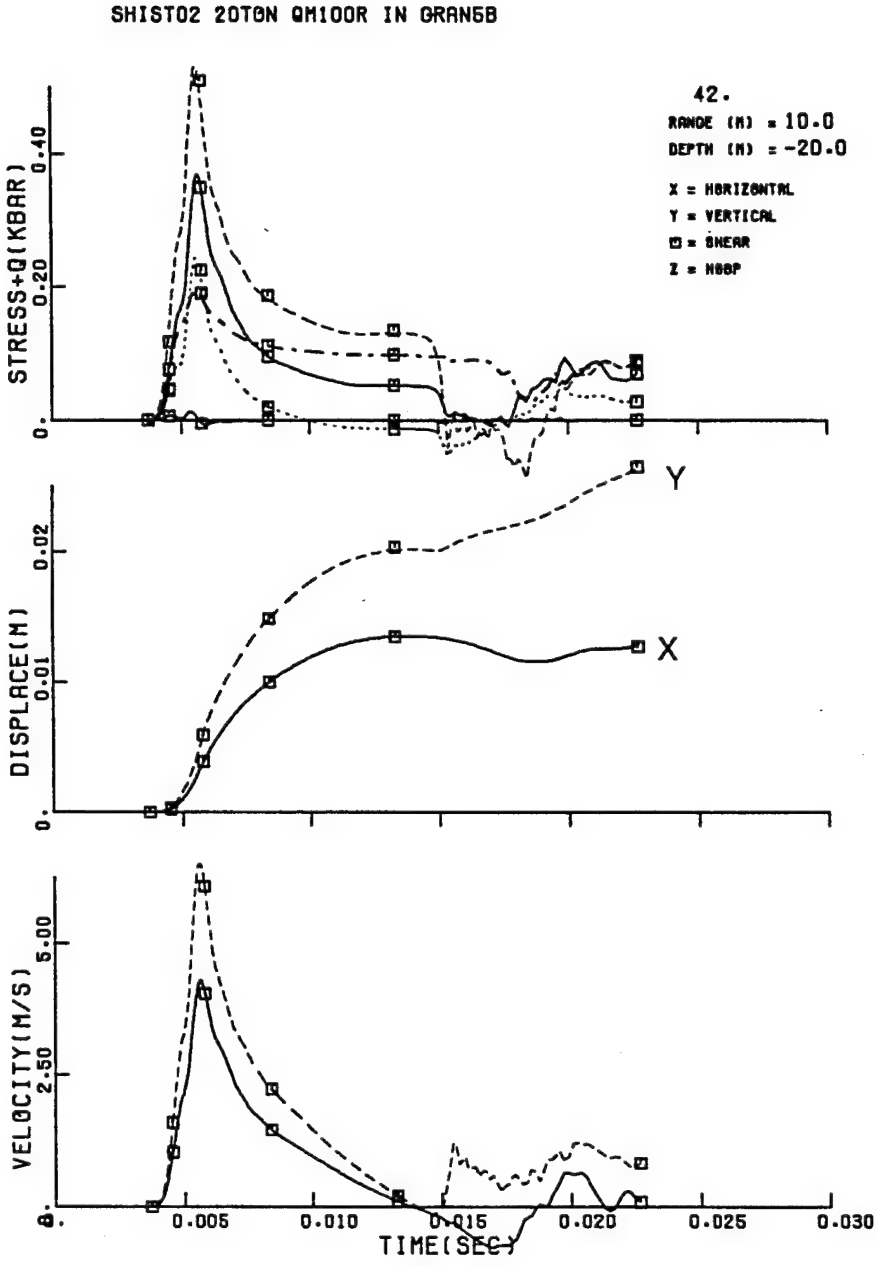


Figure 4-38. Target point 42 time history for 2DSHIST02 CRALE calculation.

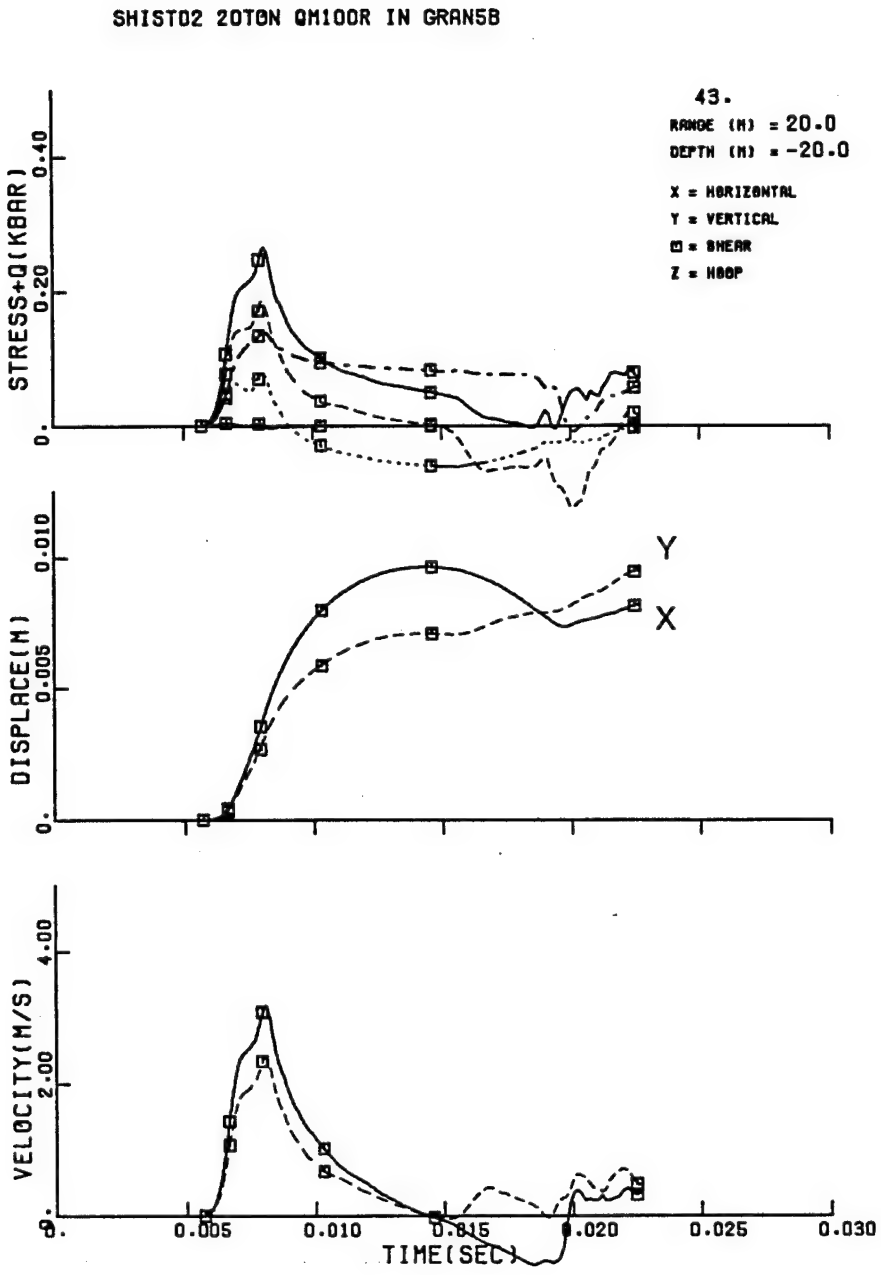


Figure 4-39. Target point 43 time history for 2DSHIST02 CRALE calculation.

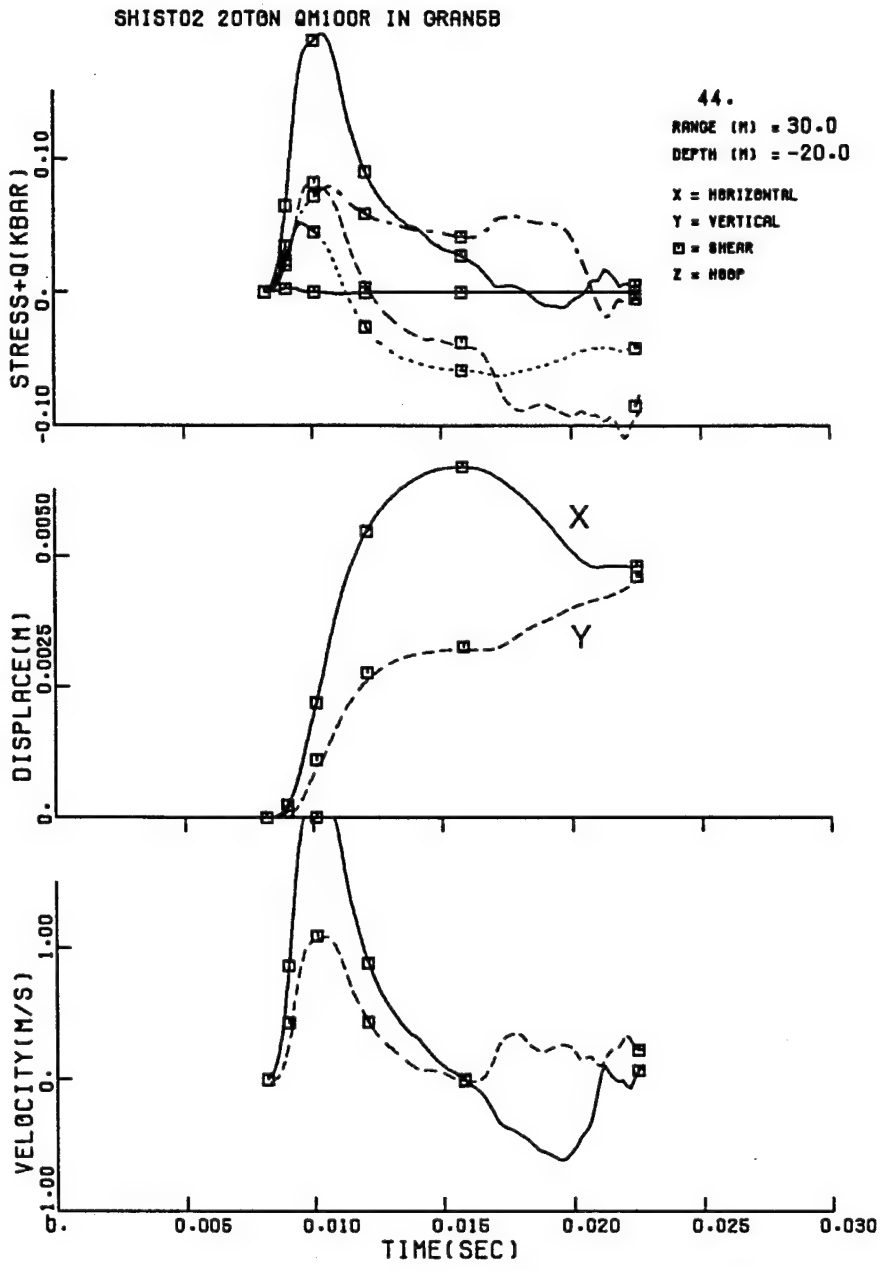


Figure 4-40. Target point 44 time history for 2DSHIST02 CRALE calculation.

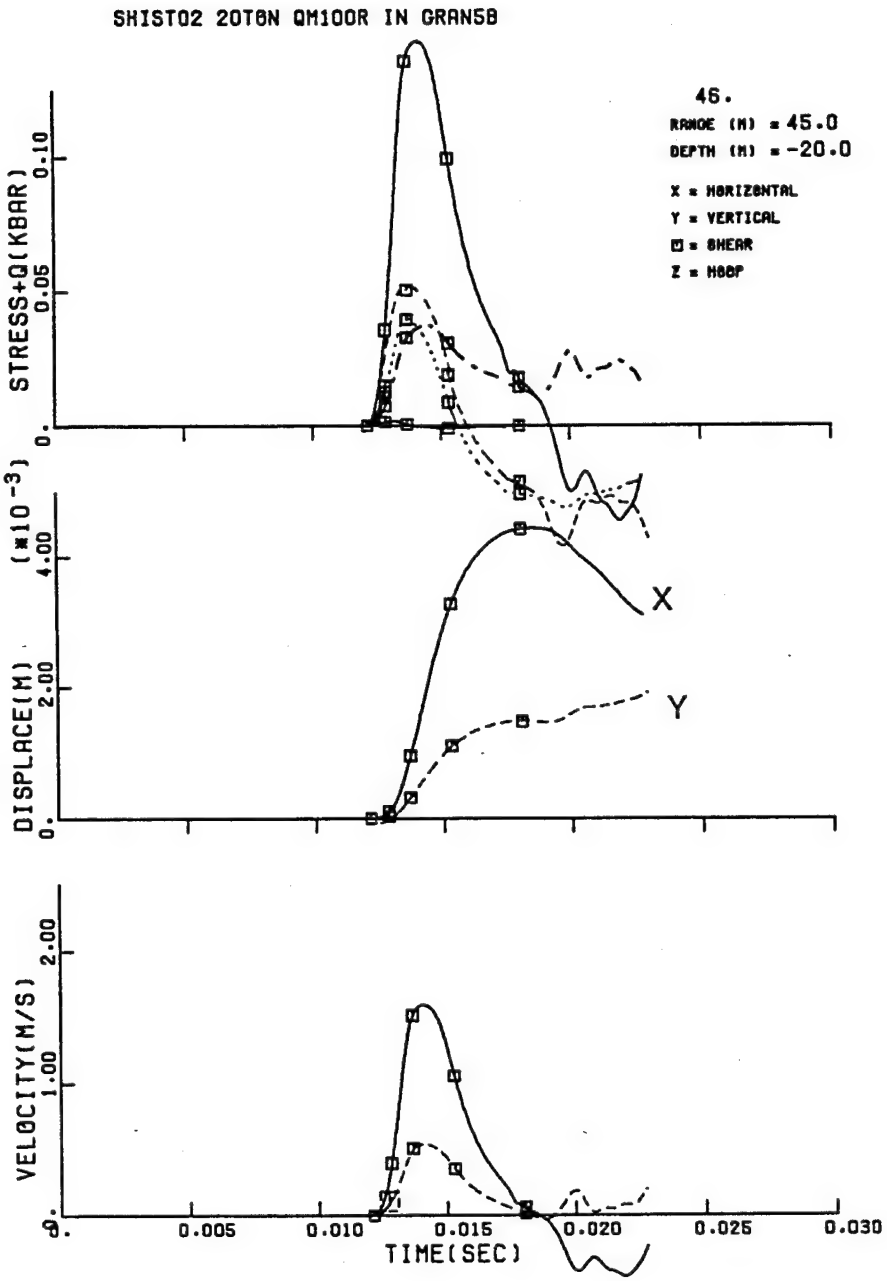


Figure 4-41. Target point 46 time history for 2DSHIST02 CRALE calculation.

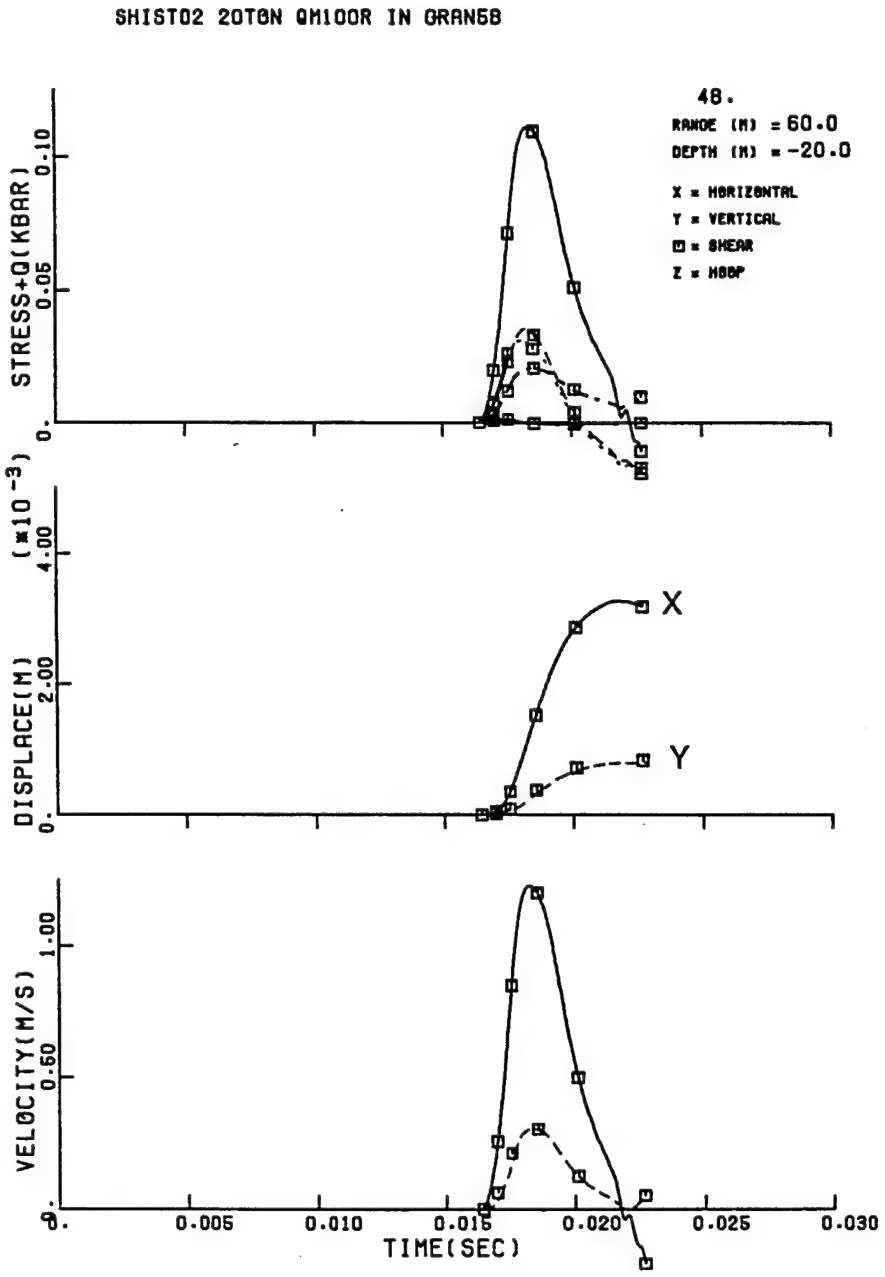


Figure 4-42. Target point 48 time history for 2DSHIST02 CRALE calculation.

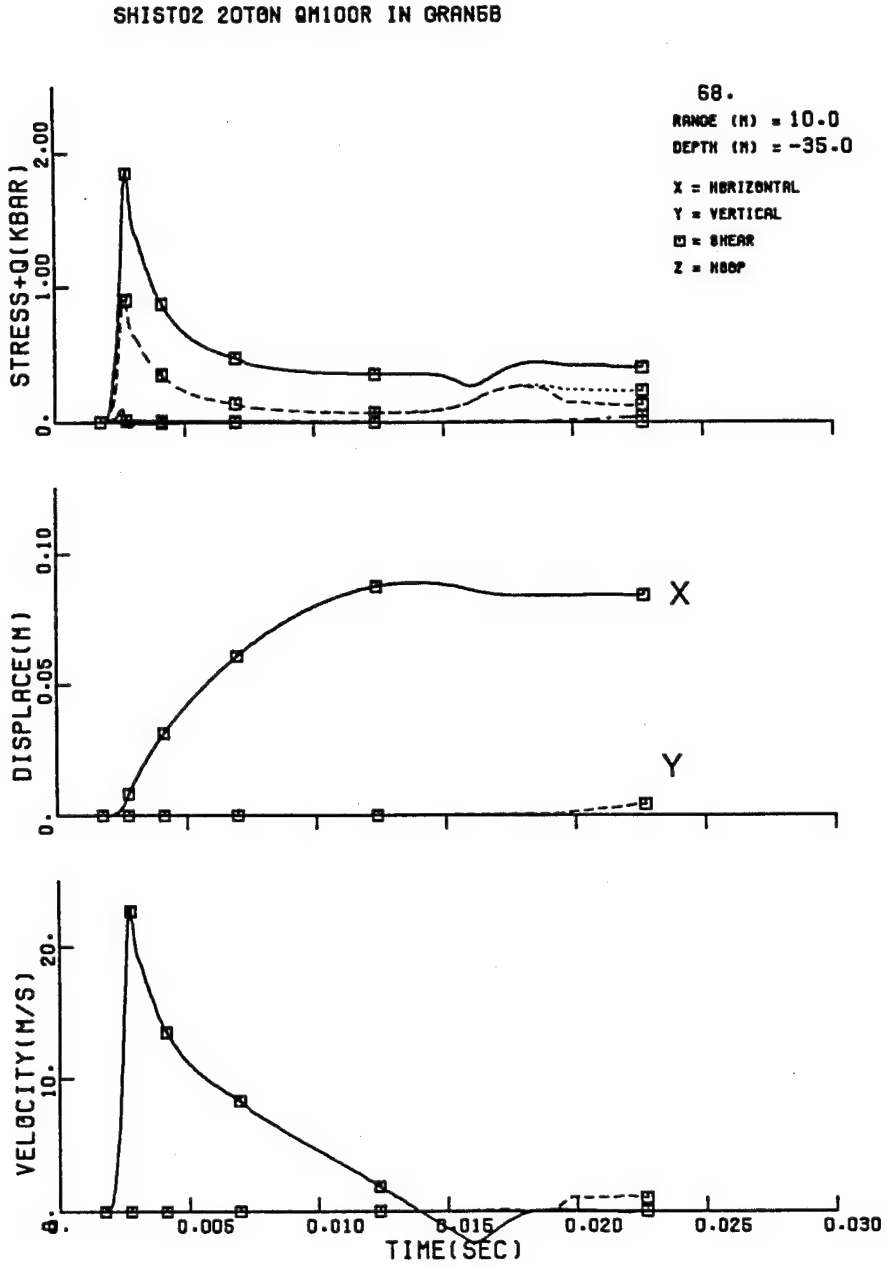


Figure 4-43. Target point 68 time history for 2DSHIST02 CRALE calculation .

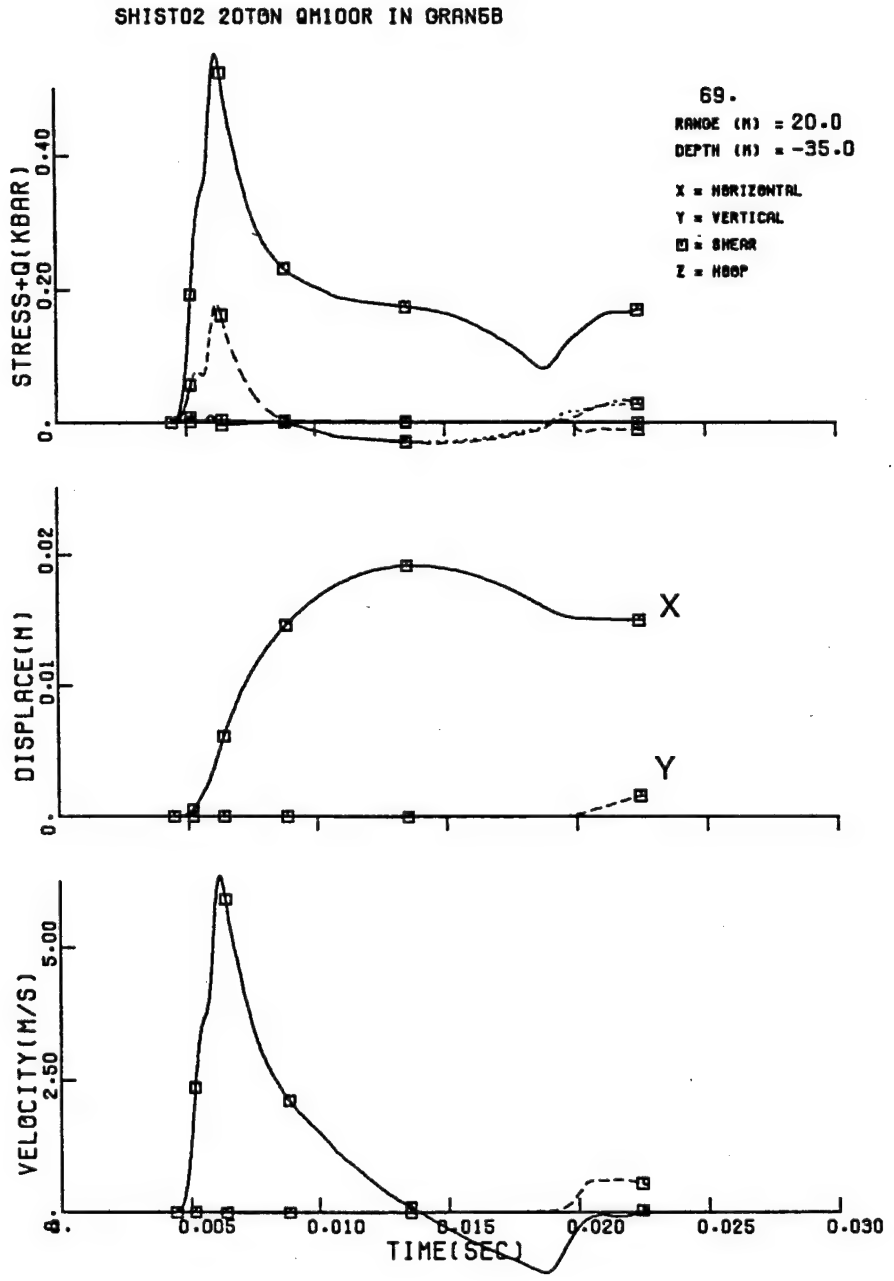


Figure 4-44. Target point 69 time history for 2DSHIST02 CRALE calculation.

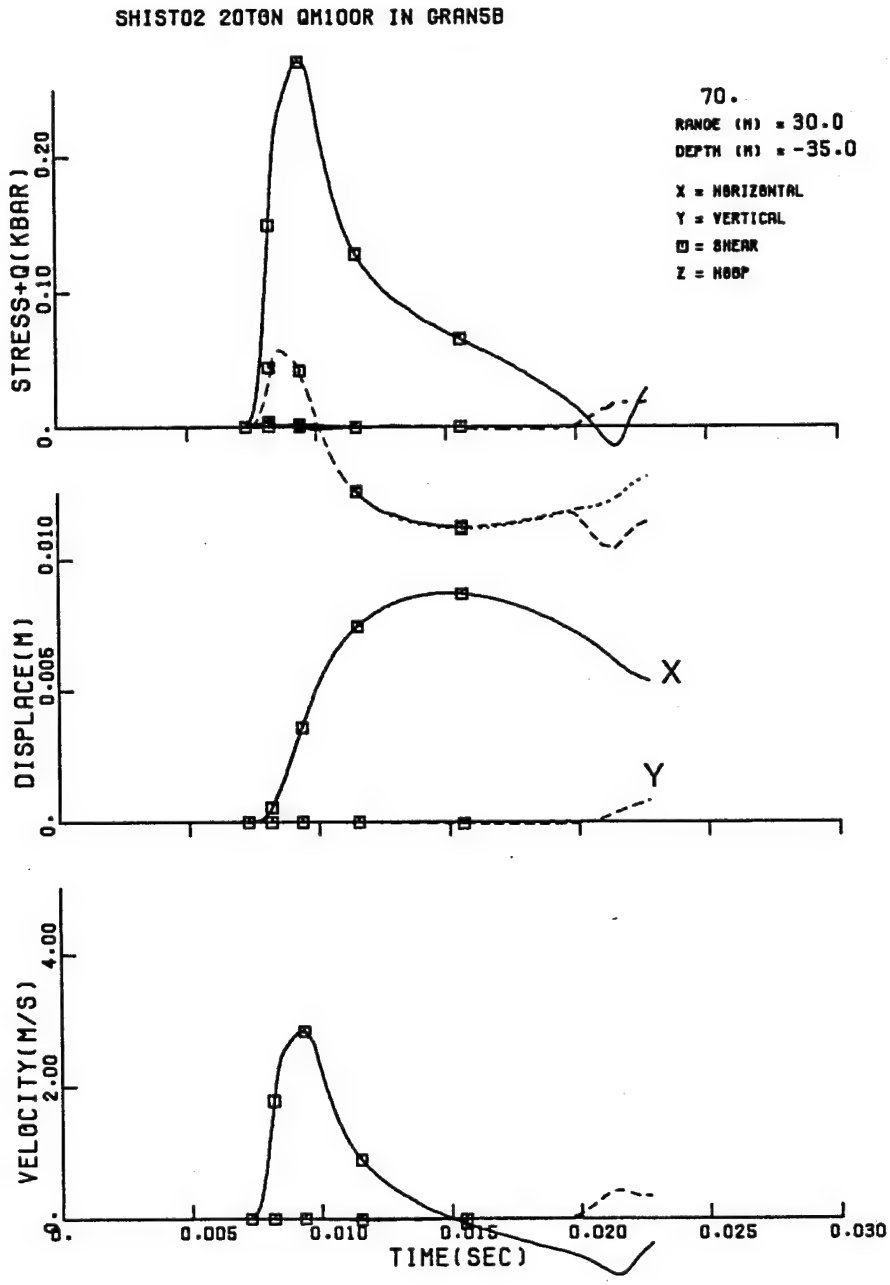


Figure 4-45. Target point 70 time history for 2DSHIST02 CRALE calculation.

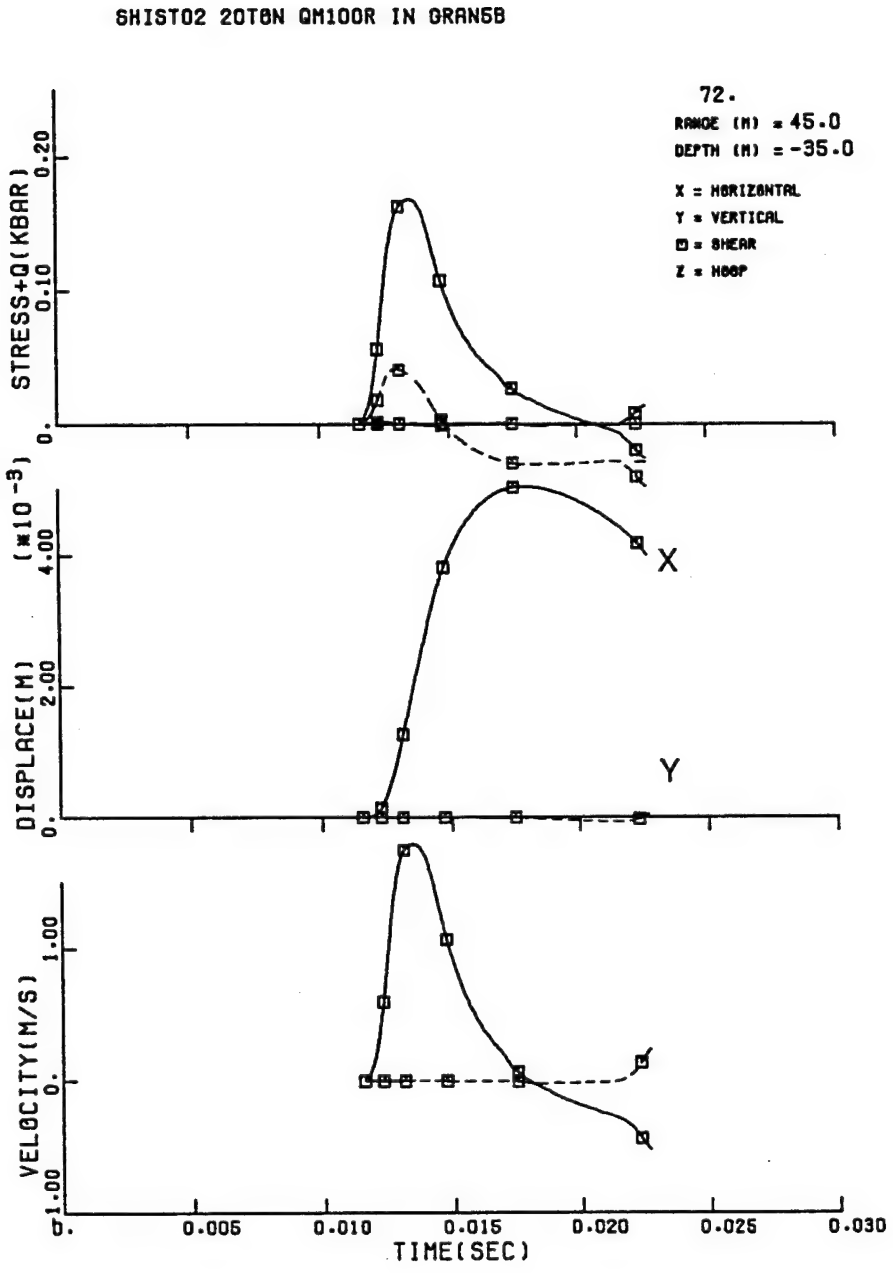


Figure 4-46. Target point 72 time history for 2DSHIST02 CRALE calculation.

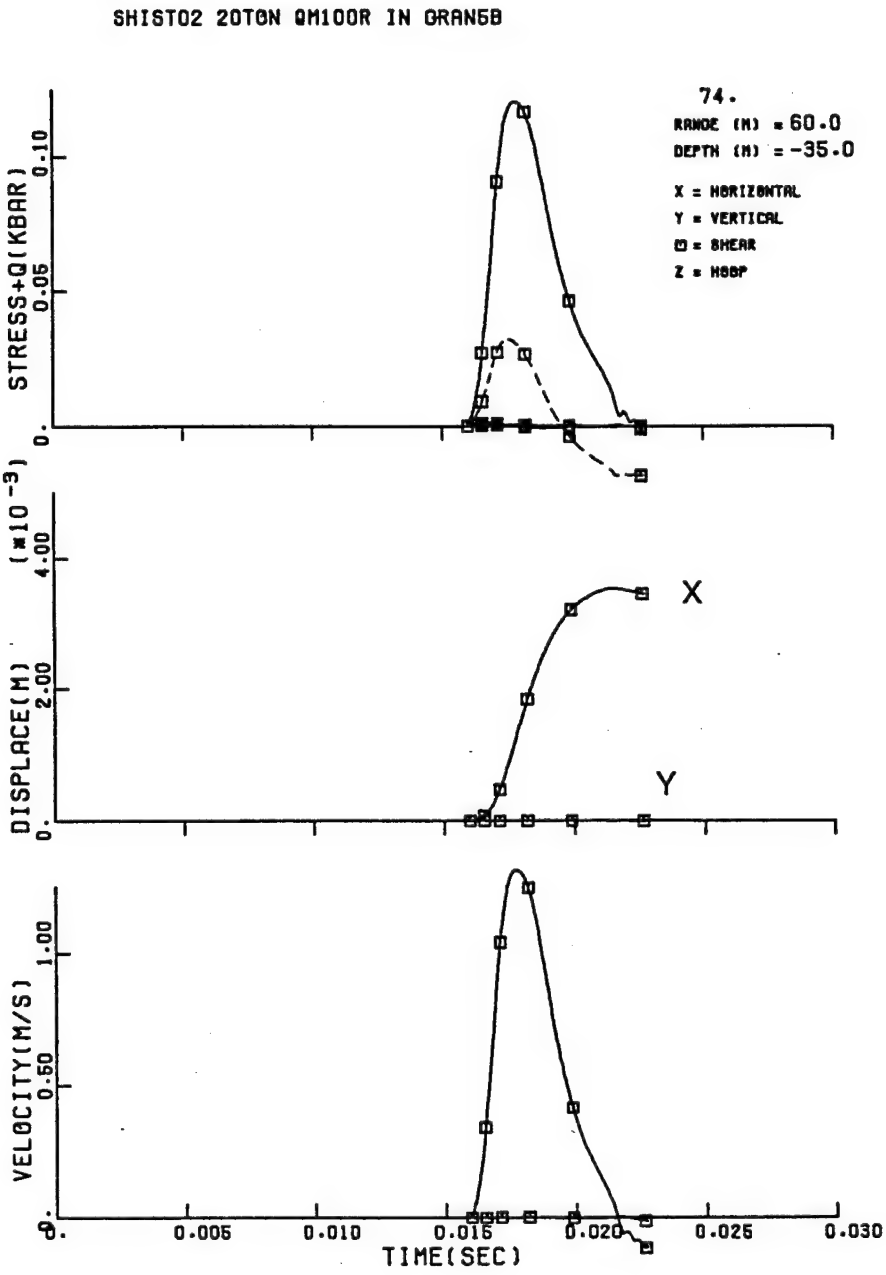


Figure 4-47. Target point 74 time history for 2DSHIST02 CRALE calculation.

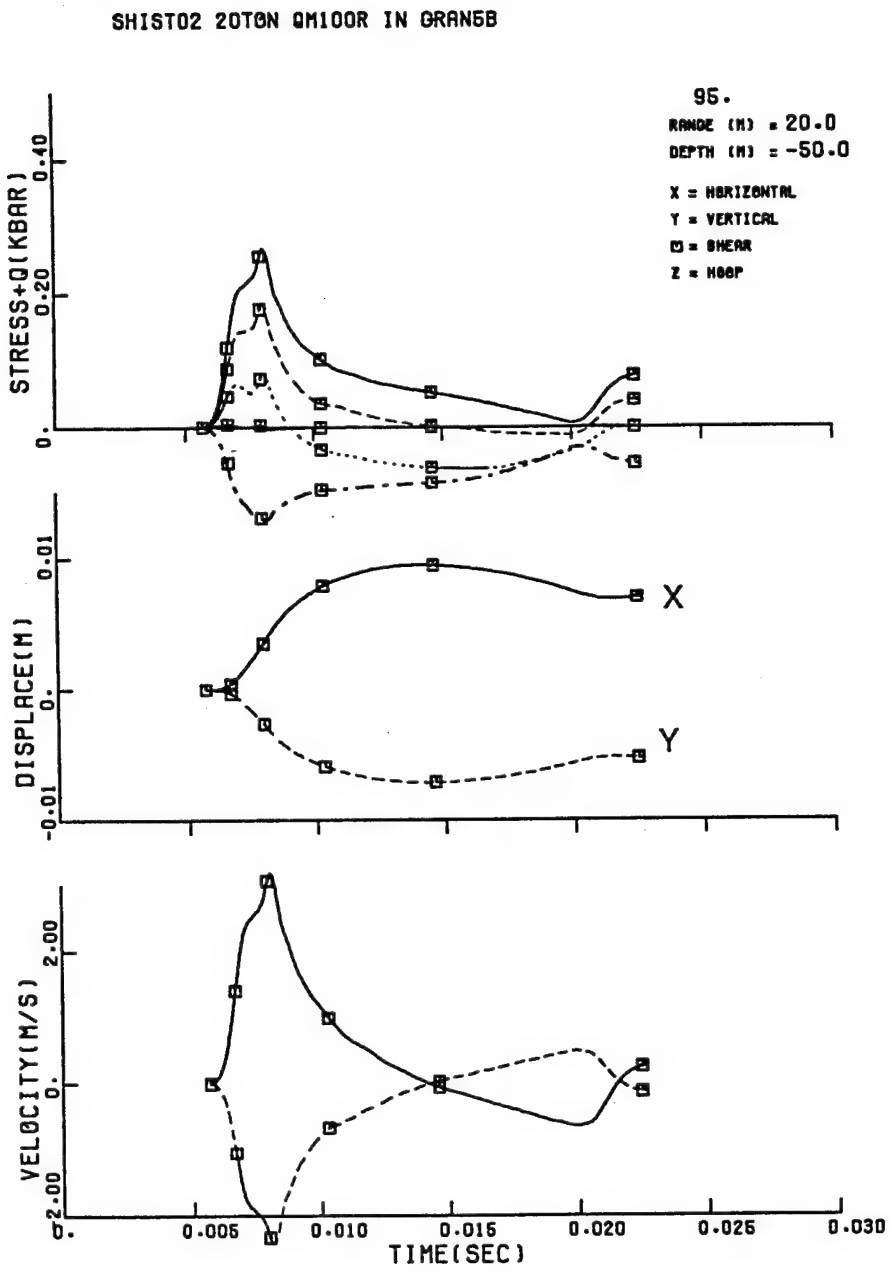


Figure 4-48. Target point 95 time history for 2DSHIST02 CRALE calculation.

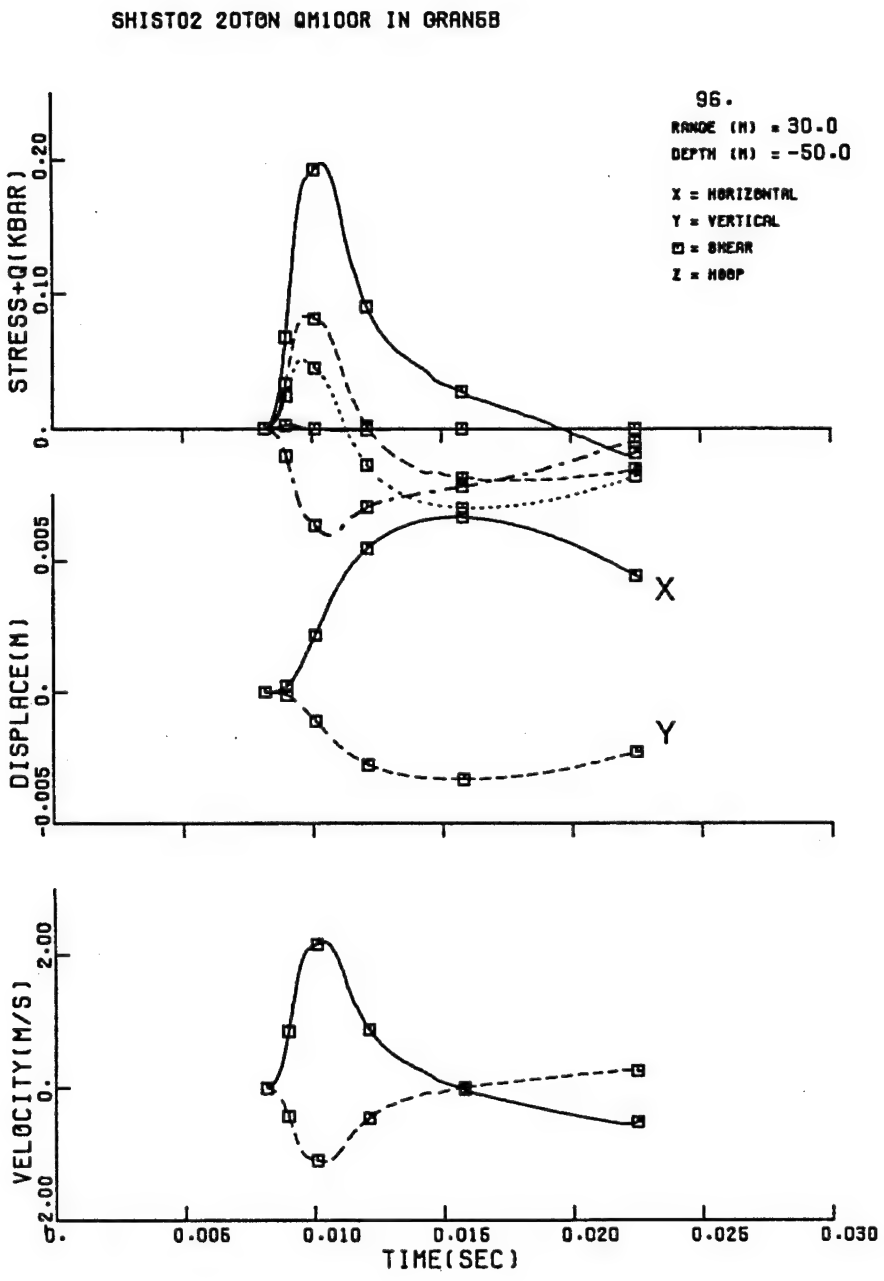


Figure 4-49. Target point 96 time history for 2DSHIST02 CRALE calculation.

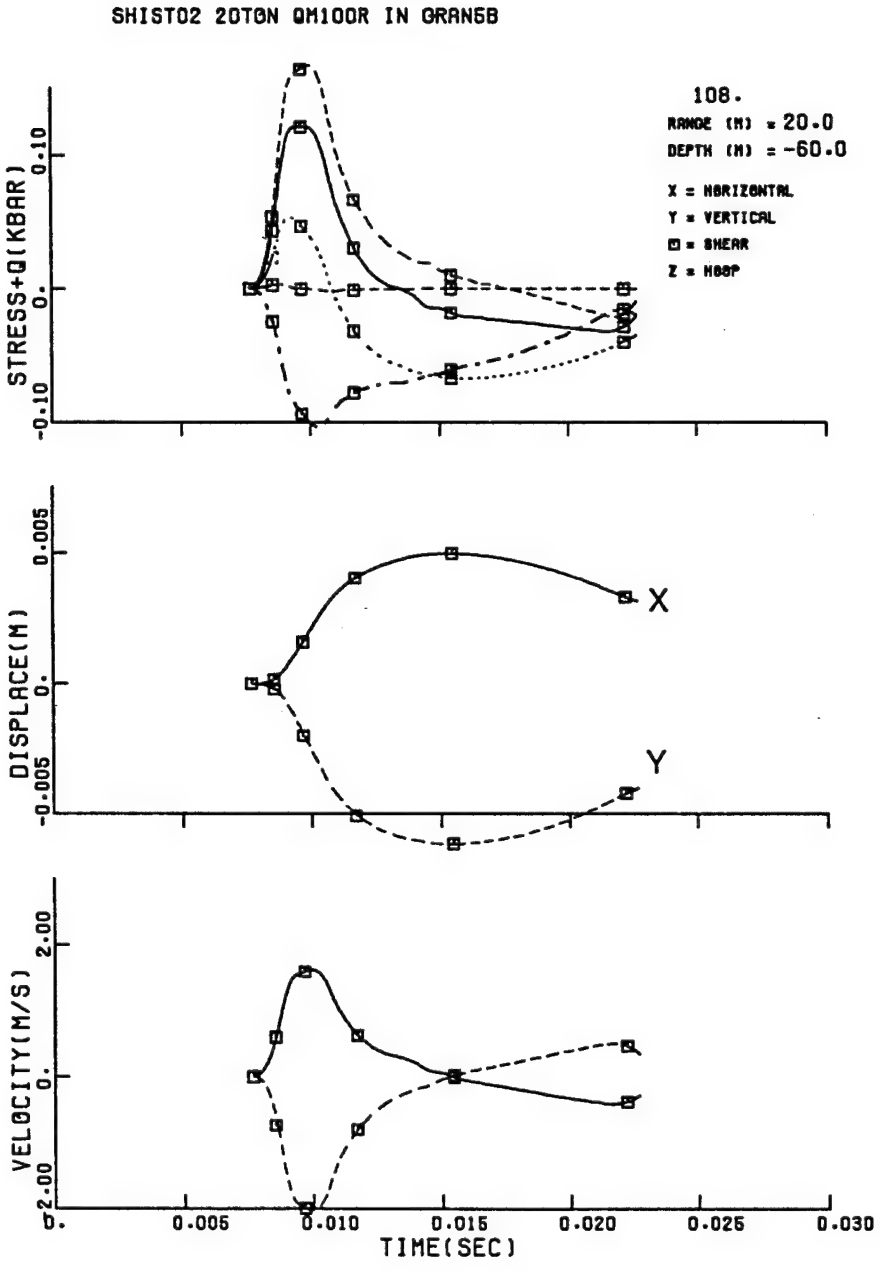


Figure 4-50. Target point 108 time history for 2DSHIST02 CRALE calculation.

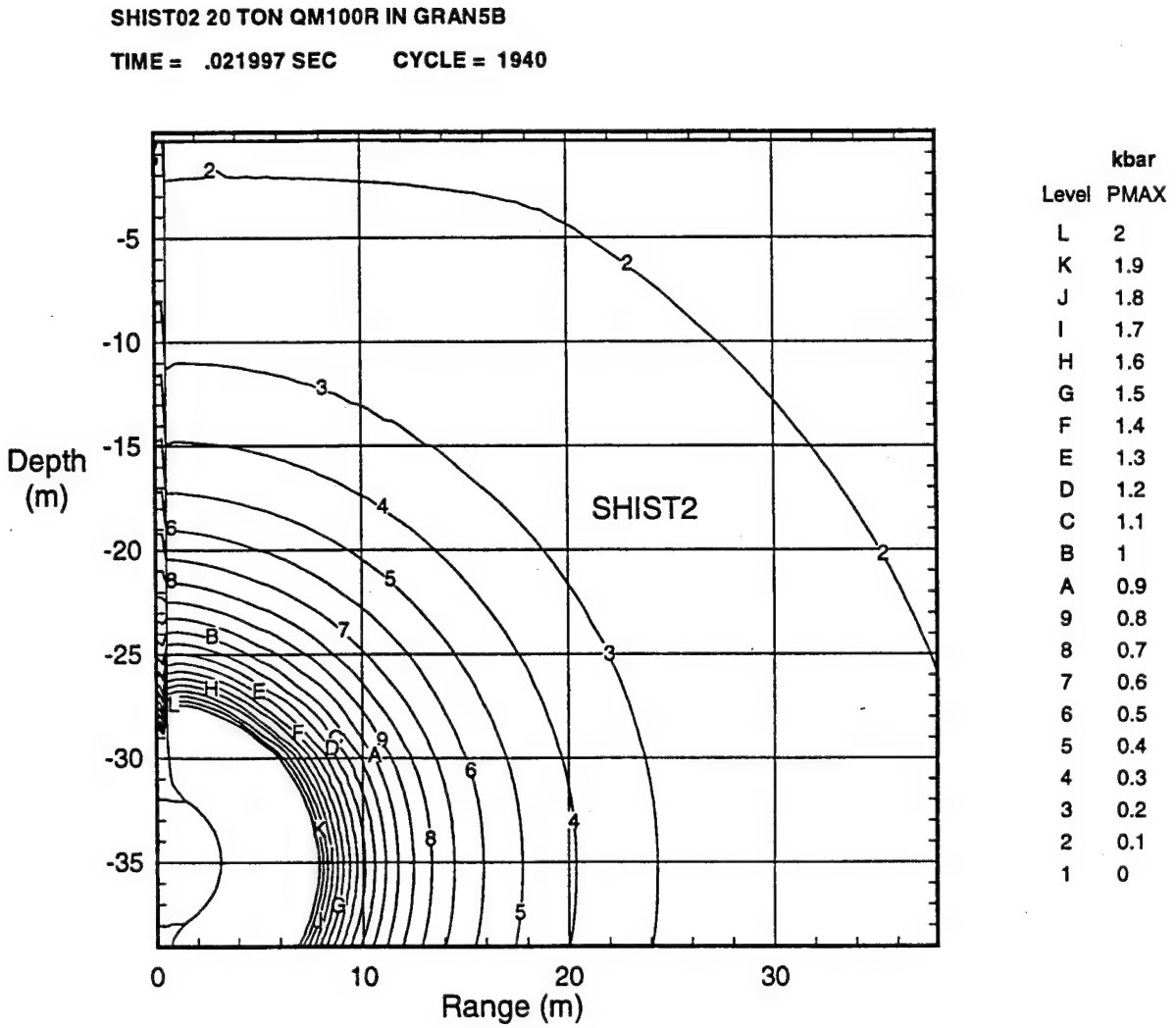


Figure 4-51. Peak stress contours for the 2DSHIST02 CRALE calculation Homogeneous SHIST2 (GRAN5B, 3,400mps, 1.1%AFV).

## 4.4 CRALE 2D CALCULATION 2DSHIST01.

**GENERIC2 (GRAN1C, 4,500 m/s) 0 to 15 meter**
**GENERIC3 (GRAN1E, 4500 m/s) depth > 15 meters**

The 2DSHIST01 calculation was run with material model GENERIC2 (GRAN1C) in the top 15 meters and material model GENERIC3 (GRAN1E) in the bottom layer. Since the seismic velocities of GENERIC1 and GENERIC2 (4,500 m/s) are higher than those expected in the field, this calculation was run primarily as a zoning study to compare with the 1D calculations run earlier. Also, since GENERIC2,3 are virtually identical materials, the site profile of this calculation can be considered homogeneous and the shock propagation is spherical until it hits the free surface. The 2D velocity and displacement waveforms from target points along the 35 meter depth radial are compared to the GENERIC3 (GRAN1E) 1D calculation in Figures 4-52 and 4-53. As can be seen, since the zoning in the 2D calculation was coarser than the 1D, the rise time of the waveforms are longer. However, it can also be seen in the displacement waveforms, that impulse has been conserved and the displacements predicted in the SHST01 2D calculation are equivalent to those in the 1D calculation. The peak stress contours from the SHIST01 2D calculation are shown in Figure 4-54.

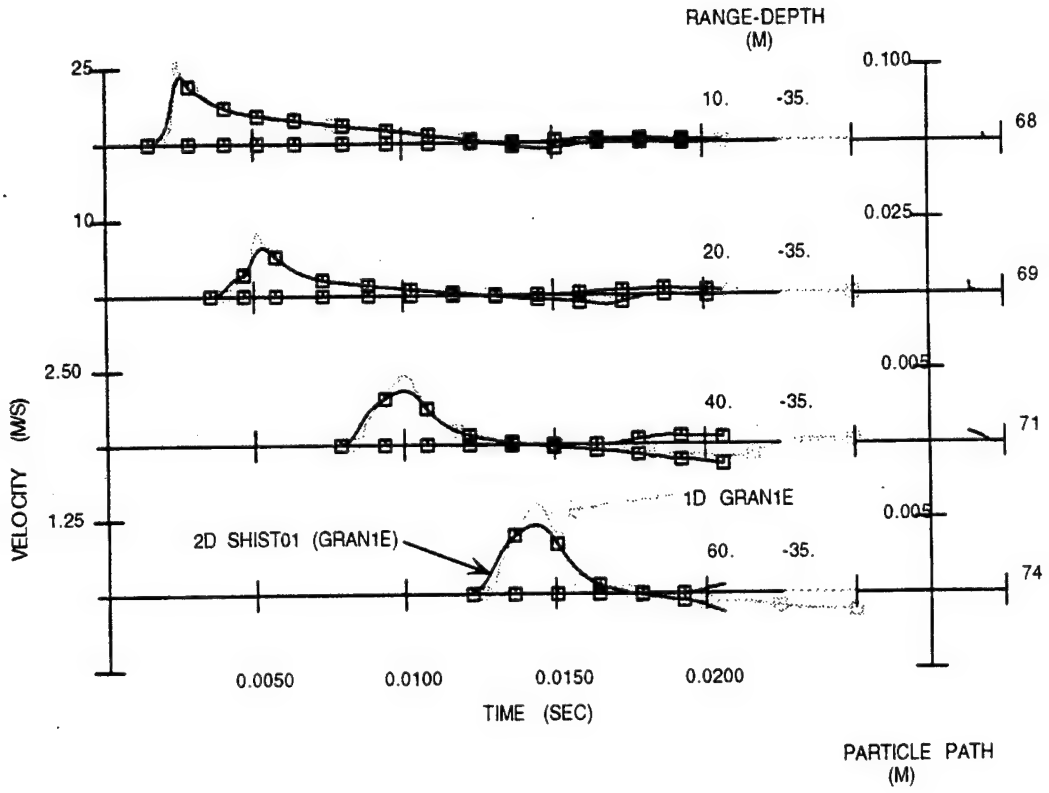


Figure 4-52. 35 meter depth radial velocities from 2DSHIST01 calculation compared to the GENERIC3 (GRAN1E) 1D calculation.

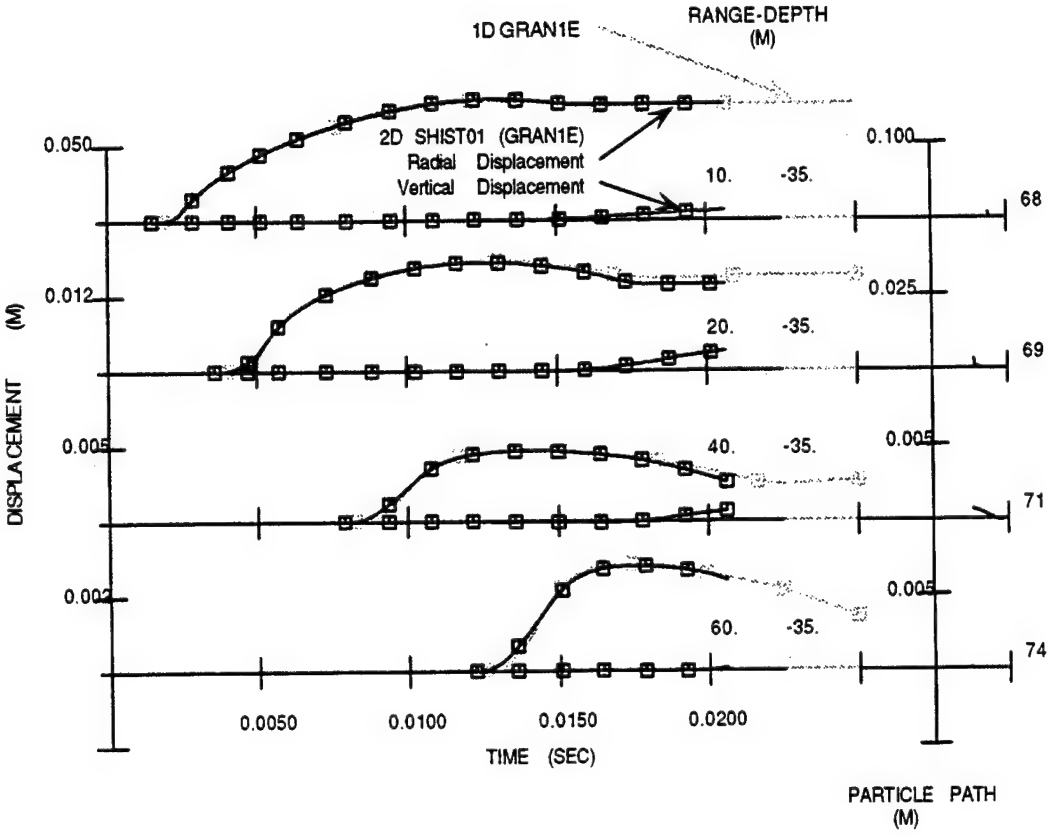


Figure 4-53. 35 meter depth radial displacements from 2DSHIST01 calculation compared to the GENERIC3 (GRAN1E) 1D calculation.

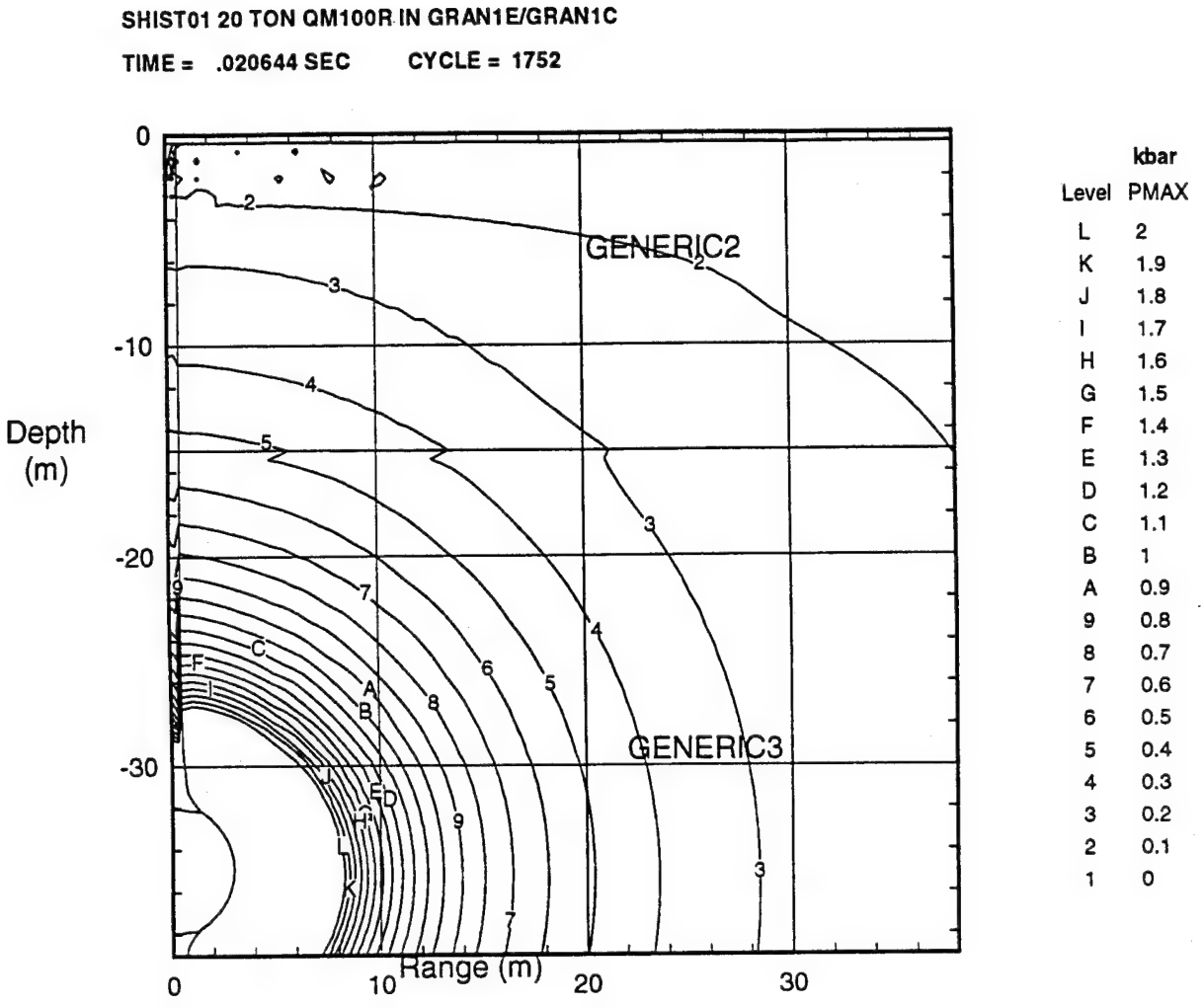


Figure 4-54. Peak stress contours for the 2DSHIST01 calculation. GENERIC2 (GRAN1C, 4,500m/s, 1%AFV) to 15 meter depth with GENERIC3 (GRAN1E, 4500m/s, 1%AFV) below.

## SECTION 5

## REFERENCES


1. Rocco, J.R., "Seismic High Explosive In-situ Source Test (SHIST) Scoping Calculations", (U) TRT letter report to Dr. Bob Reinke Field Command FCDNA/FCTT dated June 29, 1993. (UNCLASSIFIED)

2. Rocco, J.R., E.J. Rinehart, "Granite Containment Investigations: Calculations of a Simple Backfilled Tunnel With and Without a Blocking Charge", (U) DNA-TR-88-86, California Research and Technology, Pleasonton, CA, April 1990. (UNCLASSIFIED)

3. Schuster, S., "Material Modeling in the CRALE Code: Users' Manual", (U) TRT-3336TR-1 Draft, Titan Research & Technology Division, Chatsworth, CA, March 1994. (UNCLASSIFIED)

4. Martin, J.W., TerraTek letter report to Ms. Audrey Martinez FCDNA/FCTT, (U), dated October 27,1993. (UNCLASSIFIED)

5. Zelasko, J.S., "Testing and Constitutive Modeling for In-Situ Response Characterization Meeting," (U) viewgraph briefing presented on 11 July 1990 at RDA Albuquerque for Defense Nuclear Agency/SPWE, USAE Waterways Experiment Station, Vicksburg, Mississippi. (UNCLASSIFIED)

## APPENDIX A

## SHELL EQUATION OF STATE PARAMETERS

### A.1 GENERAL.

*Given:* a state of the material defined by its current

a) Density, $\rho$(g/cc) and strain state, $\varepsilon_{ij}$;

b) Specific internal energy, E (Terg/g)

*Find:* the pressure or mean stress, P (Mb) and the deviatoric stress tensor, $\sigma'_{ij}$

*Definitions:*

$\rho_o$, the initial density

$\rho_r$, the reference density, i.e., the grain density of the solid

Compression, $\eta = \rho/\rho_o$

(Note: compression is relative to the initial density)

Excess compression, $\mu = \eta - 1$

Porosity (total void volume), $v_v = 1 - \rho_o/\rho_r$

volumetric strain, $\varepsilon = -\mu/\eta$

*Then:*

$$P(\rho,E) = P_s(\rho,E) + P_v(\rho,E) \tag{A.1}$$

$$P_s = B_m\mu' - (B_m - B_o)\mu^*\left(1 - e^{-\mu'/\mu^*}\right) \tag{A.2}$$

$$P_v = \Gamma\rho E^* \; ; \qquad (E > E_m) \tag{A.3}$$

where

$$\mu' = \mu + \beta E \tag{A.4}$$

$$E^* = (E - E_m)(1 - e^{-[E-E_m]/E_m}) \tag{A.5}$$

$$^{1}\Gamma = \gamma - 1 = 0.6 + 0.023\left[\ln(\rho / E)\right]^2 + 0.14 \bullet \ln(\rho / E) + 0.05 \bullet \ln \rho \qquad \text{(A.6)}$$

Five parameters are required in Equations A.2 through A.6 to compute the pressure in a material with no porosity (voids), i.e. $\rho_o = \rho_r$, in addition to the reference/initial density. They are:

$E_m$ = minimum energy required to activate $P_v$, (Terg/g)

$B_o$ = the zero pressure bulk modulus, $dP/d\mu$ (Mb)

$B_m$ = the maximum bulk modulus, (Mb)

$\mu^*$ = the excess compression at which the bulk modulus has increased exponentially to ~$[2/3\ B_m + 1/3\ B_o]$

$\beta$ = coefficient of thermal expansion, (g/Terg);
$B_m \beta E$ is equivalent to the Gruneisen gamma term ($\Gamma \rho E$) for the energy dependence of the solid pressure.

## A.2 HYSTERESIS DUE TO AIR-FILLED POROSITY.

For a material which contains air-filled porosity, i.e., less than 100% saturation, the pores may collapse irreversibly under compression so that the behavior of the material is path dependent. Several additional steps and a new independent variable are required to compute the pressure. In the SHEL routine, the new variable, μmax ($\mu_m$), is the maximum excess compression ever attained by the material. For a material containing air-filled void spaces, the initial density, $\rho_o$, is always less then the reference density, i.e.; $\rho_o < \rho_r$.. By convention, the excess compression, μ, relative to $\rho_o$ is passed to the SHEL routine. Since the SHEL EOS algorithms are based on the reference density, $\rho_r$, the routine transforms the μ's to correspond to $\rho_r$.

---

[1]The multiplication symbol, •, has been included where needed for clarity; ln is the natural log; and γ is the gamma-law gas EOS parameter (not explicitly used).

A fundamental assumption governs the pressure behavior of the porous material under loading, namely, there is a transformation in $\mu$ to an equivalent value along the load path of the solid (void-free) material. To calculate the pressure, we first find the solid $\mu$ equivalent to $\mu_m$ and then obtain a modified $\mu'$ for the current compressional state of the material to use in Equation A.2 as follows.

*Define:*

$$\eta_z = \rho_o / \rho_r, \quad \mu_z = \eta_z - 1 \le 0, \quad \varepsilon_z = -\mu_z / \eta_z \tag{A.7}$$

Any excess compression, $\mu$ relative to $\rho_o$, can be transformed into an equivalent $\mu_r$ relative to $\rho_r$, by

$$\mu_r = \eta_z \mu + \mu_z \tag{A.8}$$

As for a nonporous solid (Equation B.4), we again augment $\mu$ and $\mu_m$ by adding the thermal contribution to both;

$$\left.\begin{aligned} \mu'' &= \mu + \beta E \\ \mu_m'' &= \mu_m + \beta E \end{aligned}\right\} \tag{A.9}$$

An offset parameter, $\Delta$, is computed next to transform the compression into the frame of the reference density;

$$\Delta = \mu_z (1 - e^{\alpha_2 \dot{\mu}_m / \varepsilon_z}) + \mu_1 (1 - e^{-\alpha_1 \dot{\mu}_m / \mu_1}) e^{\alpha_2 \dot{\mu}_m / \varepsilon_z} \tag{A.10}$$

where $\alpha_1$, $\alpha_2$ and $\mu_1$ are additional input parameters. The first term on the right-hand side of Equation B.10 provides a smooth convex curve starting at $\rho=\rho_o$ which asymptotically approaches the reference P-$\mu$ hydrostat; the second term adds a toe to

the initial loading. Physically, the first term represents the irreversible pore collapse and the breakdown of cementation bonds in the matrix, while the second term is a measure of the initial elastic response of those bonds.

$P_s$ is now computed as in Equation B.2:

$$P_s = B_m \bar{\mu} - (B_m - B_o)\mu^{*'}(1 - e^{-\bar{\mu}/\mu^{*'}}) \tag{A.11}$$

where

$$\bar{\mu} = \eta_z \mu'' + \Delta \tag{A.12}$$

and

$$\mu^{*'} = \mu^* / [\eta_z (1 - \alpha_2 e^{\alpha_2 \dot{\mu}_m / \varepsilon_z}) + \alpha_1 e^{-\alpha_1 \dot{\mu}_m / \mu_1}] \tag{A.13}$$

The assumption that unloading paths for partially collapsed porous media parallel the solid load-unload path has been used for many earth media, particularly when load-unload data were not available or inconsistent. Recommended load-unload paths for the porous shales provided by WES did not conform to this behavior. Unloading from peak pressures less than the elastic toe were elastic; as the peak pressure increased above the crush level so did the initial unload moduli. Thus the unloading paths appear to stiffen and fan out as the peak pressure increases. This effect was modeled by simply adjusting the effective maximum excess compression as the material unloaded, i.e., for $\mu_{x_1} < \mu_m < \mu_{x_2}$

$$\mu_m' = f\mu + (1 - f)\mu_m \tag{A.14}$$

where

$$f = (\mu_m - \mu_{x_1}) / (\mu_{x_2} - \mu_{x_1}) \tag{A.15}$$

and $\mu_{x_1}$ *and* $\mu_{x_2}$ are additional input parameters.

Thus, for a porous solid, six parameters must be specified, namely;

$\rho_o$ = the initial density of the material ($\neq \rho_r$)

$\alpha_1$ = relative slope of initial loading on the elastic toe to that of the non-porous solid

$\mu 1$ = amount of compression on loading toe

$\alpha 2$ = a fitting parameter that governs the elastic slope of the load curve while crushing out the voids

$\mu x1$ = minimum compression to begin fanning the unload paths

$\mu x2$ = compression at which unload path parallels zero porosity load-unload curve.

## A.3 SOLID-SOLID PHASE CHANGE.

Many materials exhibit a solid-solid phase change under compression. Based on Hugoniot and release data for silicates, it appears that under shock loading such a change is hysteretic, i.e., on unloading the material initially remains in the higher density state and does not revert to the original state until well down the release path. Such behavior can be modeled by assuming that the phase change is a function of both compression and energy.

To compute the new solid $P_s$, Equation A.2 or A.11 is again modified by replacing the constant $B_m$ and the excess compression, $\mu'$ (Equation A.4) or $\bar{\mu}$ (Equation A.12), by

$$B'_m \text{ and } \mu' - \Delta, \text{ or } \bar{\mu} - \Delta\rho \tag{A.16}$$

where

$$\Delta\rho = \begin{cases} 0 & \rho E \le (\rho E)_1; \text{ (all state 1)} \\ g\mu_2 & \rho E > (\rho E)_1 \end{cases} \tag{A.17}$$

$$B_m' = \begin{cases} B_m & \rho E \le (\rho E)_1; \text{ (all state 1)} \\ B_m + g(B_{m_2} - B_m) & \rho E > (\rho E)_1 \end{cases} \tag{A.18}$$

$$\mu_2 = \rho_2 / \rho_r - 1,$$

$$g = \frac{1 - e^{-\alpha_3[\rho E - (\rho E)_1]}}{1 + e^{-\alpha_3[\rho E - (\rho E)_1]}} \tag{A.19}$$

and $B_{m2}$, $(\rho E)_1$, $\rho_2$ and $\alpha_3$ are material constants. Thus, four additional input parameters are required for the phase change:

$\rho_2$ = the reference density of the 2nd phase

$(\rho E)_1$ = the energy per unit volume at which the phase change begins

$\alpha_3$ = a parameter setting the rate of conversion between the phases

$B_{m2}$ = the maximum bulk modulus ($d\rho/d\mu$) of the 2nd phase.

NOTE: $B_{m2}$ is relative to $\rho_r$ of the 1st phase; the modulus relative to $\rho_2$ is = $(\rho_2/\rho_r)\, B_{m2}$

**A.4 DEVIATORIC BEHAVIOR.**

The complete description of a material's stress-strain behavior requires the calculation of the deviatoric stress tensor, $\sigma'_{ij}$, in addition to the mean stress or pressure. The SHEL EOS model assumes that the stress deviators depend on the strain deviators, $\varepsilon'_{ij}$, and a yield function, Y. The stresses are calculated in two steps. First, the change in the deviators is assumed to be elastic and an incremental change is added to the previous deviators,

$$\sigma'_{ij}(n) = \sigma'_{ij}(n-1) + 2G d\varepsilon'_{ij} \qquad \text{(A.20)}$$

where G is the shear modulus of the material and $d\varepsilon'_{ij}$ is the change in the ij-th component of the deviatoric strain tensor between times n-1 and n. Furthermore, it is assumed the shear modulus can be derived from the current bulk modulus through Poisson's ratio and the standard elastic relation

$$2G = 3B(1-2\nu)/(1+\nu) \qquad \text{(A.21)}$$

After the stresses have been updated by Equation A.20 a check is made to see if the elastic changes are valid. The second invariant of the deviatoric stress tensor, $J'_2$ is compared to the square of a yield function, Y which depends only on the mean stress, P. If $J'_2$ exceeds $Y^2$, the material is deforming plastically and the deviators are proportionally reduced so that $J'_2$ is equal to $Y^2$.

For the rock media of interest, two yield surface functions are available, an exponential and a simple Drucker-Prager / Von-Mises limit with the input variable Py used as a flag. When 1/Py > 10, the yield function is

$$Y = \max\begin{cases} Y_{vm} - (Y_{vm} - Y_o)e^{-P/P_y} \\ Y_{vm} \end{cases} \qquad \text{(A.22)}$$

The four input parameters required to calculate the deviatoric stress tensor are;

- $\nu$, Poisson's ratio
- $Y_{vm}$, the limiting yield strength (kb)
- $Y_o$, the yield strength at zero pressure (kb)
- P the current pressure
- $P_y$ the pressure at which the yield function ~$(2/3\ Y_m + 1/3\ Y_o)$

When 1/Py < 10.

$$Y = \max\begin{cases} \dfrac{P}{P_y} + Y_o \\ Y_{vm} \end{cases} \qquad \text{(A.24)}$$

where

- $Y_{vm}$, the limiting yield strength
- $Y_o$, the yield strength at zero pressure (cohesion)
- P the current pressure
- $1/P_y$ the Drucker-Prager slope

## Table A-1. SHEL EOS input parameters.

| Value | Units | GENERIC2 | GENERIC3 | SHIST1 | SHIST2 | Comments |
|---|---|---|---|---|---|---|
| | | GRAN1C | GRAN1E | GRAN4B | GRAN5B | |
| $\rho_o$ | g/cc | 2.624 | 2.624 | 2.605 | 2.621 | Initial density |
| $\rho_r$ | g/cc | 2.65 | 2.65 | 2.65 | 2.65 | Reference density |
| $E_s$ | Terg/g | 0.04 | 0.04 | 0.04 | 0.04 | Min energy for $P_v$ |
| $\sigma t$ | bar | -120.0 | -120.0 | -120.0 | -120.0 | Tensile Limit |
| $B_o$ | Mbar | 0.3 | 0.3 | 0.035 | 0.1683 | Initial bulk modulus |
| $B_m$ | Mbar | 0.7 | 0.7 | 0.7 | 0.7 | Maximum bulk modulus |
| $m^*$ | -- | 0.03 | 0.03 | 0.03 | 0.03 | Rate of change of B |
| $m_1$ | -- | 0.0 | 0.0 | 0.0 | 0.0 | End of elastic toe |
| $a_1$ | -- | 0.0 | 0.0 | 0.0 | 0.0 | Rate of increase of B on elastic toe |
| $a_2$ | -- | 0.0 | 0.0 | 0.0 | 0.0 | Rate of increase of B during pore collapse |
| $m_{x1}$ | -- | 0.02 | 0.02 | 0.02 | 0.02 | Start of unload path fan |
| $m_{x2}$ | -- | 0.09 | 0.09 | 0.09 | 0.09 | End of unload path fan |
| $\rho_2$ | g/cc | 4.3 | 4.3 | 4.3 | 4.3 | Ref density of higher density phase |
| $(rE)_1$ | Te/cc | 0.007 | 0.007 | 0.007 | 0.007 | Min E/V for solid in 2nd phase |
| $B_{m2}$ | Mbar | 2.0 | 2.0 | 2.0 | 2.0 | Max B of 2nd phase solid |
| $a_3$ | -- | 18.7 | 18.7 | 2.3 | 2.3 | Rate for solid-solid phase change |
| $V_v$ | % | 1.0 | 1.0 | 1.7 | 1.1 | Porosity (total void volume) |
| b | g/Terg | 3.0 | 3.0 | 3.0 | 3.0 | Thermal expansion coef. |
| $\nu$ | -- | 0.25 | 0.25 | 0.25 | 0.25 | Poisson's ratio |
| $Y_{vm}$ | Mbar | 0.0125 | 0.0125 | 0.0125 | 0.0125 | Von Mises yield limit |
| $Y_o$ | Mbar | 0.0001 | 0.0001 | 0.0001 | 0.0001 | Cohesion |
| $1/P_y$ | Mbar | 0.30 | 30.0 | 30.0 | 30.0 | Slope Coefficient <10 linear, >10 exponential |

# APPENDIX B

# CRALE EOS INPUT DECKS

This Appendix included the CRALE input decks necessary to run the calculations discussed in this report. The CRALE EOS input parameters are discussed further in Reference 3.

## B.1 SHEL EOS MODELS SHIST1 (GRAN4B AT 1,550 M/S) AND SHIST2 (GRAN5B AT 3,400 M/S).

```
123456789-123456789-123456789-123456789-123456789-123456789-123456789-123456789-
GRAN4B 1   1  1.7% GRAN 1550 m/sec EXP yield surface
     2.605     2.650      0.04       0.0 -120.E-06
      0.30       0.7       .03       0.0     0.117       0.0      1.00      0.0
     0.020      0.09       0.0       0.0       0.0       0.0      0.05      1.0
       3.0      0.00       0.0      4.30      .007       .13       2.0      2.3
      0.25       0.0       0.0       0.0       0.0       0.0       0.0      0.0
    0.0125    0.0001      30.0       0.0       0.0       0.0       0.0      0.0

GRAN5B 1   1  1.1% GRAN 3400 m/sec EXP yield surface
     2.621     2.650      0.04       0.0 -120.E-06
      0.30       0.7       .03       0.0     0.561       0.0      1.00      0.0
     0.020      0.09       0.0       0.0       0.0       0.0      0.05      1.0
       3.0      0.00       0.0      4.30      .007       .13       2.0      2.3
      0.25       0.0       0.0       0.0       0.0       0.0       0.0      0.0
    0.0125    0.0001      30.0       0.0       0.0       0.0       0.0      0.0
```

## B.2 SHEL EOS MODELS GENERIC2 (GRAN1C AT 4,500 M/S) AND GENERIC3 (GRAN1E AT 4,500 M/S).

```
123456789-123456789-123456789-123456789-123456789-123456789-123456789-123456789-
GRAN1C 1   1  GRAN1A with new FAN
     2.624     2.650      0.04       0.0 -120.E-06
      0.30       0.7       .03       0.0     1.000       0.0      1.00      0.0
     0.020      0.09       0.0       0.0       0.0       0.0      0.05      1.0
       3.0      0.00       0.0      4.30      .007       .13       2.0      2.3
      0.25       0.0       0.0       0.0       0.0       0.0       0.0      0.0
    0.0125    0.0001       0.3       0.0       0.0       0.0       0.0      0.0
```

```
GRAN1E 1    1  GRAN1A with new FAN and EXP yield surface
     2.624     2.650      0.04       0.0 -120.E-06
      0.30       0.7       .03       0.0     1.000       0.0      1.00      0.0
     0.020      0.09       0.0       0.0       0.0       0.0      0.05      1.0
       3.0      0.00       0.0      4.30      .007       .13       2.0      2.3
      0.25       0.0       0.0       0.0       0.0       0.0       0.0      0.0
    0.0125    0.0001      30.0       0.0       0.0       0.0       0.0      0.0
```

## B.3 JWL HIGH EXPLOSIVE MODEL FOR QM-100/R (LLNL FIT).

```
123456789-123456789-123456789-123456789-123456789-123456789-123456789-123456789-
QM10R6 4    1     2ND CUT LLNL JWL FOR QM100R 8/2/93
     1.509     1.509  0.043075  0.043075      -1.0
   0.56000 11.025251      6.50  0.744978    2.8350   0.74200     .0650      0.20
```

The JWL constants of the above line are as follows:

```
      w       A(Mb)       R1     B(Mb)       R2       DetV(cm/ms)  Eo(Te/cc) Pcj(Mb)
```

## B.4 MCIST EOS MODEL CON5K4 FOR HJ7C CONCRETE.

```
123456789-123456789-123456789-123456789-123456789-123456789-123456789-123456789-
CON5K4 5    1  NEW 5KSI CONCRETE FIT TO MN CAL DATA 3/19/93 VML=5KB
     2.279     2.279      0.03       0.0 -24.0E-06     7.348     0.363
 0.0143028  0.206272      .400      .180    0.1E-7       1.0       0.3      .35
       0.0       0.0       1.0       0.0       0.0       0.0       0.0      24.
       3.0      0.03       0.0       0.0       0.0       0.0       0.0     0.95
      0.26      0.18       1.0       0.0       0.0       0.0       0.0 2.89E-3
   2.89E-3   49.5E-6     1.484       0.0       0.0       0.0    2.0E-6    1.484
```

## CONC5K4 MCIST DATA FILE (REQUIRED FOR MCIST MODEL)

| | | | |
|---|---|---|---|
| 0.00000E+00, | 0.00000E+00 | 8.28700E-03, | 9.35700E-01 |
| 1.08696E-04, | 2.83784E-02 | 8.48700E-03, | 9.46600E-01 |
| 2.17392E-04, | 5.67568E-02 | 8.68700E-03, | 9.57400E-01 |
| 1.08702E-03, | 2.83800E-01 | 8.88700E-03, | 9.68000E-01 |
| 1.28700E-03, | 3.23700E-01 | 9.08700E-03, | 9.78500E-01 |
| 1.48700E-03, | 3.57400E-01 | 9.28700E-03, | 9.88800E-01 |
| 1.68700E-03, | 3.86300E-01 | 9.48700E-03, | 9.98900E-01 |
| 1.88700E-03, | 4.12200E-01 | 9.68700E-03, | 1.00900E+00 |
| 2.08700E-03, | 4.36300E-01 | 9.88700E-03, | 1.01900E+00 |
| 2.28700E-03, | 4.60300E-01 | 1.00900E-02, | 1.02800E+00 |
| 2.48700E-03, | 4.84500E-01 | 1.02900E-02, | 1.03800E+00 |
| 2.68700E-03, | 5.08600E-01 | 1.04900E-02, | 1.04700E+00 |
| 2.88700E-03, | 5.32300E-01 | 1.06900E-02, | 1.05700E+00 |
| 3.08700E-03, | 5.55100E-01 | 1.08900E-02, | 1.06600E+00 |
| 3.28700E-03, | 5.76700E-01 | 1.10900E-02, | 1.07500E+00 |
| 3.48700E-03, | 5.96800E-01 | 1.12900E-02, | 1.08400E+00 |
| 3.68700E-03, | 6.15300E-01 | 1.14900E-02, | 1.09300E+00 |
| 3.88700E-03, | 6.32500E-01 | 1.16900E-02, | 1.10200E+00 |
| 4.08700E-03, | 6.48800E-01 | 1.18900E-02, | 1.11100E+00 |
| 4.28700E-03, | 6.64500E-01 | 1.20900E-02, | 1.12000E+00 |
| 4.48700E-03, | 6.79900E-01 | 1.22900E-02, | 1.12900E+00 |
| 4.68700E-03, | 6.95300E-01 | 1.24900E-02, | 1.13800E+00 |
| 4.88700E-03, | 7.11100E-01 | 1.26900E-02, | 1.14700E+00 |
| 5.08700E-03, | 7.27000E-01 | 1.28900E-02, | 1.15600E+00 |
| 5.28700E-03, | 7.43000E-01 | 1.30900E-02, | 1.16400E+00 |
| 5.48700E-03, | 7.58800E-01 | 1.32900E-02, | 1.17300E+00 |
| 5.68700E-03, | 7.74300E-01 | 1.34900E-02, | 1.18100E+00 |
| 5.88700E-03, | 7.89300E-01 | 1.36900E-02, | 1.19000E+00 |
| 6.08700E-03, | 8.03700E-01 | 1.38900E-02, | 1.19800E+00 |
| 6.28700E-03, | 8.17500E-01 | 1.40900E-02, | 1.20600E+00 |
| 6.48700E-03, | 8.30700E-01 | 1.42900E-02, | 1.21400E+00 |
| 6.68700E-03, | 8.43500E-01 | 1.44900E-02, | 1.22200E+00 |
| 6.88700E-03, | 8.55800E-01 | 1.46900E-02, | 1.22900E+00 |
| 7.08700E-03, | 8.67800E-01 | 1.48900E-02, | 1.23700E+00 |
| 7.28700E-03, | 8.79500E-01 | 1.50900E-02, | 1.24500E+00 |
| 7.48700E-03, | 8.91000E-01 | 1.52900E-02, | 1.25200E+00 |
| 7.68700E-03, | 9.02300E-01 | 1.54900E-02, | 1.26000E+00 |
| 7.88700E-03, | 9.13600E-01 | 1.56900E-02, | 1.26700E+00 |
| 8.08700E-03, | 9.24700E-01 | 1.58900E-02, | 1.27500E+00 |

| | | | |
|---|---|---|---|
| 1.60900E-02, | 1.28300E+00 | 2.42900E-02, | 1.61000E+00 |
| 1.62900E-02, | 1.29000E+00 | 2.44900E-02, | 1.61800E+00 |
| 1.64900E-02, | 1.29800E+00 | 2.46900E-02, | 1.62500E+00 |
| 1.66900E-02, | 1.30600E+00 | 2.48900E-02, | 1.63300E+00 |
| 1.68900E-02, | 1.31400E+00 | 2.50900E-02, | 1.64000E+00 |
| 1.70900E-02, | 1.32200E+00 | 2.52900E-02, | 1.64800E+00 |
| 1.72900E-02, | 1.32900E+00 | 2.54900E-02, | 1.65500E+00 |
| 1.74900E-02, | 1.33700E+00 | 2.56900E-02, | 1.66300E+00 |
| 1.76900E-02, | 1.34500E+00 | 2.58900E-02, | 1.67000E+00 |
| 1.78900E-02, | 1.35300E+00 | 2.60900E-02, | 1.67800E+00 |
| 1.80900E-02, | 1.36100E+00 | 2.62900E-02, | 1.68500E+00 |
| 1.82900E-02, | 1.36900E+00 | 2.64900E-02, | 1.69200E+00 |
| 1.84900E-02, | 1.37800E+00 | 2.66900E-02, | 1.70000E+00 |
| 1.86900E-02, | 1.38600E+00 | 2.68900E-02, | 1.70700E+00 |
| 1.88900E-02, | 1.39400E+00 | 2.70900E-02, | 1.71500E+00 |
| 1.90900E-02, | 1.40200E+00 | 2.72900E-02, | 1.72200E+00 |
| 1.92900E-02, | 1.41000E+00 | 2.74900E-02, | 1.73000E+00 |
| 1.94900E-02, | 1.41800E+00 | 2.76900E-02, | 1.73700E+00 |
| 1.96900E-02, | 1.42600E+00 | 2.78900E-02, | 1.74500E+00 |
| 1.98900E-02, | 1.43500E+00 | 2.80900E-02, | 1.75200E+00 |
| 2.00900E-02, | 1.44300E+00 | 2.82900E-02, | 1.76000E+00 |
| 2.02900E-02, | 1.45100E+00 | 2.84900E-02, | 1.76700E+00 |
| 2.04900E-02, | 1.45900E+00 | 2.86900E-02, | 1.77500E+00 |
| 2.06900E-02, | 1.46700E+00 | 2.88900E-02, | 1.78300E+00 |
| 2.08900E-02, | 1.47600E+00 | 2.90900E-02, | 1.79000E+00 |
| 2.10900E-02, | 1.48400E+00 | 2.92900E-02, | 1.79800E+00 |
| 2.12900E-02, | 1.49200E+00 | 2.94900E-02, | 1.80600E+00 |
| 2.14900E-02, | 1.50000E+00 | 2.96900E-02, | 1.81400E+00 |
| 2.16900E-02, | 1.50800E+00 | 2.98900E-02, | 1.82200E+00 |
| 2.18900E-02, | 1.51600E+00 | 3.00900E-02, | 1.83000E+00 |
| 2.20900E-02, | 1.52400E+00 | 3.02900E-02, | 1.83700E+00 |
| 2.22900E-02, | 1.53200E+00 | 3.04900E-02, | 1.84500E+00 |
| 2.24900E-02, | 1.54000E+00 | 3.06900E-02, | 1.85300E+00 |
| 2.26900E-02, | 1.54800E+00 | 3.08900E-02, | 1.86100E+00 |
| 2.28900E-02, | 1.55600E+00 | 3.10900E-02, | 1.86900E+00 |
| 2.30900E-02, | 1.56400E+00 | 3.12900E-02, | 1.87700E+00 |
| 2.32900E-02, | 1.57200E+00 | 3.14900E-02, | 1.88500E+00 |
| 2.34900E-02, | 1.58000E+00 | 3.16900E-02, | 1.89300E+00 |
| 2.36900E-02, | 1.58700E+00 | 3.18900E-02, | 1.90100E+00 |
| 2.38900E-02, | 1.59500E+00 | 3.20900E-02, | 1.90900E+00 |
| 2.40900E-02, | 1.60300E+00 | 3.22900E-02, | 1.91700E+00 |

| | | | |
|---|---|---|---|
| 3.24900E-02, | 1.92400E+00 | 4.06900E-02, | 2.23400E+00 |
| 3.26900E-02, | 1.93200E+00 | 4.08900E-02, | 2.24300E+00 |
| 3.28900E-02, | 1.94000E+00 | 4.10900E-02, | 2.25200E+00 |
| 3.30900E-02, | 1.94700E+00 | 4.12900E-02, | 2.26100E+00 |
| 3.32900E-02, | 1.95500E+00 | 4.14900E-02, | 2.27000E+00 |
| 3.34900E-02, | 1.96300E+00 | 4.16900E-02, | 2.27900E+00 |
| 3.36900E-02, | 1.97000E+00 | 4.18900E-02, | 2.28800E+00 |
| 3.38900E-02, | 1.97700E+00 | 4.20900E-02, | 2.29700E+00 |
| 3.40900E-02, | 1.98500E+00 | 4.22900E-02, | 2.30600E+00 |
| 3.42900E-02, | 1.99200E+00 | 4.24900E-02, | 2.31500E+00 |
| 3.44900E-02, | 1.99900E+00 | 4.26900E-02, | 2.32400E+00 |
| 3.46900E-02, | 2.00700E+00 | 4.28900E-02, | 2.33300E+00 |
| 3.48900E-02, | 2.01400E+00 | 4.30900E-02, | 2.34300E+00 |
| 3.50900E-02, | 2.02100E+00 | 4.32900E-02, | 2.35200E+00 |
| 3.52900E-02, | 2.02800E+00 | 4.34900E-02, | 2.36100E+00 |
| 3.54900E-02, | 2.03500E+00 | 4.36900E-02, | 2.37000E+00 |
| 3.56900E-02, | 2.04200E+00 | 4.38900E-02, | 2.37900E+00 |
| 3.58900E-02, | 2.04900E+00 | 4.40900E-02, | 2.38800E+00 |
| 3.60900E-02, | 2.05600E+00 | 4.42900E-02, | 2.39700E+00 |
| 3.62900E-02, | 2.06300E+00 | 4.44900E-02, | 2.40600E+00 |
| 3.64900E-02, | 2.07100E+00 | 4.46900E-02, | 2.41500E+00 |
| 3.66900E-02, | 2.07800E+00 | 4.48900E-02, | 2.42400E+00 |
| 3.68900E-02, | 2.08500E+00 | 4.50900E-02, | 2.43300E+00 |
| 3.70900E-02, | 2.09200E+00 | 4.52900E-02, | 2.44200E+00 |
| 3.72900E-02, | 2.09900E+00 | 4.54900E-02, | 2.45000E+00 |
| 3.74900E-02, | 2.10700E+00 | 4.56900E-02, | 2.45900E+00 |
| 3.76900E-02, | 2.11400E+00 | 4.58900E-02, | 2.46800E+00 |
| 3.78900E-02, | 2.12200E+00 | 4.60900E-02, | 2.47700E+00 |
| 3.80900E-02, | 2.12900E+00 | 4.62900E-02, | 2.48600E+00 |
| 3.82900E-02, | 2.13700E+00 | 4.64900E-02, | 2.49500E+00 |
| 3.84900E-02, | 2.14400E+00 | 4.66900E-02, | 2.50400E+00 |
| 3.86900E-02, | 2.15200E+00 | 4.68900E-02, | 2.51200E+00 |
| 3.88900E-02, | 2.16000E+00 | 4.70900E-02, | 2.52100E+00 |
| 3.90900E-02, | 2.16800E+00 | 4.72900E-02, | 2.53000E+00 |
| 3.92900E-02, | 2.17600E+00 | 4.74900E-02, | 2.53900E+00 |
| 3.94900E-02, | 2.18400E+00 | 4.76900E-02, | 2.54800E+00 |
| 3.96900E-02, | 2.19200E+00 | 4.78900E-02, | 2.55700E+00 |
| 3.98900E-02, | 2.20000E+00 | 4.80900E-02, | 2.56600E+00 |
| 4.00900E-02, | 2.20900E+00 | 4.82900E-02, | 2.57500E+00 |
| 4.02900E-02, | 2.21700E+00 | 4.84900E-02, | 2.58400E+00 |
| 4.04900E-02, | 2.22600E+00 | 4.86900E-02, | 2.59300E+00 |

| | |
|---|---|
| 4.88900E-02, | 2.60200E+00 |
| 4.90900E-02, | 2.61100E+00 |
| 4.92900E-02, | 2.62000E+00 |
| 4.94900E-02, | 2.63000E+00 |
| 4.96900E-02, | 2.63900E+00 |
| 4.98900E-02, | 2.64800E+00 |
| 5.00900E-02, | 2.65700E+00 |
| 5.02900E-02, | 2.66700E+00 |
| 5.04900E-02, | 2.67600E+00 |
| 5.06900E-02, | 2.68500E+00 |
| 5.08900E-02, | 2.69500E+00 |
| 5.10900E-02, | 2.70400E+00 |
| 5.12900E-02, | 2.71400E+00 |
| 5.14900E-02, | 2.72300E+00 |
| 5.16900E-02, | 2.73300E+00 |
| 5.18900E-02, | 2.74200E+00 |
| 5.20900E-02, | 2.75200E+00 |
| 5.22900E-02, | 2.76100E+00 |
| 5.24900E-02, | 2.77100E+00 |
| 5.26900E-02, | 2.78100E+00 |
| 5.28900E-02, | 2.79000E+00 |
| 5.30900E-02, | 2.80000E+00 |
| 5.32900E-02, | 2.81000E+00 |
| 5.34900E-02, | 2.82000E+00 |
| 5.36900E-02, | 2.82900E+00 |
| 5.38900E-02, | 2.83900E+00 |
| 5.40900E-02, | 2.84900E+00 |
| 5.42900E-02, | 2.85900E+00 |
| 5.44900E-02, | 2.86800E+00 |
| 5.46900E-02, | 2.87800E+00 |
| 5.48900E-02, | 2.88800E+00 |
| 5.50900E-02, | 2.89700E+00 |
| 5.52900E-02, | 2.90700E+00 |
| 5.54900E-02, | 2.91700E+00 |
| 5.56900E-02, | 2.92600E+00 |
| 5.58900E-02, | 2.93600E+00 |
| 5.60900E-02, | 2.94500E+00 |
| 5.62900E-02, | 2.95500E+00 |
| 5.64900E-02, | 2.96400E+00 |
| 5.66900E-02, | 2.97400E+00 |
| 5.68900E-02, | 2.98300E+00 |
| 5.70900E-02, | 2.99300E+00 |
| 5.72900E-02, | 3.00200E+00 |
| 5.74900E-02, | 3.01100E+00 |
| 5.76900E-02, | 3.02100E+00 |
| 5.78900E-02, | 3.03000E+00 |
| 5.80900E-02, | 3.03900E+00 |
| 5.82900E-02, | 3.04900E+00 |
| 5.84900E-02, | 3.05800E+00 |
| 5.86900E-02, | 3.06700E+00 |
| 5.88900E-02, | 3.07600E+00 |
| 5.90900E-02, | 3.08600E+00 |
| 5.92900E-02, | 3.09500E+00 |
| 5.94900E-02, | 3.10400E+00 |
| 5.96900E-02, | 3.11400E+00 |
| 5.98900E-02, | 3.12300E+00 |
| 6.00900E-02, | 3.13200E+00 |
| 6.02900E-02, | 3.14200E+00 |
| 6.04900E-02, | 3.15100E+00 |
| 6.06900E-02, | 3.16000E+00 |
| 6.08900E-02, | 3.17000E+00 |
| 6.10900E-02, | 3.17900E+00 |
| 6.12900E-02, | 3.18900E+00 |
| 6.14900E-02, | 3.19800E+00 |
| 6.16900E-02, | 3.20800E+00 |
| 6.18900E-02, | 3.21700E+00 |
| 6.20900E-02, | 3.22700E+00 |
| 6.22900E-02, | 3.23600E+00 |
| 6.24900E-02, | 3.24600E+00 |
| 6.26900E-02, | 3.25600E+00 |
| 6.28900E-02, | 3.26500E+00 |
| 6.30900E-02, | 3.27500E+00 |
| 6.32900E-02, | 3.28500E+00 |
| 6.34900E-02, | 3.29500E+00 |
| 6.36900E-02, | 3.30500E+00 |
| 6.38900E-02, | 3.31500E+00 |
| 6.40900E-02, | 3.32400E+00 |
| 6.42900E-02, | 3.33400E+00 |
| 6.44900E-02, | 3.34400E+00 |
| 6.46900E-02, | 3.35400E+00 |
| 6.48900E-02, | 3.36400E+00 |
| 6.50900E-02, | 3.37400E+00 |

| | |
|---|---|
| 6.52900E-02, | 3.38400E+00 |
| 6.54900E-02, | 3.39400E+00 |
| 6.56900E-02, | 3.40400E+00 |
| 6.58900E-02, | 3.41400E+00 |
| 6.60900E-02, | 3.42400E+00 |
| 6.62900E-02, | 3.43400E+00 |
| 6.64900E-02, | 3.44400E+00 |
| 6.66900E-02, | 3.45400E+00 |
| 6.68900E-02, | 3.46400E+00 |
| 6.70900E-02, | 3.47400E+00 |
| 6.72900E-02, | 3.48400E+00 |
| 6.74900E-02, | 3.49400E+00 |
| 6.76900E-02, | 3.50400E+00 |
| 6.78900E-02, | 3.51400E+00 |
| 6.80900E-02, | 3.52400E+00 |
| 6.82900E-02, | 3.53400E+00 |
| 6.84900E-02, | 3.54400E+00 |
| 6.86900E-02, | 3.55300E+00 |
| 6.88900E-02, | 3.56300E+00 |
| 6.90900E-02, | 3.57300E+00 |
| 6.92900E-02, | 3.58300E+00 |
| 6.94900E-02, | 3.59200E+00 |
| 6.96900E-02, | 3.60200E+00 |
| 6.98900E-02, | 3.61200E+00 |
| 7.00900E-02, | 3.62100E+00 |
| 7.02900E-02, | 3.63100E+00 |
| 7.04900E-02, | 3.64100E+00 |
| 7.06900E-02, | 3.65000E+00 |
| 7.08900E-02, | 3.66000E+00 |
| 7.10900E-02, | 3.66900E+00 |
| 7.12900E-02, | 3.67900E+00 |
| 7.14900E-02, | 3.68800E+00 |
| 7.16900E-02, | 3.69800E+00 |
| 7.18900E-02, | 3.70700E+00 |
| 7.20900E-02, | 3.71700E+00 |
| 7.22900E-02, | 3.72600E+00 |
| 7.24900E-02, | 3.73600E+00 |
| 7.26900E-02, | 3.74500E+00 |
| 7.28900E-02, | 3.75500E+00 |
| 7.30900E-02, | 3.76400E+00 |
| 7.32900E-02, | 3.77400E+00 |
| 7.34900E-02, | 3.78300E+00 |
| 7.36900E-02, | 3.79300E+00 |
| 7.38900E-02, | 3.80200E+00 |
| 7.40900E-02, | 3.81200E+00 |
| 7.42900E-02, | 3.82100E+00 |
| 7.44900E-02, | 3.83100E+00 |
| 7.46900E-02, | 3.84000E+00 |
| 7.48900E-02, | 3.85000E+00 |
| 7.50900E-02, | 3.85900E+00 |
| 7.52900E-02, | 3.86900E+00 |
| 7.54900E-02, | 3.87800E+00 |
| 7.56900E-02, | 3.88800E+00 |
| 7.58900E-02, | 3.89700E+00 |
| 7.60900E-02, | 3.90700E+00 |
| 7.62900E-02, | 3.91700E+00 |
| 7.64900E-02, | 3.92600E+00 |
| 7.66900E-02, | 3.93600E+00 |
| 7.68900E-02, | 3.94600E+00 |
| 7.70900E-02, | 3.95500E+00 |
| 7.72900E-02, | 3.96500E+00 |
| 7.74900E-02, | 3.97500E+00 |
| 7.76900E-02, | 3.98500E+00 |
| 7.78900E-02, | 3.99400E+00 |
| 7.80900E-02, | 4.00400E+00 |
| 7.82900E-02, | 4.01400E+00 |
| 7.84900E-02, | 4.02400E+00 |
| 7.86900E-02, | 4.03400E+00 |
| 7.88900E-02, | 4.04400E+00 |
| 7.90900E-02, | 4.05400E+00 |
| 7.92900E-02, | 4.06400E+00 |
| 7.94900E-02, | 4.07400E+00 |
| 7.96900E-02, | 4.08500E+00 |
| 7.98900E-02, | 4.09500E+00 |
| 8.00900E-02, | 4.10500E+00 |
| 8.02900E-02, | 4.11600E+00 |
| 8.04900E-02, | 4.12600E+00 |
| 8.06900E-02, | 4.13700E+00 |
| 8.08900E-02, | 4.14700E+00 |
| 8.10900E-02, | 4.15800E+00 |
| 8.12900E-02, | 4.16900E+00 |
| 8.14900E-02, | 4.17900E+00 |

| | |
|---|---|
| 8.16900E-02, | 4.19000E+00 |
| 8.18900E-02, | 4.20100E+00 |
| 8.20900E-02, | 4.21200E+00 |
| 8.22900E-02, | 4.22300E+00 |
| 8.24900E-02, | 4.23400E+00 |
| 8.26900E-02, | 4.24500E+00 |
| 8.28900E-02, | 4.25600E+00 |
| 8.30900E-02, | 4.26700E+00 |
| 8.32900E-02, | 4.27900E+00 |
| 8.34900E-02, | 4.29000E+00 |
| 8.36900E-02, | 4.30100E+00 |
| 8.38900E-02, | 4.31200E+00 |
| 8.40900E-02, | 4.32400E+00 |
| 8.42900E-02, | 4.33500E+00 |
| 8.44900E-02, | 4.34700E+00 |
| 8.46900E-02, | 4.35800E+00 |
| 8.48900E-02, | 4.37000E+00 |
| 8.50900E-02, | 4.38100E+00 |
| 8.52900E-02, | 4.39300E+00 |
| 8.54900E-02, | 4.40400E+00 |
| 8.56900E-02, | 4.41600E+00 |
| 8.58900E-02, | 4.42800E+00 |
| 8.60900E-02, | 4.43900E+00 |
| 8.62900E-02, | 4.45100E+00 |
| 8.64900E-02, | 4.46300E+00 |
| 8.66900E-02, | 4.47400E+00 |
| 8.68900E-02, | 4.48600E+00 |
| 8.70900E-02, | 4.49800E+00 |
| 8.72900E-02, | 4.50900E+00 |
| 8.74900E-02, | 4.52100E+00 |
| 8.76900E-02, | 4.53300E+00 |
| 8.78900E-02, | 4.54500E+00 |
| 8.80900E-02, | 4.55600E+00 |
| 8.82900E-02, | 4.56800E+00 |
| 8.84900E-02, | 4.58000E+00 |
| 8.86900E-02, | 4.59200E+00 |
| 8.88900E-02, | 4.60400E+00 |
| 8.90900E-02, | 4.61500E+00 |
| 8.92900E-02, | 4.62700E+00 |
| 8.94900E-02, | 4.63900E+00 |
| 8.96900E-02, | 4.65100E+00 |
| 8.98900E-02, | 4.66200E+00 |
| 9.00900E-02, | 4.67400E+00 |
| 9.02900E-02, | 4.68600E+00 |
| 9.04900E-02, | 4.69800E+00 |
| 9.06900E-02, | 4.71000E+00 |
| 9.08900E-02, | 4.72100E+00 |
| 9.10900E-02, | 4.73300E+00 |
| 9.12900E-02, | 4.74500E+00 |
| 9.14900E-02, | 4.75700E+00 |
| 9.16900E-02, | 4.76800E+00 |
| 9.18900E-02, | 4.78000E+00 |
| 9.20900E-02, | 4.79200E+00 |
| 9.22900E-02, | 4.80400E+00 |
| 9.24900E-02, | 4.81600E+00 |
| 9.26900E-02, | 4.82700E+00 |
| 9.28900E-02, | 4.83900E+00 |
| 9.30900E-02, | 4.85100E+00 |
| 9.32900E-02, | 4.86300E+00 |
| 9.34900E-02, | 4.87500E+00 |
| 9.36900E-02, | 4.88600E+00 |
| 9.38900E-02, | 4.89800E+00 |
| 9.40900E-02, | 4.91000E+00 |
| 9.42900E-02, | 4.92200E+00 |
| 9.44900E-02, | 4.93400E+00 |
| 9.46900E-02, | 4.94600E+00 |
| 9.48900E-02, | 4.95700E+00 |
| 9.50900E-02, | 4.96900E+00 |
| 9.52900E-02, | 4.98100E+00 |
| 9.54900E-02, | 4.99300E+00 |
| 9.56900E-02, | 5.00500E+00 |
| 9.58900E-02, | 5.01600E+00 |
| 9.60900E-02, | 5.02800E+00 |
| 9.62900E-02, | 5.04000E+00 |
| 9.64900E-02, | 5.05200E+00 |
| 9.66900E-02, | 5.06400E+00 |
| 9.68900E-02, | 5.07500E+00 |
| 9.70900E-02, | 5.08700E+00 |
| 9.72900E-02, | 5.09900E+00 |
| 9.74900E-02, | 5.11100E+00 |
| 9.76900E-02, | 5.12300E+00 |
| 9.78900E-02, | 5.13400E+00 |

| | |
|---|---|
| 9.80900E-02, | 5.14600E+00 |
| 9.82900E-02, | 5.15800E+00 |
| 9.84900E-02, | 5.17000E+00 |
| 9.86900E-02, | 5.18200E+00 |
| 9.88900E-02, | 5.19300E+00 |
| 9.90900E-02, | 5.20500E+00 |
| 9.92900E-02, | 5.21700E+00 |
| 9.94900E-02, | 5.22900E+00 |
| 9.96900E-02, | 5.24000E+00 |
| 9.98900E-02, | 5.25200E+00 |
| 1.00100E-01, | 5.26400E+00 |
| 1.00300E-01, | 5.27600E+00 |
| 1.00500E-01, | 5.28800E+00 |
| 1.00700E-01, | 5.29900E+00 |
| 1.00900E-01, | 5.31100E+00 |
| 1.01100E-01, | 5.32300E+00 |
| 1.01300E-01, | 5.33500E+00 |
| 1.01500E-01, | 5.34600E+00 |
| 1.01700E-01, | 5.35800E+00 |
| 1.01900E-01, | 5.37000E+00 |
| 1.02100E-01, | 5.38200E+00 |
| 1.02300E-01, | 5.39300E+00 |
| 1.02500E-01, | 5.40500E+00 |
| 1.02700E-01, | 5.41700E+00 |
| 1.02900E-01, | 5.42900E+00 |
| 1.03100E-01, | 5.44000E+00 |
| 1.03300E-01, | 5.45200E+00 |
| 1.03500E-01, | 5.46400E+00 |
| 1.03700E-01, | 5.47500E+00 |
| 1.03900E-01, | 5.48700E+00 |
| 1.04100E-01, | 5.49900E+00 |
| 1.04300E-01, | 5.51100E+00 |
| 1.04500E-01, | 5.52200E+00 |
| 1.04700E-01, | 5.53400E+00 |
| 1.04900E-01, | 5.54600E+00 |
| 1.05100E-01, | 5.55700E+00 |
| 1.05300E-01, | 5.56900E+00 |
| 1.05500E-01, | 5.58100E+00 |
| 1.05658E-01, | 5.59054E+00 |
| 1.24657E-01, | 6.75405E+00 |
| 1.39134E-01, | 7.83243E+00 |
| 1.57073E-01, | 9.25135E+00 |
| 1.74922E-01, | 1.08405E+01 |
| 1.89103E-01, | 1.24297E+01 |
| 2.06272E-01, | 1.43028E+01 |

# DISTRIBUTION LIST

**DNA-TR-95-43**

**DEPARTMENT OF DEFENSE**

DEFENSE INTELLIGENCE AGENCY
ATTN: DT-1

DEFENSE NUCLEAR AGENCY
ATTN: DFSP
ATTN: DFTD D LINGER
ATTN: SPWE
ATTN: SPWE E TREMBA
2 CY ATTN: SSTL
ATTN: TDTV F RENSVOLD

DEFENSE TECHNICAL INFORMATION CENTER
ATTN: DTIC/OCP

FIELD COMMAND DEFENSE NUCLEAR AGENCY
ATTN: FCTN B HARRIS-WEST
ATTN: NVTV

FIELD COMMAND DEFENSE NUCLEAR AGENCY
ATTN: FCTT-T E RINEHART
ATTN: FCTT DR BALADI
ATTN: FCTT J HUGHES
ATTN: FCTTS J LEVERETTE
ATTN: FCTTS LT COL LEONARD
ATTN: FCTTS DR REINKE
ATTN: FCTTS P THOMPSON

**DEPARTMENT OF THE ARMY**

U S ARMY ENGR WATERWAYS EXPER STATION
ATTN: E JACKSON CEWES-SD-R
ATTN: J ZELASKO CEWES-SD-R

**DEPARTMENT OF THE AIR FORCE**

PHILLIPS LABORATORY
ATTN: PL/SUL

**DEPARTMENT OF ENERGY**

EG&G, INC
ATTN: D EILERS

LAWRENCE LIVERMORE NATIONAL LAB
ATTN: DONALD LARSON
ATTN: F HEUZE
ATTN: B DUNLAP
ATTN: LEWIS GLENN
ATTN: J RAMBO
ATTN: J WHITE
ATTN: W C MOSS
ATTN: R WARD
ATTN: TECH LIBRARY

LOS ALAMOS NATIONAL LABORATORY
ATTN: DAVID KING
ATTN: FRED APP
ATTN: T KUNKLE
ATTN: T MCKOWN
ATTN: J FRITZ
ATTN: C MORRIS
2 CY ATTN: REPORT LIBRARY
ATTN: J N JOHNSON
ATTN: THOMAS DEY
ATTN: TOM WEAVER

SANDIA NATIONAL LABORATORIES
ATTN: DIV 9321 W BOYER
ATTN: MIKE FURNISH
2 CY ATTN: TECH LIB 3141

**DEPARTMENT OF DEFENSE CONTRACTORS**

DEFENSE GROUP, INC
ATTN: ROBERT POLL

ENSCO INC
ATTN: P FISHER

JAYCOR
ATTN: CYRUS P KNOWLES

KAMAN SCIENCES CORP
ATTN: DASIAC

KAMAN SCIENCES CORPORATION
2 CY ATTN: DASIAC

KTECH CORP
ATTN: E SMITH
ATTN: FRANK DAVIES
ATTN: L LEE

LOGICON R & D ASSOCIATES
ATTN: J RENICK

MAXWELL LABORATORIES INC
ATTN: DR E PETERSON
ATTN: J BAKER
ATTN: J MORRIS
ATTN: P COLEMAN
ATTN: S PEYTON

SCIENCE APPLICATIONS INTL CORP
ATTN: DAN PATCH
ATTN: JACK KLUMP
ATTN: L SCOTT
ATTN: MARTIN FOGEL
ATTN: MR M MCKAY

SRI INTERNATIONAL
ATTN: DR JIM GRAN
ATTN: MARK GROETHE
ATTN: P DE CARLI

TECH REPS, INC
ATTN: F MCMULLAN
ATTN: R NAEGELI

TERRA TEK, INC
ATTN: W MARTIN

TITAN CORPORATION (THE)
ATTN: A FREDERICKSON
2 CY ATTN: J M THOMSEN
2 CY ATTN: J R ROCCO
ATTN: S SCHUSTER
2 CY ATTN: V E KOIK

**DIRECTORY OF OTHER**

MARYLAND UNIVERSITY OF
ATTN: RICHARD DICK